Effects of Riparian Vegetation on Transitional and Equilibrium River Morphology

by

ZHU Runye

Department of Civil and Environmental Engineering
Nagoya University

Supervised by

Associate Professor TSUBAKI Ryota

Submitted in partial fulfillment of the requirements for the degree of
DOCTOR OF ENGINEERING

December 2021

1 ABSTRACT

The interaction between vegetation, water flow and geomorphology has created diverse fluvial landforms on the Earth. Investigating the interaction between these elements also has significant engineering value. The interaction has been studied extensively in last decades. By using numerical model that developed rapidly in the last decade, vegetation effects, i.e., vegetation distribution and flexibility, on the transitional and equilibrium river morphology are discussed in this study. The effects of vegetation transect distribution on braided river morphology, and effect of flexibility on reach-scale river morphology has been firstly demonstrated. The problems are investigated through simplified scenarios aiming to understand the fundamental interaction between vegetation and river morphology. The results have compensated the bio-hydro-geomorphology interaction triangle and deepened the understanding of the interaction.

Firstly, a numerical experiment is performed to investigate the effects of floodplain vegetation combined with various initial low water channel planforms on the meandering development in a gravel-bedded river. Three different low water channels, whose wavelengths are determined by an empirical criterion of the mobility of alternate bars through river bends, are studied. Two different floodplain covers are considered: a bare floodplain and a vegetated floodplain. The simulation configurations are based on the Otofuke River at Hokkaido. Results show that with suitable initial low water channel planform and floodplain vegetation, meandering develops in a gravel-bed river without periodic vegetation establishment on bare bars. The sinuosity in the simulation is close to the river in the field. Meandering develops from two processes in gravel-bed rivers, (1) alternate bar growth with an erodible bank and (2) growth from the initial low water channel bend. The wavelength and amplitude of developed meandering are similar. The results suggest that appropriate initial low water channel and floodplain vegetation is sufficient condition for meandering initiation in a gravel-bed river. Furthermore, vegetation establishment

on the floodplain is not a necessary condition for meandering development in short-term river morphology development. This chapter demonstrated vegetation on the floodplain can bring serious damage to river embankment in a vegetated river, and implies the important role of water edge vegetation in the formation of channel meandering.

Since the combination effect of floodplain vegetation and channel planform may induce serious embankment failure, countermeasures are necessary for the management of a vegetated river. In the Satsunai River in Hokkaido, reopening of a closed channel on floodplain is used as a measure to reduce embankment failure risks and remove vegetation coverage. To evaluate the performance of the reopened side channel, the morphological change of river reach (between 31.0 km and 28.8 km from the downstream confluence) during the 2019 flushing flood is simulated by the hydro-morphological model, iRIC Nays2DH. Results show that numerical simulation can capture the trend of river morphological change around the bifurcation introduced by the reopening, but the erosion in the reopened side channel is overestimated compared to field-measured data. The morphology of the side channel is quite stable to the flushing flood based on the field measurement after both 2019 and 2020 flushing floods. The inactive morphological response of the reopened side channel to the flushing flood is inefficient in reactivating the river bed. By narrowing the inlet of another side channel near the bifurcation, more discharge has entered the bifurcation and increased the efficiency of the reopened side channel according to the simulation. The results suggest that by artificially changing the low water channel planform and redirecting the flow, short-term morphological responses can be modified to meet river management requirements. Combined with previous chapter, appropriately modifying the floodplain, e.g., artificially creating a new watercourse on the floodplain, can reduce the risks brought by vegetation expansion.

Second, the effect of vegetation distribution on river morphology in a braided river is studied. Vegetation distribution along river transects is controlled by hydrological conditions and flow disturbance. It can also be influenced by human activities. As one of the most dynamic river

patterns, braided river can be significantly influenced by vegetation encroachment, while the effect of vegetation distribution along river transects on braided river characteristics is still unknown. A depth-averaged hydro-morphodynamic model is employed to study the influence of vegetation transect distribution as the development of numerical model in the last decade has proved its efficiency in studying the interaction between vegetation and river morphology. Rather than discussing specific reason that induces different vegetation distribution and their effects on river morphology, the problem is generalized and studied by varying the vegetation habitat extension. Two patterns of transect distribution of vegetation have been investigated: (1) Vegetation establishment near the low water channel; and (2) Vegetation establishment on bar tops and keeps distance from the low water channel. The model has successfully reproduced the reduction in braiding index of a vegetated braided river. The results show that transect distribution of vegetation has a significant influence on the statistical properties of braiding river bed elevation. Bed variance increases with the increase of vegetation habitat area in both distribution patterns. Skewness and kurtosis decrease and increase with the increase of vegetation habitat area in case of type (1) distribution, respectively. With a distribution type (2), the relationships between skewness, kurtosis, and vegetation habitat area are opposite. These results have provided an extra explanation for the discrepancy in the skewness between field observation and laboratory experiment and show implications for managing vegetated braided rivers with a gravel bed. For restoration project in a vegetated braided river, vegetation near water edge should be removed rather than vegetation on bar top. This chapter shows that only with a vegetation belt that is close to the water edge, the river morphology can be significantly influenced. The results further prove the importance of water edge vegetation in the fluvial system.

Finally, the effect of vegetation flexibility on river morphology is investigated. The flexibility of riparian vegetation affects the flow around vegetation patches and alters bed shear stress below and surrounding the patches. To investigate the effects of vegetation flexibility in a fluvial

bio-hydro-morphodynamic simulation, a model to predict flexible vegetation reconfiguration is incorporated to a bio-hydro-morphodynamic model based on Delft3D. The effects of vegetation flexibility in a gravel bed river with alternate bars have been studied. *Phragmites japonica*, which is an extensively existing reedy grass in riparian environment is the target vegetation. Results show that vegetation flexibility impacts river hydrodynamics and morphology development processes. With flexibility accounted for, the water depth decreases, averaged Shields stress in vegetation patch increases, and active channel width widens. Erosion and deposition in the channel are reduced. The significance of flexibility depends on multiple factors, i.e., stem density growth rate, rigidity, and sediment size. With a fast stem density growth rate or large gravel size, the difference between flexible and rigid cases can be neglected. Compared to previous chapters, the effect of flexible water edge vegetation is demonstrated in this chapter. With flexibility considered, the floodplain formation rate can be better estimated.

In this thesis, the effects of riparian vegetation on transitional and equilibrium river morphology have been studied. The results demonstrate the significant influence of vegetation, i.e., its distribution and flexibility, on river morphology. The results emphasize the necessity to understand the geomorphological influence of water edge vegetation, including its spatial distribution and mechanical properties.

2 ACKNOWLEGEMENTS

First and foremost, I would like to thank my supervisor, Prof. Ryota Tsubaki, for his enlightening advice, great support, and immense patience. Without his support and help, this work cannot be possible. Every discussion with him is insightful. The field surveys to Satsunai River, which were led by Prof. Tsubaki, have shown me the wonders and profound natures of river system.

I would also like to thank Prof. Toda, Prof. Obana, and Prof. Tashiro for their valuable suggestions and comments on this work during the laboratory seminar. Additionally, I would like to express gratitude to the committee members, Prof. Akahori, Prof. Mizutani, and Prof. Toda, for their insightful suggestions on my thesis.

Special thanks also belong to Prof. Iwasaki for providing the source code of Nays2DH.

I also want to thank the lab members and staff in the Hydraulic Lab. They provide kind help to foreign students. I would like to thank Mr. Yuji and Mr. Hamaguchi, for their help during field surveys. I am grateful to Mrs. Wada for her help in dealing with the complicated documents.

I would like to give profound thanks to Ms. Lian Jiani, for her immense support.

Finally, I would like to thank the Japanese Government (Monbukagakusho: MEXT) Scholarship, which provided financial support and made my study in Japan possible.

Table of Contents

3 LIST OF FIGURES

1 Introduction

1.1 Research background

The interaction between vegetation, river flow and morphology is complicated. Conceptual models have been proposed to explain the interaction (Castro and Thorne, 2019; Tsujimoto, 1999). An example of the conceptual models is depicted in **Figure 1.1**. The interaction between vegetation, flow, and geomorphology is called the bio-hydro-geomorphology triangle. However, it has various names in different literature, e.g., eco-morphodynamic (D'Alpaos et al., 2016). In this thesis, the effect of vegetation on geomorphology is the main focus.

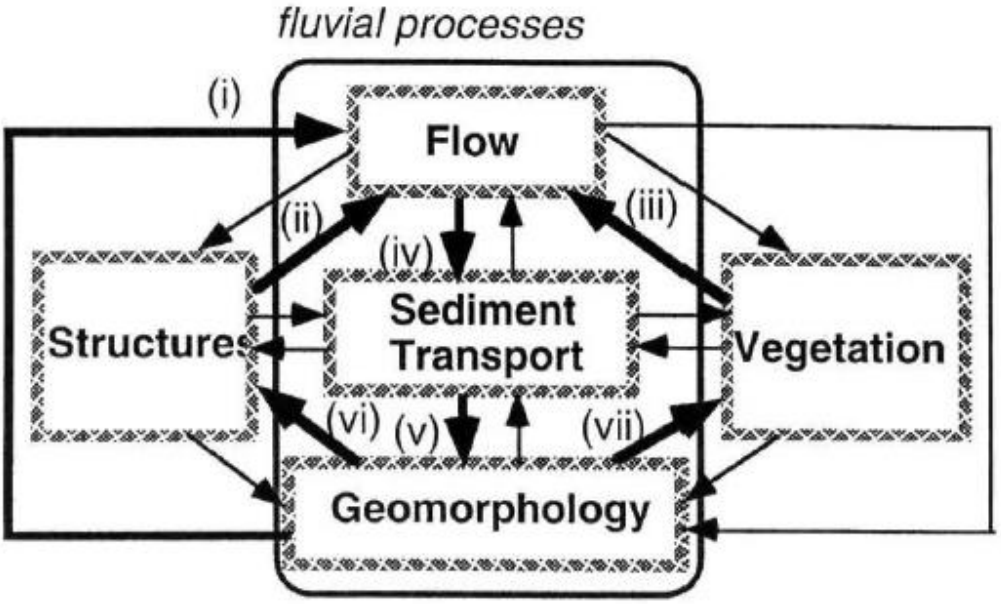

Figure 1.1 A conceptual model showing the interaction between vegetation, river flow, and geomorphology (Tsujimoto, 1999).

1.1.1 Fluvial process: Interaction between hydrodynamic and river morphology

The interaction between river hydraulics and river morphology has created a diverse pattern of river planform. River planforms can be classified to several patterns, while a threshold

between patterns does not exist (Carson, 1984; Leopold and Wolman, 1957; Nanson and Knighton, 1996). River morphology can transform from single-thread river to multi-thread river continuously. A classification of channel patterns is depicted in **Figure 1.2**. Channel pattern is related to multiple factors, such as bankfull discharge, water depth, and channel width or bed slope. Several predictors, empirical or physically based, have been proposed to predict the channel pattern with certain parameters.

A predictor related the bankfull discharge and a critical bed slope is shown as follows (Leopold and Wolman, 1957):

$$S_c=0.013Q_{bf}^{-0.44}$$

where S_c is the channel slope, Q_{bf} is the bank-full discharge. However, it is realized that this predictor can distinguish the meandering and braiding is because the channel slope is partly related to channel sinuosity. Therefore, the predictor is not used anymore.

A better predictor relies on an independent value from the river morphology is developed by van den Berg (1995). The predictor is expressed as the following formula:

$$\omega=900D_{50}^{0.42}$$

where ω is the transitional stream power and D_{50} is the median river bed grain size.

Crosato and Mosselman (2009) proposed a simple predictor based on forced bar theory. The predictor is expressed as the following formula:

$$m^2=\frac{0.17g(b\text{-}3)}{\sqrt{\frac{\rho_s\text{-}\rho}{\rho}D_{50}}}\frac{B^3 i}{CQ}$$

where the m is the bar mode that represents bar numbers in one cross-section, b is the nonlinearity of the sediment transport (b is 10 in a gravel bed river, and 5 in a sandy bed river), ρ_s and ρ is sediment density and water density respectively, D_{50} is the median bed grain size, B is the channel width, i is the longitudinal bed slope, C is the Chezy roughness and Q is the bankfull discharge. The river tends to be braiding if the river is wide, steep and bedload transport is dominated.

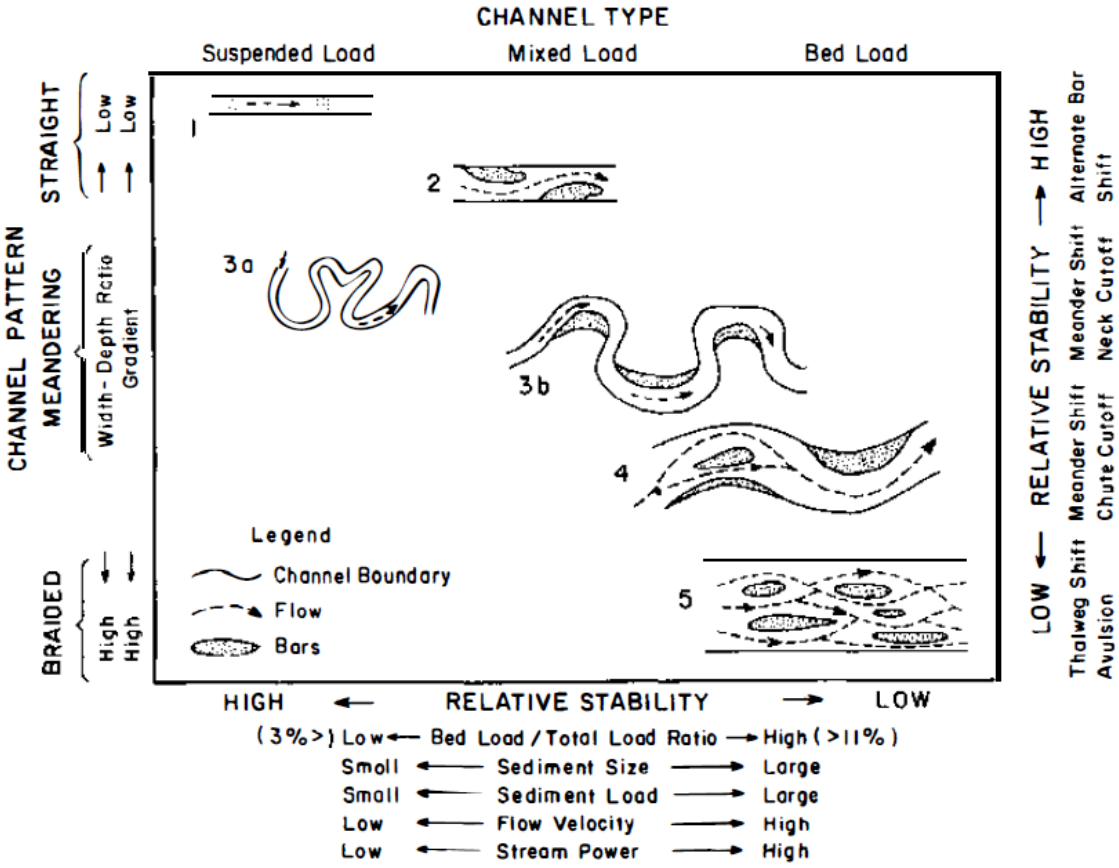

Figure 1.2 River pattern classifications based on river stability, sediment load and other paraameters (Schumm, 1985).

1.1.2 Vegetation effects

1.1.2.1 On hydrodynamics

Vegetation in the fluvial environment exerts drag force on the water flow (Luhar and Nepf, 2013). Thus, the roughness of the river bed increases due to the occurrence of aquatic vegetation. Velocity within the vegetation patch is found to decrease due to the increase of bed roughness (Nepf et al., 1997). Due to the reduced velocity, the bed shear stress decreases. For emergent vegetation, the depth-averaged flow velocity is reduced. While for submerged vegetation, the water is deflected to the area without vegetation; thus, the distribution of the velocity profile is changed: between the lower vegetated part and upper part, there is a shear stress layer. It is found turbulence stress drives the water flow in the vegetation canopy. Meanwhile, the bed slope plays

an important role (Raupach et al., 1991). The relative importance of turbulent stress or bed slope is determined by water depth and vegetation height (Nepf and Vivoni, 2000).

The effects of vegetation on flow velocity are mainly determined by the parameter *ah*, where *a* is the front area per square meter and *h* is the vegetation height (Nepf, 2011). If the vegetation is sparse ($ah<<0.1$), the velocity profile along the vertical direction is close to the turbulent boundary-layer profile. With dense vegetation, the velocity profile can be described by a two-layer model (Baptist et al., 2007; Nepf, 2011). The criteria for dense vegetation is that $ah>0.1$.

In an open channel partially covered by vegetation, the flow is deflected to water course without vegetation cover. Such flow may influence the flow field that is far from the vegetation patch. The effect is called the far-field effect (Bywater-Reyes, 2015). Experiments and simulations have investigated flow field around vegetation patch that has simple geometry. Z. Chen et al. (2012) has confirmed the wake structure behind a porous obstruction and its implications for aquatic vegetation. The flow velocity around the patch increases due to reduced cross-section area, and behind the patch, the velocity reduces in the wake area. The occurrence of wake structure is also confirmed by numerical simulation (Kim et al., 2018). The wake structure also has an influence on sediment deposition patterns. However, in natural conditions, multiple vegetation patches exist in the same river reach; thus, they may interact with each other (Ghani et al., 2019; Meire et al., 2014). Velocity between patches is found to be enhanced, and the area with an increased velocity reduces its longitudinal size with a decrease in the gap between patches (Meire et al., 2014).

1.1.2.2 On sediment transport

As vegetation influences the velocity around vegetation patches and within the vegetation, it affects sediment transport. Since shear stress within the vegetation patch is reduced, vegetation is regarded that favors the capture of fine sediment in the patch (López and García, 1998). Flume experiments find suspended load also deposits behind vegetation patch in the wake region and recirculation zone due to reduced shear stress (Kim et al., 2018). However, since the vegetation

patch diverts the incoming flow and increases the flow velocity around the patch, erosion also happens around the vegetation patch (Rominger et al., 2010). Follett and Nepf (2012) investigated the sediment patterns around a limited reedy vegetation patch and found sediment is redistributed around the patch. Erosion around the lateral edge increased with dense stem density. An interesting discovery is that they did not observe net deposition in the reach scale. The experiment also suggests that sediment redistribution around vegetation patches depends on the sediment supply condition upstream. Kim et al. (2015) has demonstrated by laboratory experiment that sediment pattern is highly related to upstream sediment supply condition. Without enough sediment transported from the upstream, erosion occurred around the patch and on the leading edge. With Shields stress higher than the transport criteria, deposition happens in the vegetation patch. Vegetation also prevents bank sediment from entering the river corridor by increasing bank stability. Vegetation stabilize the river bank and reduces bank erosion by combing the sediment particles with its root system, as shown in **Figure 1.3** (Tal and Paola, 2010; Van Dijk et al., 2013).

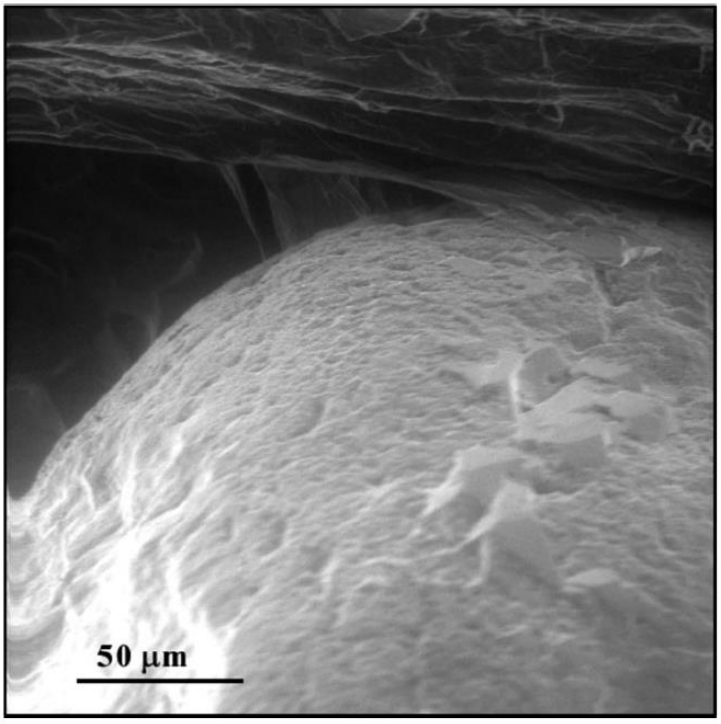

Figure 1.3 Photo shows a sediment grain attaches to vegetation root (Tal and Paola, 2010).

1.1.2.3 On river morphology

Vegetation is shown to affect sediment transport; thus, it also influences river morphology (Gurnell, 2014). Riparian vegetation reduces channel width by strengthening the channel bank and its expansion (Zen and Perona, 2020). Vegetation on floodplain and point bars reduces the occurrence of chute cutoff (Dijk et al., 2014). In braided river, vegetation expansion and growth may lead to a reduction in the braiding intensity and finally transform the river pattern from braiding to dynamic meandering (Bertoldi et al., 2015; Gran and Paola, 2001; Tal and Paola, 2010, 2007). The transformation is demonstrated by flume experiment (**Figure 1.4**). Researchers suggest the occurrence of vegetation on the Earth has changed the landform (Gibling and Davies, 2012). Vegetation on the floodplain maintains the channel width and keeps river meandering (Asahi et al., 2013). Vegetation in braided river creates habitat and forms, and such process has formed the island-braided river pattern (Edwards et al., 1999; Gurnell et al., 2001). Vegetation's role in creating various river morphological patterns is dynamic rather than static (Camporeale et al., 2013; Solari et al., 2016). River morphology response differently to vegetation life stage due to different frontal area and flood resistance (Kyuka et al., 2021; A. Vargas-Luna et al., 2016). Interestingly, the distribution approach of vegetation seeds during seeds dispersal period has a different influence on river morphology development (Van Dijk et al., 2013). With seed dispersed by water flow (hydrochory), vegetation can increase the braiding intensity. Not only can alive vegetation change the river morphology, vegetation debris generated by floods or other reasons can also impact morphological development. Woody debris is found to reduce river braiding intensity, channel width, and bed elevation skewness (Mao et al., 2020). Debris of invasive grassy vegetation may increase the risks of vegetation expansion and change the river morphology (van Oorschot et al., 2017).

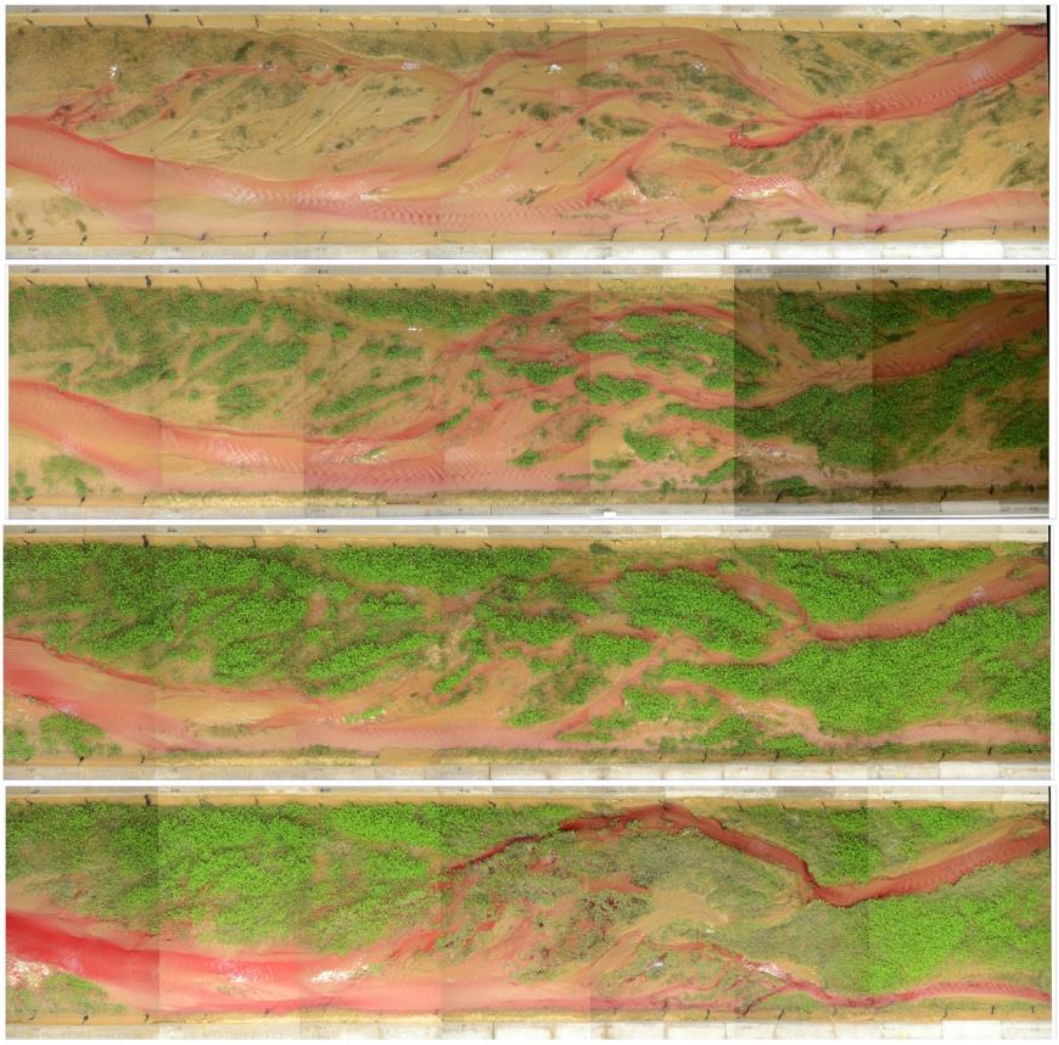

Figure 1.4 Transformation from braiding to dynamic meandering due to the expansion of vegetation (Bertoldi et al., 2015).

The relationship between vegetation characteristics and river pattern can be described the following formula (Millar, 2005, 2000):

$$S^{*}=0.0002D_{50}^{0.61}\phi'^{1.75}Q^{-0.25}$$

where S^{*} is a critical slope, D_{50} is the bed grain size, ϕ' is the angle of repose affected by vegetation, Q is bank-full discharge. If the river bed slope is larger than the critical slope, the river tends to be braiding; otherwise, it tends to be single-thread.

1.1.3 Vegetation dynamic

Vegetation dynamic is classified into five processes: seed dispersal, recruitment, growth, succession, and mortality (Solari et al., 2016). In river channels, seeds are mainly distributed by water flow and wind. Seed transported by water flow is named as hydrochory. Hydrochory has various forms, and two forms are related to long-distance transport: seeds transported by surface flow and seeds transported on the river bed (Parolin, 2006). Hydrochory is influenced by three factors: hydrological regime, geomorphology units and phenology (Merritt and Wohl, 2006, 2002). Water flow velocity is described as the major driver of seed floating or deposition. With a small increase in water flow velocity, the distance of seed transport increases significantly (Johansson and Nilsson, 1993). Increased shear stress with the increase of flow velocity reduces the ability of seed to settle on the river bed (Hyslop and Trowsdale, 2012). For vegetation recruitment, a good conceptual model is the recruitment box model (Mahoney and Rood, 1998). In the recruitment box model, the seed dispersal period is related to the annual water elevation change and recruitment zone (**Figure 1.5**). Vegetation growth is related to the temporary change of vegetation stem density, diameter, root depth and etc. The growth of vegetation is related to multiple factors, e.g., sunlight conditions (Sakai et al., 2013). Models describing vegetation growth is few. Perucca et al. (2007) employed a process-based logistic model to describe the growth of vegetation. The model is described as the following:

$$\frac{\partial B}{\partial t} = \gamma B(1 - B/B_{st})$$

where B is the vegetation biomass, B_{st} is the biomass carry capacity of the local environment, and γ is a parameter that is related to vegetation growth time scale. Similar growth model has been widely used, e.g., Camporeale and Ridolfi (2006).

Sakai (2013) has employed a more realistic model describing the change of vegetation biomass. This model considers the effects of several biological processes on vegetation biomass change. The model is described by the following equation:

$$\frac{\partial B}{\partial t} = P - R + \frac{\partial}{\partial x}\left(k_x \frac{\partial B}{\partial t}\right) + \frac{\partial}{\partial t}\left(k_y \frac{\partial B}{\partial t}\right)$$

Where *P* is the biomass generated by photosynthesis, *R* is the biomass consumed by respiration, k_x and k_y is diffusion coefficient describing the spatial diffusion of vegetation biomass. This model is a mixture of process-based model and physic-based model. The process of photosynthesis is estimated by the following formula:

$$P = \frac{I}{I + I_{ci}} P_{max}$$

Where *I* is light intensity in the vegetation patch, I_{ci} is the saturation constant for light intensity. The process of respiration is described by the following formula:

$$R = \gamma P + \mu B$$

Where γ and μ are parameters.

Pearlstine et al. (1985) proposed a model that describes the increase of tree diameter.

$$\frac{\partial D}{\partial t} = \frac{1 - DH/D_{max}H_{max}}{274 + 3b_2 D - 4b_3 D^2}$$

Where *D* is the tree diameter at breast height, *H* is the tree height, D_{max} and H_{max} are the maximum diameter and height, b_2 and b_3 are parameters that are determined by vegetation species.

Vegetation mortality can be attributed to multiple reasons. Johnson (2000) indicated that drought is a major reason for seedlings. Seedlings on the bare ground cannot survive without suitable moisture conditions and water surface declining rate (Amlin and Rood, 2002). A fast decline rate of water table may induce vegetation mortality. While a best declining rate exist which is about 1 cm per day (González et al., 2010).

Vegetation is also destructed due to uprooting by erosion and water flow. Erosion-induced destruction of riparian vegetation may account for half of vegetation destruction during a large flood (Cooper et al., 1999). Two types of uprooting mechanisms are determined by Edmaier et al. (2011), namely Type I and Type II (**Figure 1.6**). Type I uproot is purely induced by flow drag force acting on the above-ground part of the vegetation. Type II uproot is a combination of

substrate erosion and drag force. With bed eroded the anchoring force induced by root system decreases. When the anchoring force is smaller than the drag force, the vegetation is uprooted. Since erosion occurs in the Type II uproot, a time delay exists, while in Type I uproot there is not time delay. A method to calculate the critical erosion depth for Type II uproot is proposed by Calvani et al. (2019). The depth L_e could be solved by the following equation:

$$aL_e^2 + bL_e + c = 0$$

$$a = 1$$

$$b = -2\left(\frac{1}{N_R}\sum_{i=1}^{N_R} L_{r,i} + \frac{\tau_{bed} + c'}{(\gamma_{sat} - \gamma_w) f \ \ tan(\phi')}\right)$$

$$c = \frac{1}{N_R}\sum_{i=1}^{N_R} L_{r,i} - 2\frac{\tau_{bed}\left(\pi H_p D_p + A_l\right) + B}{(\gamma_{sat} - \gamma_w)\pi N_R D_r f \ \ tan(\phi')} + \frac{2c'}{(\gamma_{sat} - \gamma_w) f \ \ tan(\phi')}\frac{1}{N_R}\sum_{i=1}^{N_R} L_{r,i}$$

where c' is the cohesion of bed soil, ϕ' is the shear stress angle of soil, L_r is the length of root depth, D_r is the diameter of root, H_p is the height of vegetation, D_p is the diameter of stem above ground, A_l is the leaf area, τ_{bed} is bed shear stress, N_R is the number of roots, γ_w and γ_s are unit weight of water and soil, respectively. For non-cohesive river bed, c' is zero.

In addition to erosion, vegetation can also be destroyed by burial. Experiment in a meandering channel has confirmed that under certain flow conditions, burial-induced destruction is much riskier to the vegetation than the erosion-induced destruction (Kui et al., 2014). Kui et al. (2014) show that burial is related to vegetation density and vegetation height. Dense vegetation is found to have a higher risk of being buried in the experiment. It is explained by the higher drag force exerted on water flow when the vegetation patch is dense.

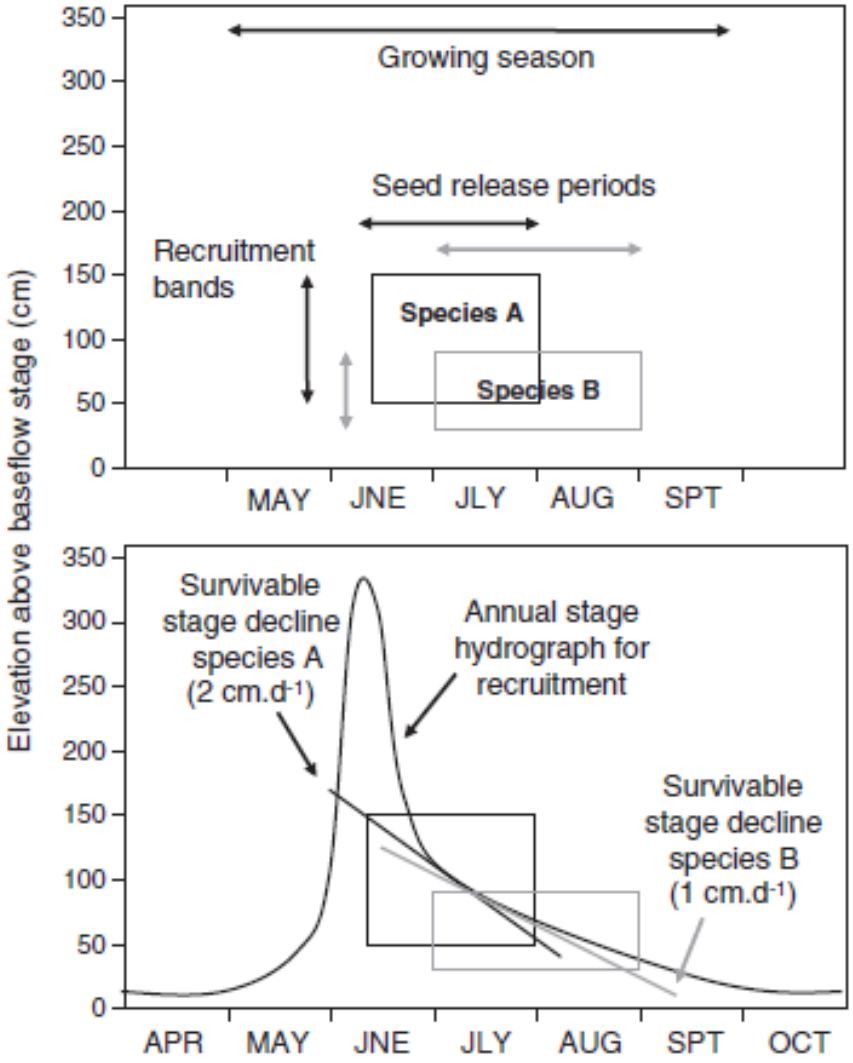

Figure 1.5 Recruitment box model. Seed dispersal is related to water elevation. From C. Camporeale et al. (2013).

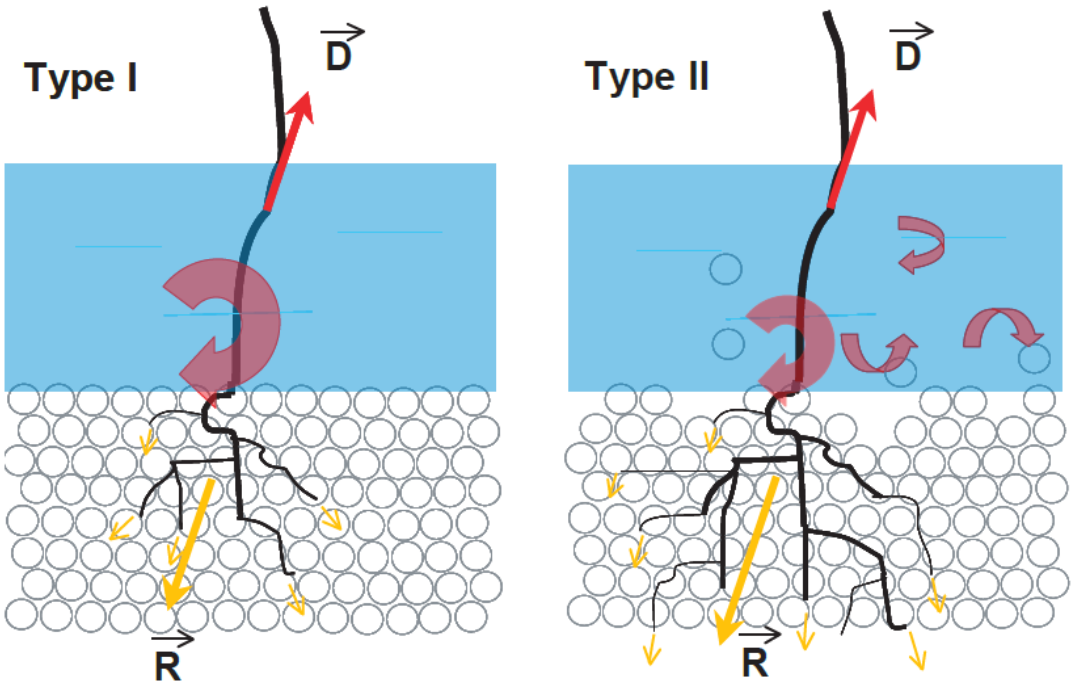

Figure 1.6 Two types of uproot mechanisms of riparian vegetation (Edmaier et al., 2011).

1.1.4 Representing vegetation in numerical model and flume experiment

The interaction between vegetation and fluvial geomorphology can be investigated through multiple methods, including field survey (Bertoldi et al., 2011), analytical analysis (D'Alpaos et al., 2016), flume experiment (Tal and Paola, 2010), and numerical simulation (van Oorschot et al., 2016). In this section, representing vegetation in numerical simulations and flume experiment are the focus since both methods provide highly controllable conditions but simplified vegetation conditions.

There are multiple approaches to account for the effect of vegetation in a numerical geomorphological simulation. As a pioneering work, Murray and Paola (2003) built a cellular automaton model to investigate the effect of vegetation on a braiding river morphology. In their model, the vegetation effect was accounted for by reducing sediment flux in vegetated places and strengthening river banks by reducing lateral sediment transport.

However, the most frequently employed approaches of account for vegetation effect in numerical simulation are changing bed roughness or adding a source term representing drag force to the momentum equations. The drag force is calculated by the following formula:

$$F_D = \frac{1}{2}\rho C_D a h_v u_v^2$$

Where ρ is the water density, C_D is the drag coefficient, u_v is the mean flow velocity, h_v is vegetation height and a is projected plant area per volume which is the product of stem diameter and stem numbers per square meter.

Multiple models have been proposed to account for the vegetation effect by changing bed roughness. By analytical analysis and employing generic programming, Baptist et al. (2007) proposed the following formula to calculate Chezy roughness coefficient in a vegetated channel with submerged vegetation:

$$C_b' = C_b + \frac{\sqrt{g}}{\kappa} ln\left(\frac{h}{h_v}\right)\sqrt{1 + \frac{C_D a h_v C_b^2}{2g}}$$

where C_b' is the Chezy coefficient with the vegetation effect, C_b is the Chezy coefficient of bare bed, h is the water depth, g is the gravitational acceleration. For emergent vegetation, the Chezy coefficient is calculated as follows:

$$C_b' = \sqrt{\frac{1}{\frac{1}{C_b^2} + \frac{C_D a h}{2g}}}$$

Barfield et al. (1979) proposed a formula to account for vegetation effect based on hydraulic radius. The hydraulic radius R_{BF} is determined by:

$$R_{BF} = h - h_v + \frac{s h_v}{2h_v + s}$$

Where s is the distance of stems within vegetation patch. The bed shear stress then is calculated by:

$$\tau = \rho g R_{BF} i$$

where i is the channel bed slope.

By comparing with field results and flume experiment results (including roughness and sediment transport rate), the Baptist formula shows the best agreement (Vargas-Luna et al., 2015). However, the accuracy for sparse vegetation worsens since Baptist formula is based on two-layer model that does not appropriate for sparse vegetation patches.

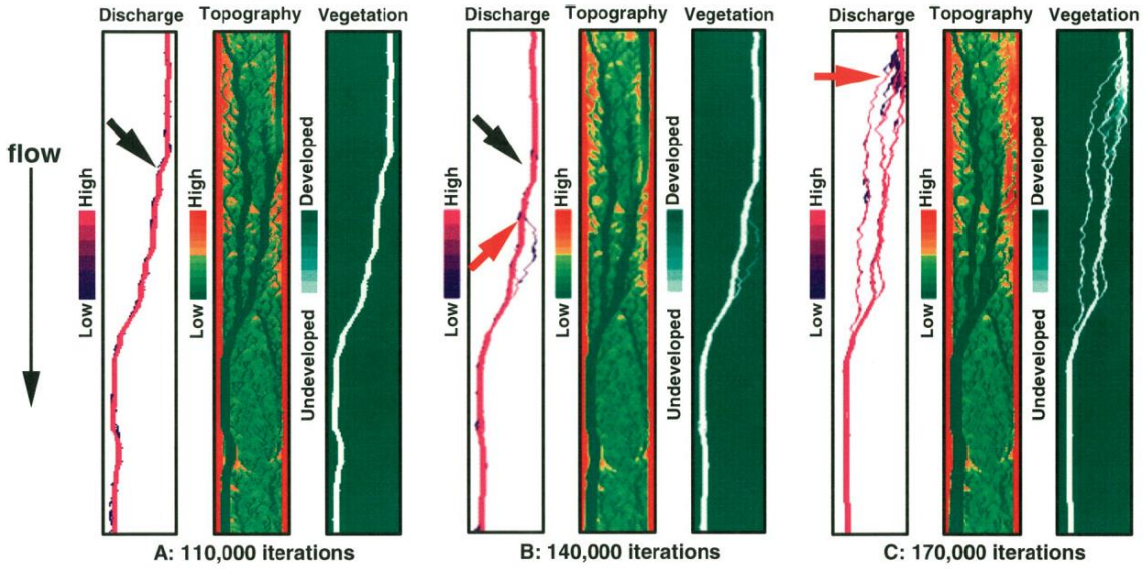

Figure 1.7 Single thread channel forms undergoing vegetation expansion in a braided river (Murray and Paola, 2003).

1.1.5 Advances in modelling bio-geomorphology interaction by depth-averaged model

With the fast increase of computational resources, the simulation of the bio-geomorphology by depth-averaged shallow water model combined with the Exner equation has developed rapidly in the last decades. Although numerical models have not been a standard solution for such problems, it has been applied to solve several interesting problems (Stecca et al., 2019). Crosato and Saleh (2011) investigated the effects of floodplain vegetation in a braided river with a fine gravel bed. They demonstrated that floodplain vegetation could concentrate flow to the main channel during an overbank flood, and prevent the river morphology from being braiding. They also found that Baptist formula overestimated the vegetation effect when vegetation is sparse. Sakai et al. (2013) simulated the effects of vegetation on alternate bars and

mid-channel bars, accounting for the competence between trees and grassy vegetation. Bertoldi et al. (2014) demonstrated that two distinct vegetation distribution patterns exist when varying the river stream power, and rapid change of river bed statistical properties can be observed. Oorschot et al. (2016) has developed a bio-morphology model based on Delft3D. The simulation results based on this model show that river morphology response quite differently to dynamic vegetation than static vegetation. The model has been applied to various problems, including the effect of climate change and alien vegetation invasion (van Oorschot et al., 2018, 2017). Jourdain et al. (2020) investigated the effects of vegetation on alternate bar characteristics by numerical model and obtained results that quantitatively agreed with theoretical predictions.

1.2 Research problems and objectives

Early research compared different vegetation cutting methods and their influence on water depth and velocity (Leu et al., 2008). The results suggest different locations of vegetation patches left by the vegetation cutting processes have different influences on river hydrodynamics, and water edge vegetation may have the largest influence (**Figure 1.8**b). However, its influence on river morphology has not been studied. Water edge vegetation is assumed to play an important role in vegetation habitat expansion by promoting fine sediment deposition (Corenblit et al., 2009). During this process, flexibility cannot be neglected. With the development of numerical simulation techniques, investigating the effects of vegetation on river morphology in a highly controllable way is becoming possible. In this study, vegetation influence on river morphology in gravel bed rivers is going to be examined, and possible river management measures and their influences are discussed. Gravel bed rivers are considered since they may experience river morphology change, e.g., the transformation from braiding to dynamic meandering, undergoing the influence of vegetation. Moreover, gravel bed river generally has relatively high stream energy and less stable river morphology; thus, it provides various habitat for the fluvial ecological system.

Following are the specific problems that will be tackled in the thesis. The topic that is discussed in this thesis and their position in the interaction are depicted in the red box in **Figure 1.9**. The schematic of research topics are shown in Table 1. By investigating such problems, not only the understanding of riparian vegetation can be advanced, but also the understanding of the role played by water edge vegetation can be improved.

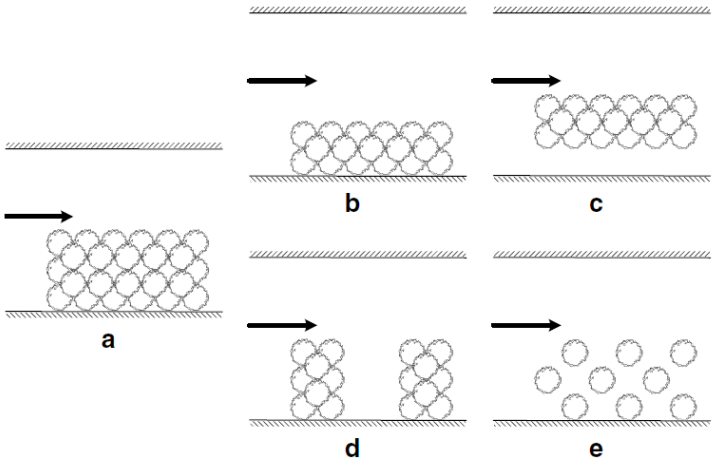

Figure 1.8 Different vegetation cutting methods (Leu et al., 2008). Arrows represent flow direction.

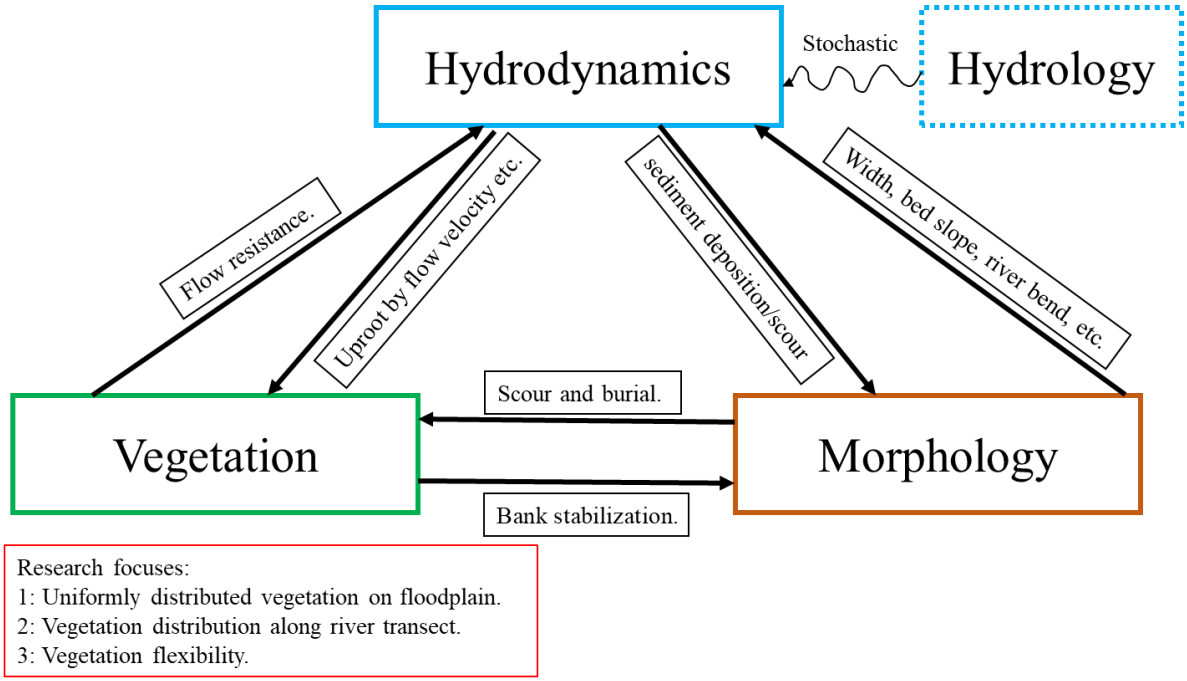

Figure 1.9 Schematic figure showing the position of this thesis in the bio-hydro-geomorphology interaction triangle. The black box shows the processes that influence the elements in the triangle. The red box shows the focuses and research focuses in this thesis.

Table 1 Research focuses and schematic figures.

Research focuses	Schematic
1. Effects of Uniformly distributed vegetation on floodplain and initial channel planform	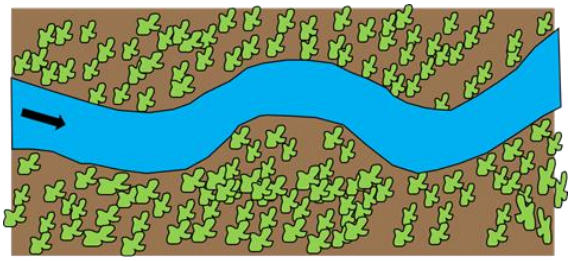
2. Effects of vegetation distribution along river transect on river morphology	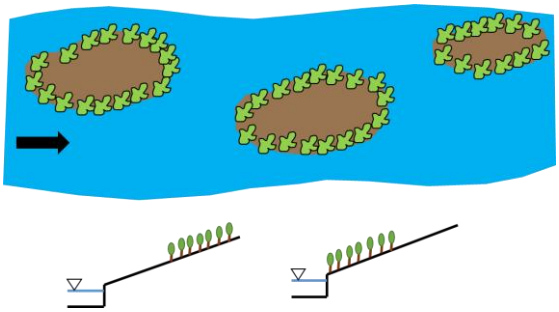
3. Effects of vegetation flexibility on river morphology	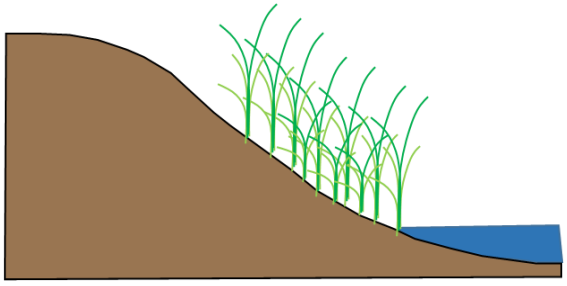

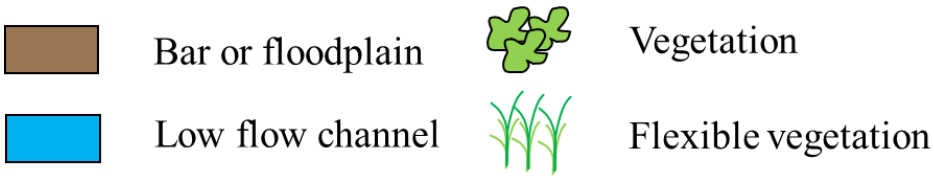

1.2.1 Combined effect of floodplain vegetation and low water channel planform on the transitional development of river morphology

This problem is going to tackle the effect of uniformly distributed vegetation on floodplain, as shown in the red box of **Figure 1.9**. With human impact on river hydrology increases, e.g., dam operation, vegetation is expanding in fluvial environment and induces serious management

risks. With vegetation expansion, the river is going to be a single thread. In a river encountering vegetation expansion problem, floodplain and low water channel both affected water flow. Hence they can influence the river morphology development. The floodplain vegetation can reduce the sediment entering the river flow; thus, it can affect the river morphology development. For a long-term study, which is generally investigated in early research, the river equilibrium state is not affected by the initial river morphology (Baar et al., 2019). However, transitional development may differ depending on the initial morphology. Clarifying the role played by floodplain vegetation and the low water channel planform on the transitional morphological development would be valuable for river management.

1.2.2 Morphological effects of vegetation distribution along river transect in a braided gravel river

This problem is going to tackle the effect of vegetation distribution along river transects on the dynamic equilibrium state of river morphology, as shown in the red box of **Figure 1.9**. In a real river, vegetation distribution along river transect is determined by several factors: hydrological conditions, morphological change and vegetation species. Vegetation transect distribution is tightly related to flow variability (stochastic properties, as shown in the dash blue box in **Figure 1.9**), which is difficult to simulate in a 2-dimensional model due to its high randomness. The distribution of vegetation can also be modified by human activities, such as vegetation removal. To investigate different factors that induce various vegetation distribution is difficult; thus, the problems can be generalized and investigated by varying the vegetation habitat extension. Different habitat extension implicitly reflects the factors that induces the variability of vegetation distribution. With a deeper understanding of the effect of vegetation transect distribution, better vegetation control measures can be designed.

1.2.3 Effects of vegetation flexibility on river morphology development in a gravel bed

river

This problem is going to tackle the effect of vegetation flexibility on the dynamic equilibrium state of river morphology, as shown in the red box of **Figure 1.9**. However, numerical model regarding bio-geomorphology interaction has developed rapidly in the last decade. The flexibility of certain type of vegetation is generally neglected, e.g., reedy grass. However, field survey has shown that reedy grass is flexible. Thus, investigating the effects of considering vegetation flexibility on river morphology development is important. The question is, what is the influence of neglecting vegetation flexibility, and in what situation the flexibility can be neglected. With a better understanding of modeling flexibility in a bio-geomorphology model, better measures to prevent vegetation expansion might be designed.

1.3 Contents of the thesis

The structure of the thesis is shown in **Figure 1.10**.

Chapter 1 includes the research background and the research problems. The effect of vegetation on the bio-hydro-geomorphology interaction is introduced in this chapter. Three problems that are neglected are identified in this chapter.

In Chapter 2, the effects of the uniformly distributed vegetation on floodplain with various low water channel on the transitional response of channel morphological development is investigated.

In Chapter 3, the effects of the reopened and closed channel on the transitional morphological response are investigated. This chapter depends on a real vegetated braided river. Short term morphological response of the initial channel is used as a river management measure. Both Chapter 2 and Chapter 3 focus on the transitional response of river morphology.

In Chapter 4, the effects of vegetation distribution along river transect on braided river morphology are investigated. In this chapter, the extension of vegetation habitat is the metric to

be studies since it implicitly reflects the influence of stochastic properties of hydrology conditions.

In Chapter 5, the effects of vegetation flexibility on river morphology and water flow are investigated. The study shows that flexibility has an influence when stem density and bed grain size fall in a certain range.

In Chapter 6, conclusions and further research are described.

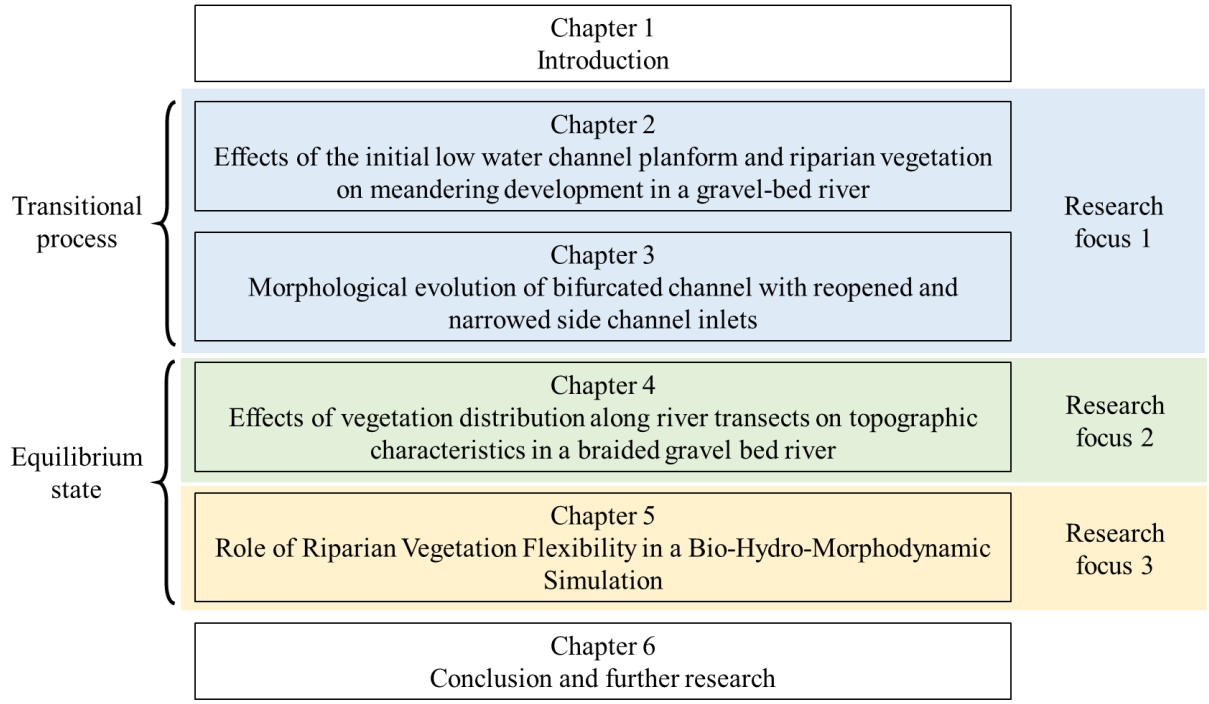

Figure 1.10 The structure of the thesis. Research problems correspond to the problems in **Figure 1.9**.

2 Effects of the floodplain vegetation and low water channel planform on meandering development in a gravel-bed river

2.1 Introduction

During a flood event in 2011, a meandering has developed from the low water channel in the Otofuke River in Hokkaido and induced disastrous failure of embankment in Figure 2.1 (Kawamura and Watanabe, 2015). A similar disaster occurred in 2016 in the same river (Okabe et al., 2018). Laboratory experiments and numerical simulations have indicated that meandering development in the Otofuke River could be induced by initial river topography, i.e., alternate bars (Nagata et al., 2013). Yamaguchi and Ito (2014) have shown that the river can still be meandering without initially developed alternate bars, but the meandering cannot be maintained for a long time. The bank erosion accompanying the meandering development is also related to floodplain vegetation cover. Obtaining a better understanding of meandering development in gravel bed river would be helpful to prevent similar disasters, while the process is quite complicated.

Meandering initiation and formation have long attracted attention from both geomorphologists and river engineers. By linearizing the shallow water equations, incipient meandering is attributed to the alternate bar formation and channel curvature (Seminara and Tubino, 1989). A movable bed experiment with a fixed wall has shown that the low water channel curved with a certain wavenumber could introduce steady perturbation in the river bend and amplify the meandering (Garcia and Niño, 1993). Numerical simulation has shown single upstream bend can trigger meandering that can migrate to the downstream in the Otofuke River (Nagata et al., 2014). However, a study about the influence of initial low water channel geometry is lacking.

Figure 2.1 River meandering developed during the 2011 flood in the Otofuke River (Kawamura and Watanabe, 2015).

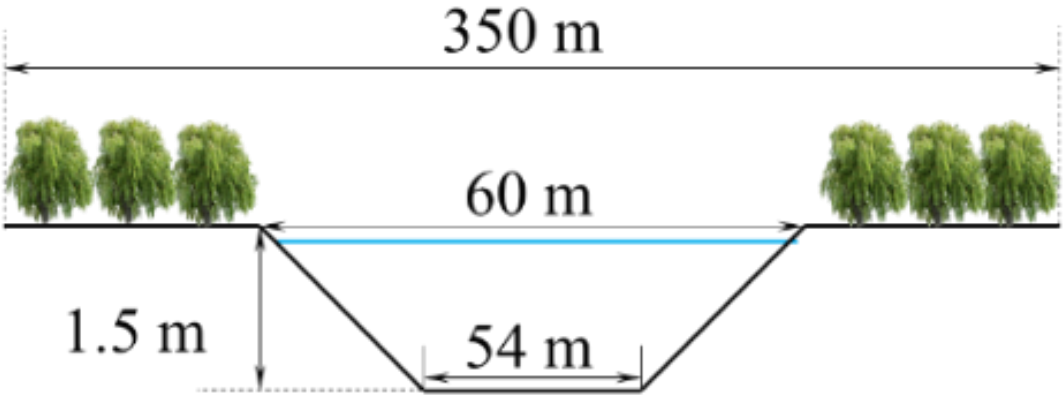

Figure 2.2 The cross-sectional configuration of the initial channel.

Another important factor influencing meandering in a gravel-bed river is vegetation. Without floodplain vegetation, gravel-bed river tends to be braided (Iwasaki et al., 2016a). Studies suggest vegetation establishment on bars is a key factor for sustaining dynamic meandering from a long-term point of view (Braudrick et al., 2009; Weisscher et al., 2019): With vegetation establishment on bare bars, shear stress is reduced, and chute-cutoff is difficult to occur (Dijk et al., 2014). Without vegetation recruitment on bare bars, floodplain vegetation alone is found enough to enhance bank erosion in a braided flume channel (Kyuka and Yamaguchi, 2018). Thus, a reasonable assumption is that vegetation alone can trigger meandering in a gravel bed river.

Previous studies have shown both initial planform of low water channel and vegetation can be triggers of river meandering. However, whether vegetation or planform alone can trigger the meandering has not been clearly studies. This study aims to investigate the influence of initial low water channel planform and vegetation effect on meandering initiation in a gravel-bed river. The study is performed by non-linear numerical simulation since the model can capture non-linear effects, e.g., chute-cutoff (Dijk et al., 2014), that influence meandering development. Different initial low water channels are designed with referring to an empirical criterion that determines the mobility of free alternate bars through river bends.

2.2 Methods

2.2.1 Numerical model

Nays2DH is employed to solve the shallow water equations and to predict the morphological change by the sediment mass conservation equation (Shimizu et al., 2020). The effect of vegetation on flow is accounted for by adding a source term in the momentum equations:

$$F_D(s,n) = \frac{1}{2} C_D \rho a_s U(s,n)^2 \tag{1}$$

where $F_D(s,n)$ is the drag force in the streamwise direction s and transverse direction n directions, C_D is the drag coefficient, $\rho$is the water density, a_s is the vegetation density, which is the product of vegetation stem number per area and representative diameter, $U(s,n)$ is the depth-averaged velocity. Vegetation effect in strengthening the bank stability through combining the sediment particles is not accounted for in this study. The effect of vegetation in protecting the river bank is represented by reducing shear stress within the vegetation patch.

In Nays 2DH, the transverse bedload transport is calculated by:

$$q_n = q_b \left[\frac{v}{\sqrt{u^2 + v^2}} \frac{h}{r} N - \gamma \frac{\partial z_b}{\partial n} \right] \tag{2}$$

where q_n is the transverse bedload transport rate, q_b is the total bedload transport rate calculated by bedload transport formula, u and v are the near-bed velocity components along

with the streamwise and transverse directions, h is the water depth, r is the streamline radius, N (= 7) is a calibration parameter for secondary flow, γ is a positive calibration parameter depending on the Shields number, z_b is the bed elevation. The transverse bedload transport in the vegetated near-bank region could be reduced due to a decreased q_b.

An angle of repose θ_c is used to determine the occurrence of a bank collapse. If the bed slope exceeds θ_c, the elevation is adjusted to be bed slope smaller than θ_c.

2.2.2 *Initial low water channel planforms*

In this study, compound channels are used as the initial bed (**Figure 2.2**). The configuration of the low water channel and parameters are based on the Otofuke River. The Otofuke River is chosen as an example of a gravel bedded river with a vegetated floodplain. In addition, the river morphology is braiding if there is no vegetation cover in the Otofuke River (Iwasaki et al., 2016a); therefore, this configuration is suited to investigate the impact of vegetation.

The width and depth of the low channel are 60 m and 1.5 m, respectively. The width of the initial bed is 54 m due to a sloped channel bank. The total width of the channel is 350 m (**Figure 2.2**). The total length of the simulation domain is 6,200 m. The channel slope is 1/130. The grid resolution in the lateral direction and longitudinal direction is 3 m and 5 m, respectively.

The centerlines of the low water channel meandering follow sine-generated curves. Three wavelengths, 200 m, 600 m, and 1200 m, are used, whereas the meandering angle is kept to 15°. The sinuosity of the initial low water channel is about 1.02, which is a typical value for the rivers in Japan (Fukuoka et al., 1997). Three wavelengths of the initial low water channel are selected to cover two regimes based on an empirical criterion that determines the mobility of alternate bars through river bend (Whiting and Dietrich, 1993). In Whiting and Dietrich (1993), vegetation is not accounted for. The regimes are shown in **Figure 2.3** by the solid line. The bar migration regime predicted by the approximated relation is read as:

$$\frac{M}{B} = (cos\,\omega\, sin\,\omega)^{-1} + 2 \qquad (3)$$

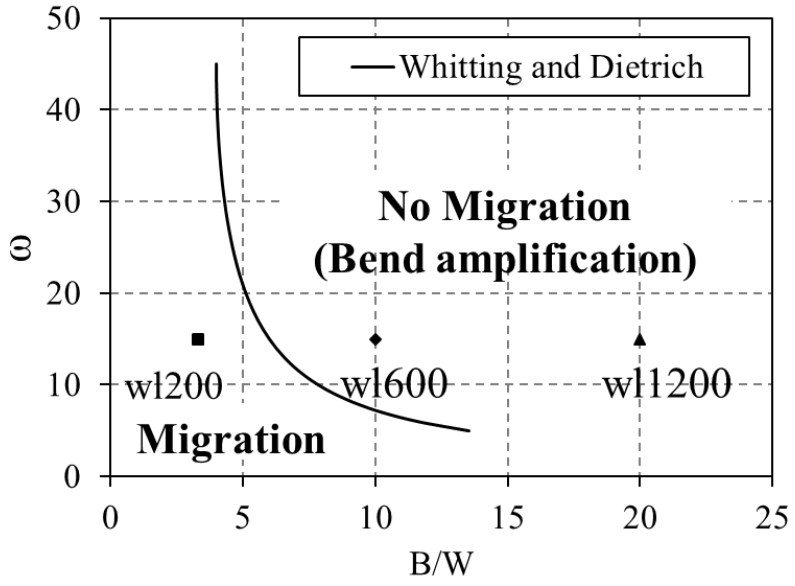

Figure 2.3 The bar migration regime predicted by formula (3).

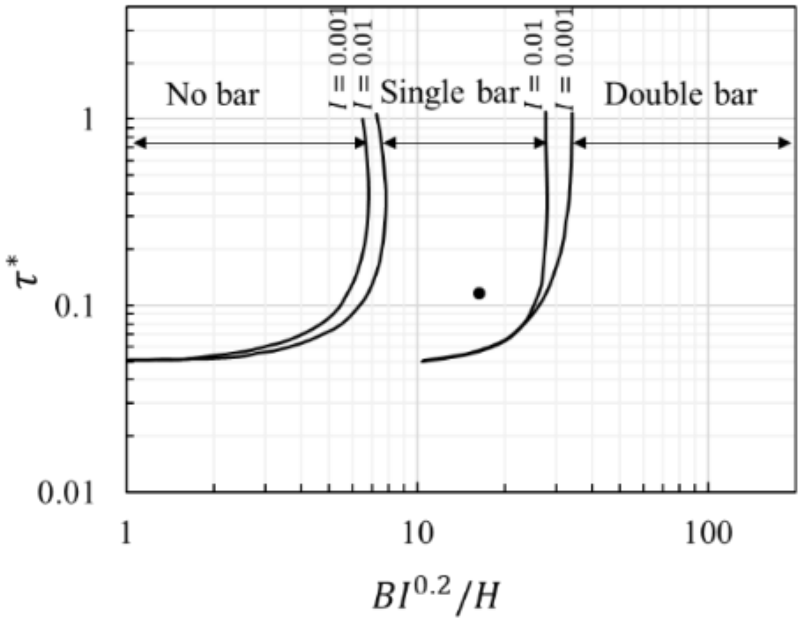

Figure 2.4 River morphology classification (Kuroki and Kishi, 1984). The black circle represents the initial low water channel of wl-200.

where M is the wavelength of the meandering channel, B is the channel width, and ω is the meandering angle. If the left-hand side of formula (3) is smaller than its right-hand side, alternate bars can migrate through the river bend, and meandering is difficult to develop. If the

left-hand side of formula (3) is greater than its right-hand side, the alternate bars do not migrate in the bend, and the bend tends to amplify.

The parameter space is divided into two regimes by the curve predicted by the approximated relation. Above the curve is the no-migration regime, and below the curve is the migration regime. The case wl-200 is located in the migration regime predicted by formula (3). The case wl-600 is located in the no migration regime. The case wl-1200 is also located in the no-migration regime, while experimental results indicated alternate bars could migrate through bends when *M/W* is large.

2.2.3 Simulation conditions

The total simulation time is 122 hours: the first 22 hours are used for vegetation colonization and discharge increase. Hence, the total duration time for the flood is 100 hours. Vegetation grows on dry grids where the water depth is smaller than the criterion that is set to 0.1 m in this study. The representative sediment diameter is set to 55 mm (Iwasaki et al., 2016a). Ashida-Michiue formula is used for bedload flux calculation. Manning's roughness coefficient is 0.028, which is calculated by the Manning-Strickler formula. Fine sediment on the floodplain is neglected in this study for following reasons: 1. The discharge is close to bankfull discharge; thus, fine sediment covering the floodplain has less significant influence on the morphological change; 2. The major morphological change occurs near the interface of floodplain and main channel, where the shear stress is relatively high, so the fine sediment can be easily washed out; 3. The 55 mm grain size has been proved by multiple numerical simulations that can reproduce morphological change in the field in a short time perspective (e.g. one flood event), which also suggests that fine sediment on the floodplain can be ignored. 4. To keep the model simple.

Vegetation density and erosion criterion for the vegetation, which depends on mature willow, are set to 0.1 m^{-1} and 0.5 m, respectively (Iwasaki et al., 2016a). A modification of the original Nays2DH model is made to account for the erosion-induced vegetation destruction: If the

erosion in a vegetated grid is deeper than the erosion criterion, the grid is regarded as a bare grid. The bank height in the Otofuke River is about 1.5 m; therefore, the critical angle of repose is set to 0.56 (Iwasaki et al., 2016a). Input sediment at the inlet is calculated based on the equilibrium condition.

Since this study focuses on the interaction between the initial low water channel and the migration of free alternate bars, the discharge for simulation is designed to form alternate bars in the low water channel. According to the river morphology regime theory (Kuroki and Kishi, 1984), alternate bars will form in the initial low water channel (**Figure 2.4**). Since the sinuosity of the initial low water channels is small, the difference in slope between the three cases is minor, and only one dot is visible in **Figure 2.4**. In the Otofuke River during the 2011 flood event, the bankfull discharge is between 300 and 400 m^3/s, and a larger discharge keeps meandering migration (Yamaguchi and Ito, 2014). Therefore, in this study, the discharge is set to 400 m^3/s to ensure the morphological change occurrence and the formation of the alternate bars.

2.3 Results

2.3.1 River morphology without vegetation

Morphological development with a floodplain without vegetation cover is firstly tested. The results are shown in **Figure 2.5**. The time at the right-upper corner represents the duration time after the discharge has achieved 400 m^3/s.

In the wl-200 case (**Figure 2.5**a), the low water channel becomes straight first, and then alternate bars develop from the upstream after 20 hours. The alternate bars development and river meandering coexist until the 60^{th} hour. After the 60^{th} hour, chute cut-off happens, and the channel soon becomes braiding.

In wl-600 case (**Figure 2.5**b), no migrating alternate bars have been found in the low water channel, while the bends amplify until about the 20^{th} hour. After the 20^{th} hour, chute cut-off occurs and transforms the morphology into braiding.

In the wl-1200 case (**Figure 2.5**c), similar to wl-200 case, alternate bars are generated and are able to migrate through the bend, and the river becomes braided after the occurrence of chute cut-offs after about 40 hours.

The thalwegs in wl-200 and wl-600 before the channel becomes braided through chute-cutoff are depicted in **Figure 2.6**. The averaged amplitude in wl-200 is 161 m and is 167 m in wl-600. Since the determining factor of chute-cutoff is gradient difference between chute channel and main channel (Dijk et al., 2014), the thalwegs are similar in wavelength and amplitude, although the phase of the amplitude differs in the two cases,. The duration needed for the channel becoming braiding is different in wl-200 and wl-600 since in wl-600 the migrating alternate bar does not occur, and the meandering starts to grow earlier.

2.3.2 River morphology development with floodplain vegetation

The morphology developments in rivers with vegetated floodplains with different initial low water channel geometries are depicted in **Figure 2.7**. The river morphological development is clearly different depending on the initial geometry by comparing **Figure 2.7** to **Figure 2.5**. Meandering has developed and kept for a longer duration due to the existence of vegetation on the floodplain.

In the wl-200 case (**Figure 2.7**a), the planform of the initial low water channel has disappeared after 20 hours. Alternate bars are formed after 30 hours, and then the low water channel starts to widen. After 40 hours, the alternate bars along the channel have started to erode the low water channel bank. By comparing the bar location in 40^{th} hours and 60^{th} hours, the alternate bars have stopped migrating, and their amplitude starts to grow. A thalweg with a typical meandering shape has formed. Between 60 hours and 100 hours, the bars keep growing. The development is similar to straight channel, except braiding has not yet started (Yamaguchi and Ito, 2014). The migrating alternate bars before the 20^{th} hour is consistent with the prediction of formula (3).

Similar to case wl-200, the initial meander amplifies in case wl-600 (**Figure 2.7**b). After 20 hours, the concave banks are eroded, and the convex banks start to grow. Alternate bars have not developed in the main channel, and the river bends do not migrate. The alternate bars have been suppressed by the initial predominant channel bend. After 100 hours, the major morphological change is still the growth of the river bends. The river morphology keeps meandering, except several chute-cutoff happen at around 2 km. The morphological development follows the prediction of the formula (3); namely, the results suggest that river bends enable the meandering to develop from this regime, where no alternate bars are generated.

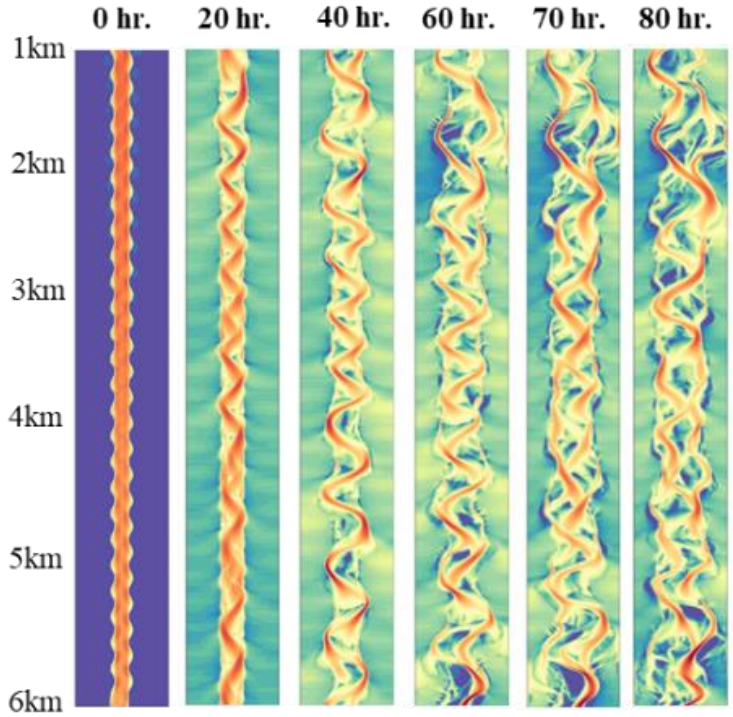

(a) wl-200 without vegetation.

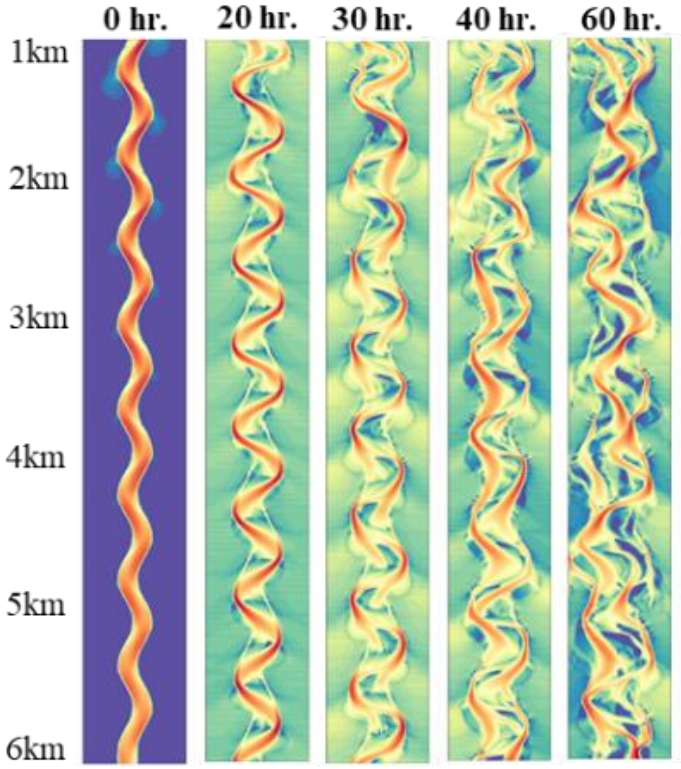

(b) wl-600 without vegetation.

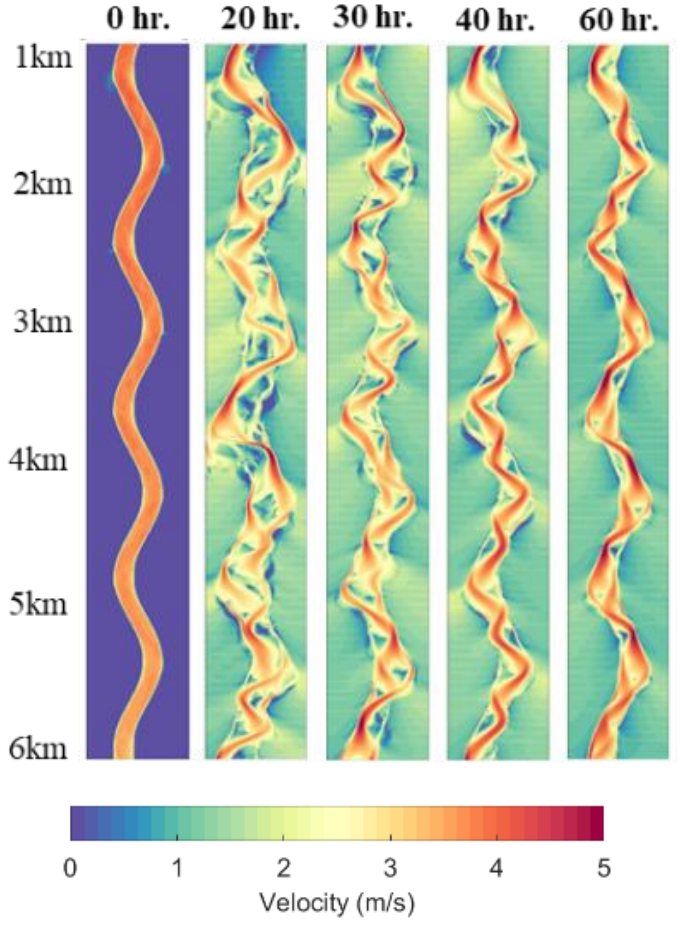

(c) wl-1200 without vegetation.

Figure 2.5 River morphology development without vegetation on the floodplain. Contour shows the velocity magnitude.

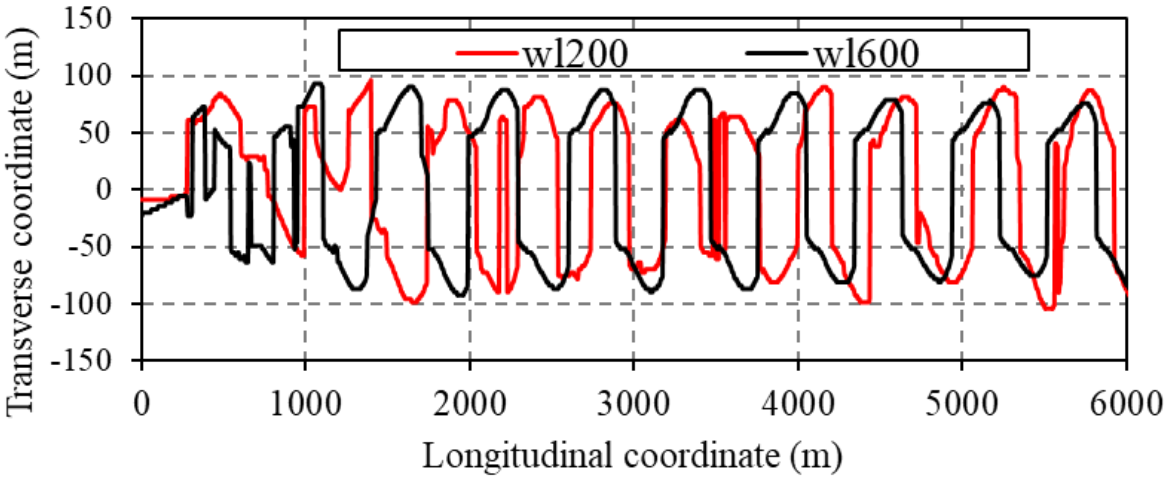

Figure 2.6 Thalwegs in wl-200 and wl-600 before chute-cutoff occurrence.

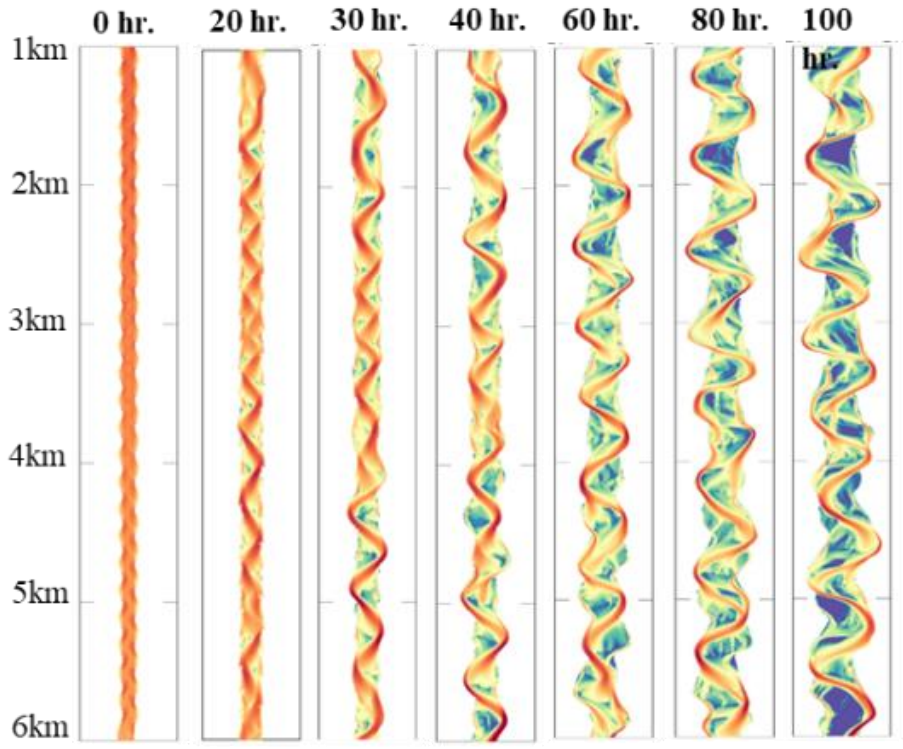

(a) wl-200 with vegetated floodplain.

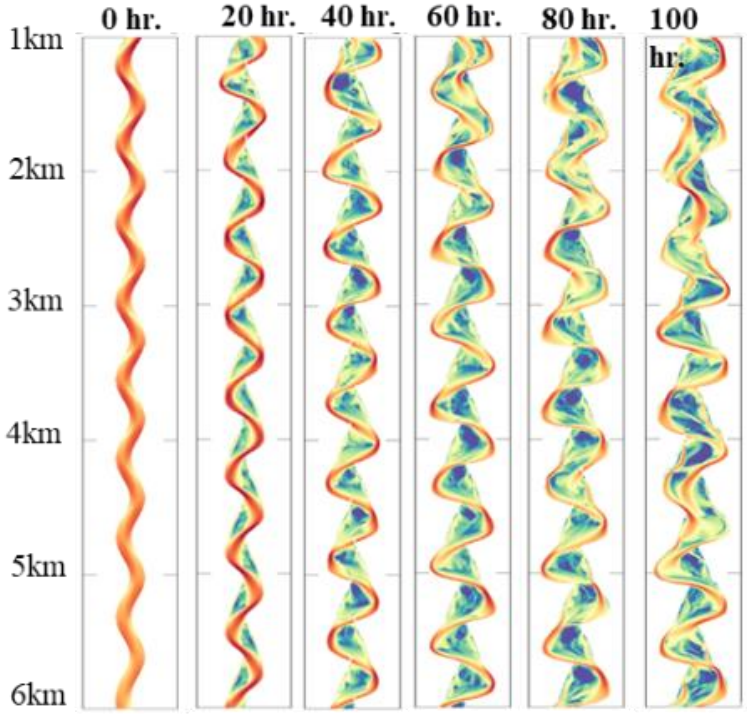

(b) wl-600 with vegetated floodplain.

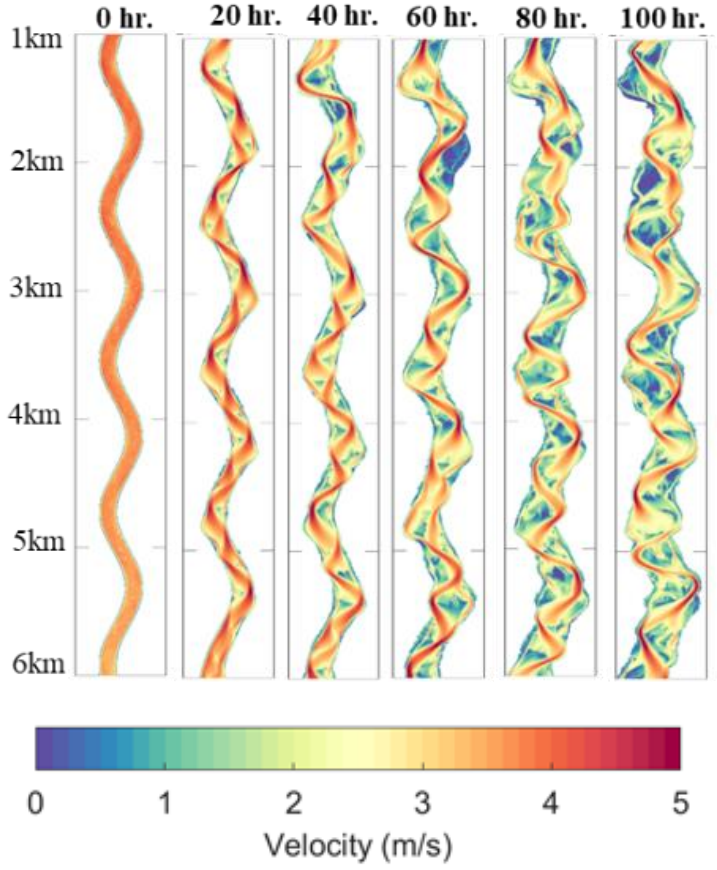

(c) wl-1200 with vegetated floodplain.

Figure 2.7 River morphology development with floodplain vegetation. Contour shows the velocity

magnitude, and white parts represent vegetation cover area.

With a longer wavelength of the initial low water channel in wl-1200, alternate bars occur again in the river bends after 20 hours (**Figure 2.7**c). Alternate bars grow with a longer wavelength, and deflected main flow starts to erode the river bank. Unlike case wl-600, convex banks in the wl-1200 can be eroded either, e.g., at around 2 km and 4 km. Chute-cutoff frequently happens in the channel. After 100 hours, the river morphology is more braided than wl-200 and wl-600. Since migrating alternate bars are observed at the beginning of the simulation, the results are inconsistent with the formula (3), which predicts the bar is unable to migrate through the bend. Similar bar migration has been observed by Whiting and Dietrich (1993) in an experimental flume with a fixed bank.

2.4 Discussions

2.4.1 Comparison with bifurcation instability theory

According to Dijk et al. (2014), when chute-cutoff happens, inlet step differences between the main channel and chute channel decrease, and a plug bar will block the main channel. Elevation development of one chute-cutoff event is shown in **Figure 2.8**. The elevation of the main channel and chute channel are shown in **Figure 2.9**. Before the chute-cutoff, a gradient advantage existed in the chute channel since it has a shorter length. At the inlet of the main channel, the elevation was higher after the chute-cutoff since a plug bar formed at the inlet. The inlet elevation of the chute channel became lower. During the formation of chute-cutoff, the inlet step difference becomes smaller. The development of the chute cutoff is qualitatively consistent with the chute development in field.

After the occurrence of chute channel on the point bar, a bifurcation has formed between the main channel and the chute channel. Thus, the development of the chute-cutoff event should

follow the prediction of bifurcation instability theory. The relation of sediment transport and discharge can be described by the nodal point relation (Wang et al., 1995):

$$\frac{\mathrm{Q_{schute}}}{Q_{smain}} = \frac{Q_{chute}^{k}}{Q_{main}} \frac{W_{chute}^{1-k}}{W_{main}}$$

$\mathrm{Q_s}$ is the sediment transport rate, Q is the discharge and W is the width. For $k<n/3$, where n is determined by the bedload transport formula, the bifurcation will be unstable. Bedload transport is proportional to $\mathrm{v^n}$ (v is the velocity magnitude). Since Ashida-Michiue formula is used in the simulation, *n* is about 3.8 (obtained by fitting the bedload-velocity curve). **Figure 2.10** shows the discharge ratio and sediment transport ratio during the chute-cutoff event. The slope was smaller than the stability criteria predicted by the theory in the right region of the dashed line, which means the chute-channel would be the dominant channel. Thus, the development was consistent with the theoretical prediction. Based on these results, the numerical model of this research can reproduce the chute cutoff qualitatively and quantitatively.

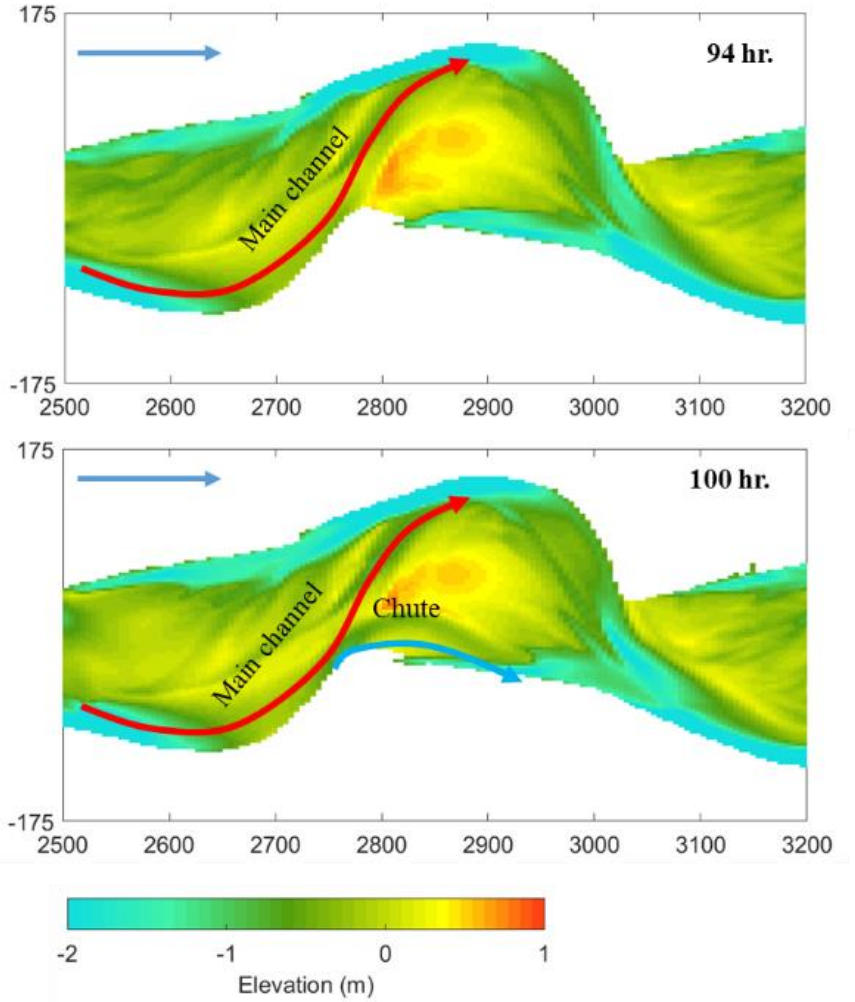

Figure 2.8 One chute-cutoff event in wl-600 with vegetated floodplain.

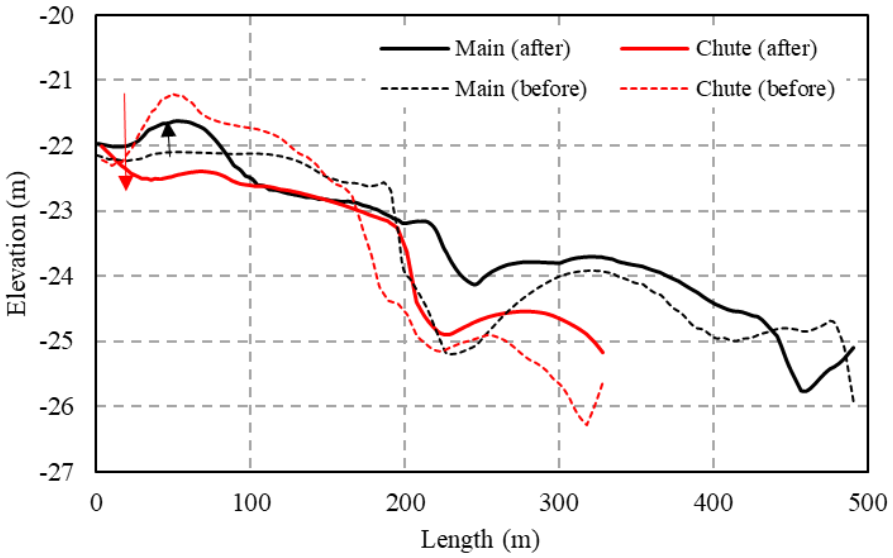

Figure 2.9 Elevation of main channel and chute channel before and after the chute cutoff event.

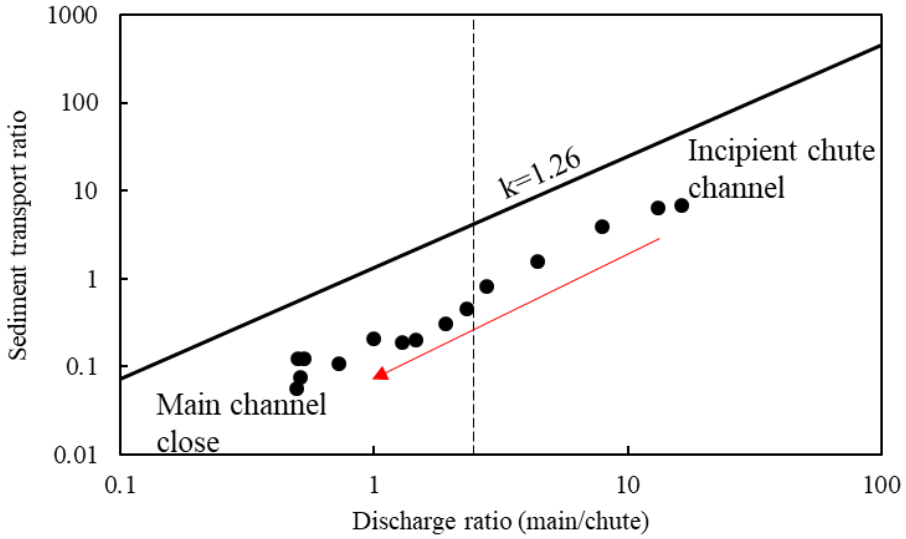

Figure 2.10 Discharge ration and sediment transport ratio during the chute cutoff event. Black line is the stability criteria of bifurcation predicted by theory.

2.4.2 Vegetation effect in alternate bar growth

Figure 2.11 compares the distribution of water depth and bedload transport in a typical meander in wl-200 with (upper) and without vegetation (lower). The area where the water depth is less than 0.5 m, corresponding to the floodplain, is represented by the white in the figure. Without vegetation cover, active bedload flux is observed around the bank (black box in **Figure 2.11**a). Due to sediment entrainment, the outer bank migrates to the downstream (red line in **Figure 2.11**a), and leads to the bar tail limb elongation and channel widening (solid red line in **Figure 2.11**a). With vegetation cover (**Figure 2.11**b), the sediment entrainment from the bank reduces because the effective bed shear stress near the bank is reduced (black box with a solid line in **Figure 2.11**b); thus, the outer bank hardly moves downstream. With a limited downstream migration, the location with the highest Shields number moves to upstream gradually, and the location keeps in phase with the bend apex (**Figure 2.12** and the orange triangles in **Figure 2.11**). Therefore, the outer bank migration is restricted in the lateral direction, and the bend gradually becomes tighter. The tighter bend increases the angle between the

incoming flow and the potential chute channel on the bar (**Figure 2.11**, black arrows), which makes the chute-cutoff difficult to occur.

Vegetation on the point bar was found to delay chute-cutoff in previous research by reducing shear stress within the vegetation patch (Iwasaki et al., 2016a), and bar-floodplain conversion by vegetation establishment is necessary for modeling meandering (Weisscher et al., 2019). In this study, vegetation does not grow on the newly deposited bars, but the sinuosity of the developed meandering channel is about 1.52, which was close to the sinuosity of real meandered gravel bed river (Braudrick et al., 2009). Bank erosion is enhanced by uniform vegetation cover, which is consistent with the results in a braided river (Kyuka and Yamaguchi, 2018). The results show that vegetation can still play an important role in triggering the meandering in a gravel bed river without vegetation recruitment on point bars.

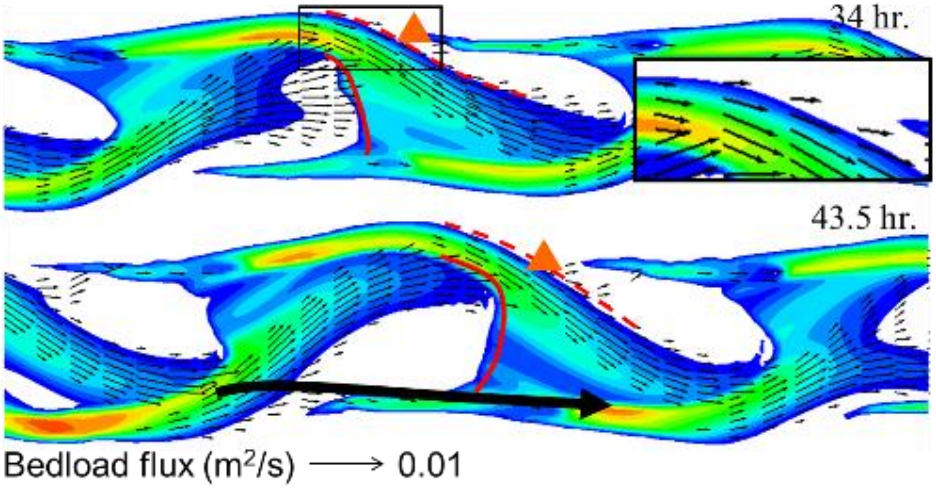

(a) Floodplain without vegetation cover.

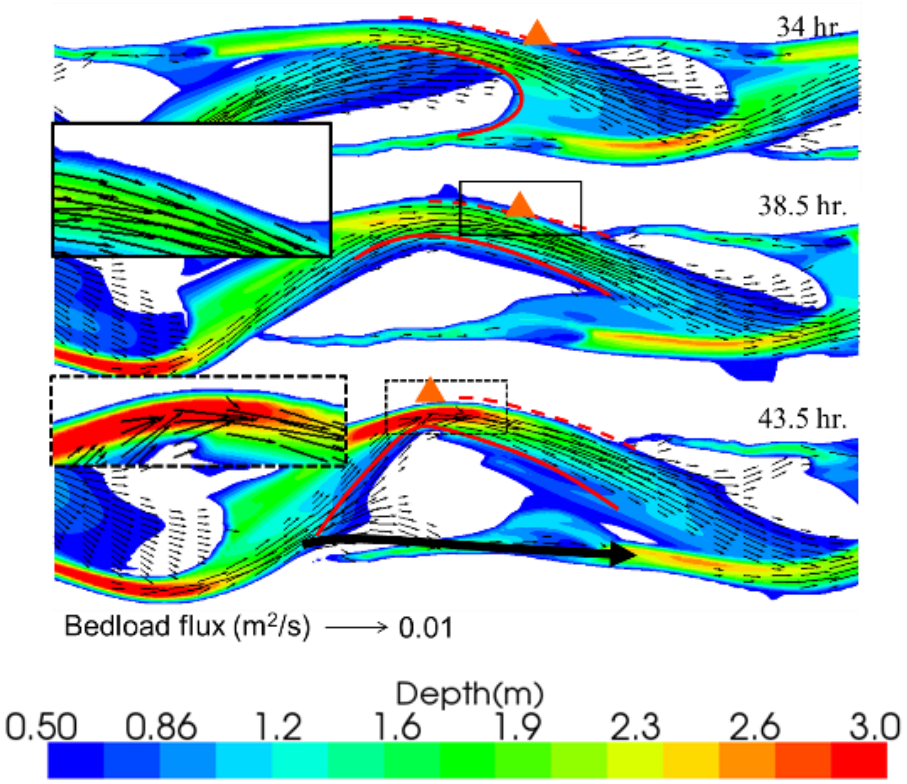

(b) Floodplain with vegetation cover.

Figure 2.11 Water depth and bedload transport in a typical meander in wl-200.

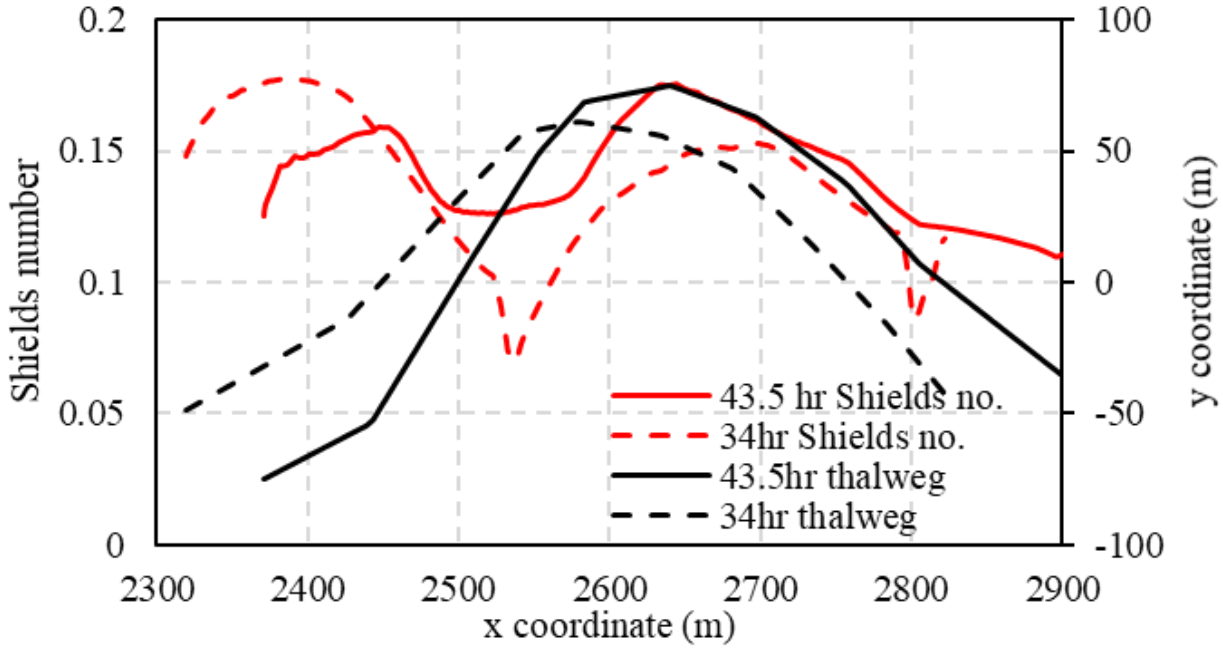

Figure 2.12 Thalweg and Shields number in wl-200 case with floodplain vegetation.

2.4.3 Meandering development from the initial low water channel

The results of morphological development in vegetated cases show two types of meandering development. The first type (found in case wl-200) is meandering development from alternate bars. Alternate bars firstly develop in the low water channel, and the bank eroded by the alternate bars induces and amplifies meandering. The second type (found in case wl-600) is the meandering developed from channel bend. The initial channel bend suppresses the formation of alternate bars, and curvature flow in the bend amplifies the meandering. The meandering in wl-200 is developed by the resonance between alternate bars and bank curvature (Seminara and Tubino, 1989).

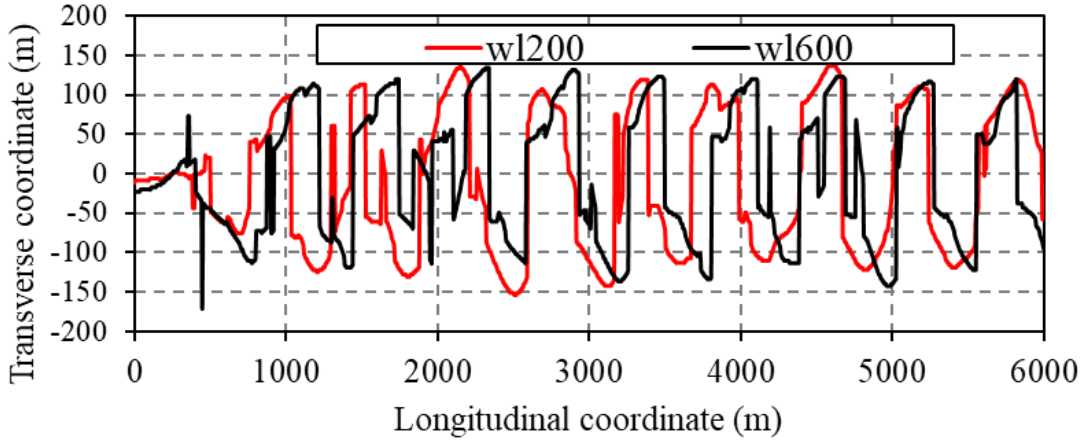

Figure 2.13 Thalwegs at the 100th hour in wl-200 and wl-600 with floodplain vegetation.

Figure 2.13 depicts the thalwegs, determined by the lowest elevation of each section, in wl-200 and wl-600 at 100 hours. Although the phases of the meandering are different between the two cases, the wavelength and meandering amplitude are similar between wl-600 and wl-200. The results imply that with different meandering development types, the developed meandering geometry is similar.

2.5 Conclusions

A numerical experiment is performed to investigate the influence of uniformly distributed floodplain vegetation and low water channel planform on meandering development. Three initial low water channels are prepared, and vegetated and bare floodplains are compared. Initial channel morphology affects the duration before braiding occurrence without floodplain vegetation. Low water channel planform can influence the transitional process for a relatively short period without floodplain vegetation cover. With vegetation coverage on floodplain, the bank erosion is enhanced in the outer bank of point bars, and meandering with sinuosity close to gravel rivers in the field can develop from both initial channels in the migration regime and no-migration regime. It is concluded that vegetation recruitment on bare bars is not a necessary condition for meandering initiation in vegetated gravel rivers, and vegetated floodplain combined with a suitable initial channel is one sufficient condition. The bar growth is restricted to the lateral direction because its downstream migration is limited by vegetation, and the phase lag between the bend apex and high shear zone becomes small. The results demonstrate that vegetation on floodplain plays a more important role than the initial low water channel planform.

3 Morphological response of bifurcated channel with reopened and narrowed side channel inlets to artificial flush flood

3.1 Introduction

As the results shown in the Chapter 2, vegetation on the floodplain may induce significant bank erosion during short-term flood impact. To reduce such risk, artificial modification of the initial planform is performed in some rivers in Japan. Such modifications do not only aim to reduce the bank failure possibilities but also have ecological objectives. The multiple targets of artificial modification to the river planform require the measure to reduce bank failure risks and activate morphological change at the same time.

The Satsunai River is a tributary of the Tokachi River in Hokkaido, Japan. Due to a decreased annual peak discharges, the river morphology has become relatively stable, and the flood plain has been covered with stable vegetation. However, riparian vegetation species *Salix arbutifolia* has reduced its habitat because this species prefers bare gravel bars but the bars in the river has covered by other vegetation adapted to a more stable environment. To destabilize the bed form of Satsunai River for keeping the area of bare gravel bars, the river morphology manipulation including the reopening of closed side channels on vegetated floodplain had been implemented. Such measures, i.e., artificially modifying the initial river morphology, have been found effective in reactivating the river bed while reducing the risk of embankment failure (Sumitomo et al., 2016). A side channel was reopened its inlet in Feb. 2019 is depicted by the purple line in **Figure 3.1** and focused in this study.

River flow has bifurcated after the reopening of the side channel (**Figure 3.1**). The bifurcation may have the potential to be closed again during floods(Bolla Pittaluga et al., 2003; Kleinhans

et al., 2013). The morphological change of the side channel may influence its efficiency in the destabilization of the river morphology. The morphological change around the bifurcation depends on the budget of sediment transported into and outgo from the bifurcation (Wang et al., 1995). However, the quantitative prediction of the morphological change around the bifurcation from a long-term perspective is a challenging task, and factors influence the morphological evolution are still unclear.

To predict and evaluate the effects of the side channel reopening, the numerical simulation would be an effective approach. However, the accuracy of the numerical simulation depends on several factors and the predictive ability of numerical simulation for such a complicated process is not well understood. The uniform grain size assumption has been widely used in engineering and research and this study also uses this assumption. Another reason for using a uniform grain size model is that grain size distribution is quite inhomogeneous in both horizontal and vertical directions in the field, and the number of data points of grain size distribution measurement was insufficient to prepare the simulation grid covering the domain.

In June 2019, a flushing flood was discharged at Satsunai River. The flood provided a precious opportunity to verify the simulation model and observe the evolution of the reopened side channel. In this paper, the applicability of numerical simulation with uniform sediment assumption in predicting the river morphological change is discussed, and then a measure is proposed to improve the performance of the reopened side channel in destabilizing the river morphology by narrowing the inlet of another side channel around the bifurcation. With careful design of the measure to change the initial planform, the short-term response of river morphology can be modified to meet the requirements on reducing embankment failure risks and creating habitat for certain vegetation species.

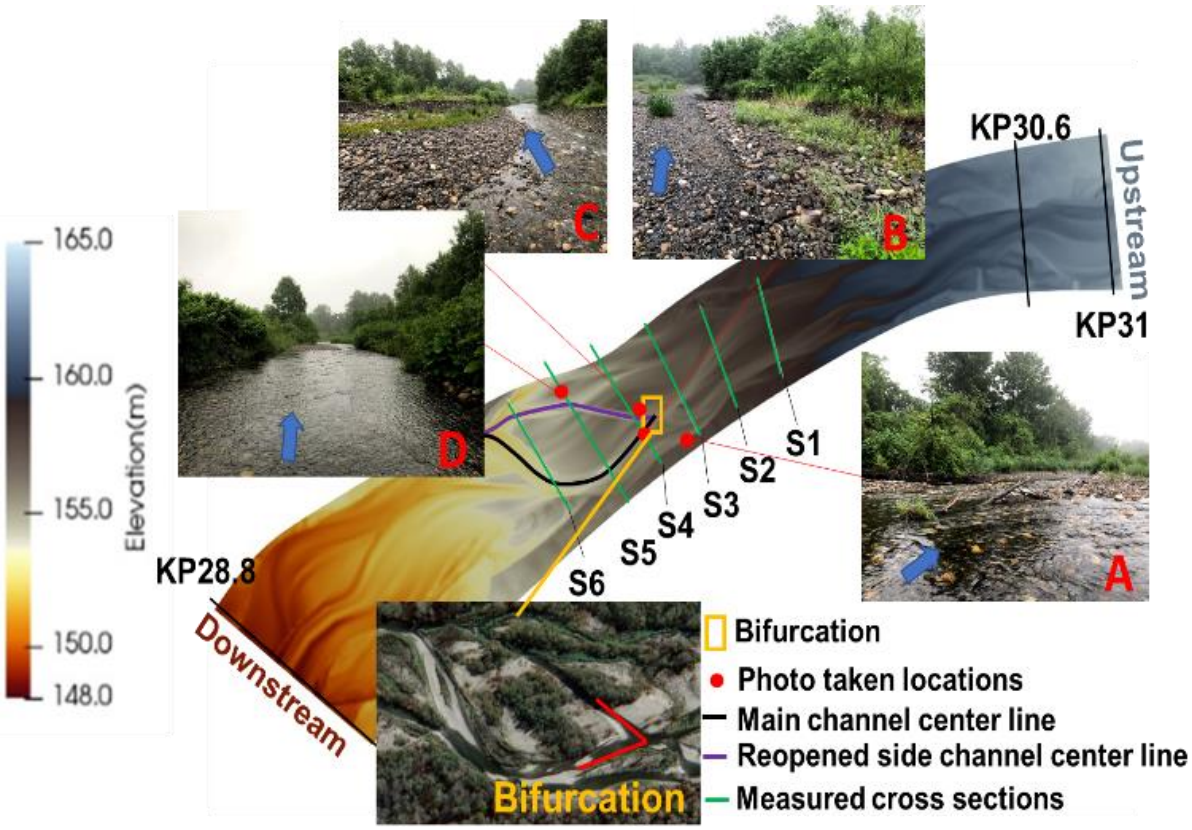

Figure 3.1 Simulation domain and photos of the field.

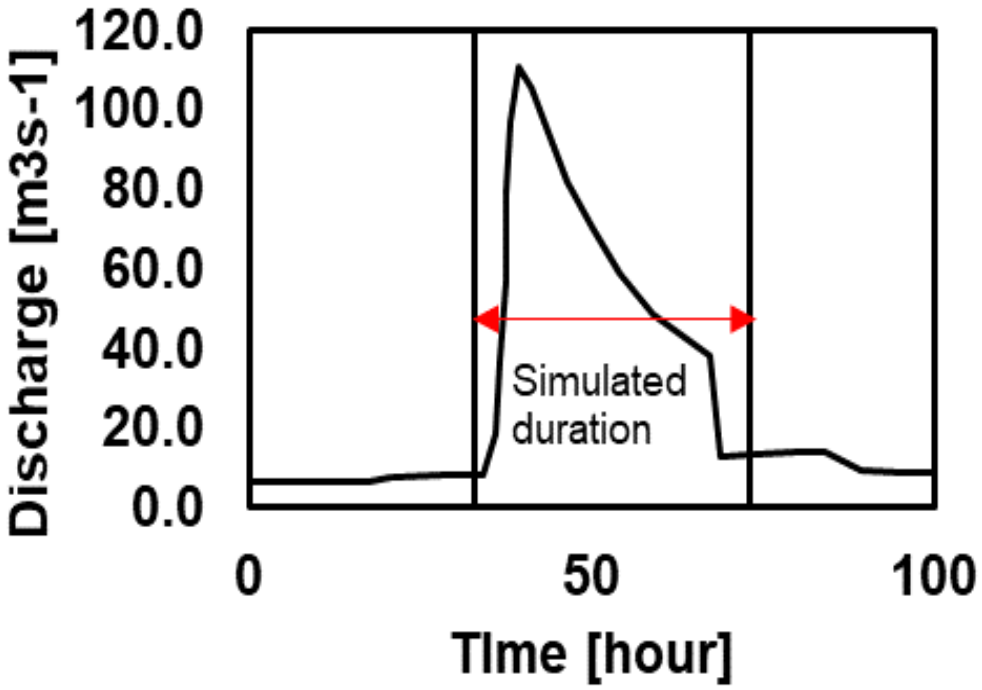

Figure 3.2 Hydrograph of flushing flood in June, 2019.

3.2 Simulation

The simulation was performed by the iRIC Nays2DH model (Shimizu et al., 2020). **Figure 3.2** shows the hydrograph of the flushing flood which was based on the record at the dam and there was no major tributary among the dam and the site. The maximum discharge was around 110 m^3/s. The flood lasted for 35 hours. The river morphology did not change during the low discharge, hence in the simulation, only the flood duration had represented aiming to reduce the simulation time. The initial topography was obtained from DEM data with a resolution of 2.5 m x 2.5 m. The simulation domain is as shown in **Figure 3.1**, which is between KP31.0 and KP28.8 from the confluence with the Tokachi River. The result of a case whose grid size was equal to 1.2 m x 1.2 m showed a minor difference with a case whose grid size equal to 2.5 m x 2.5 m, and the erosion and deposition pattern were the same (**Figure 3.3**). Thus, the 2.5 m x 2.5 m grid was used. Because the floodplain was hardly submerged during the flushing flood, the domain does not cover whole the river width to increase the computational efficiency with keeping the grid density in the channel. The total grids number was 112941, with 801 grids in the stream-wise direction and 141 grids in the transverse direction.

In the field survey, the sediment diameter D_{60} as a representative diameter had increased after the 2019 flushing flood. Between KP31 and S1 sections, the D_{60} was 77.5 mm after the flushing flood. Between S1 and S6, the sediment diameter D_{60} was from 62.5 mm to 68.5 mm after the flushing flood.

In the simulation, a uniform grain model is used and single grain size can be specified in the simulation. The uniform grain size of 35 mm, 53.5 mm, 60 mm and 73.5 mm had been tested and the run with 73.5 mm diameter provided the bedform after the 2019 flushing flood corresponded well to the field data and this grain size had been used for the following analysis.

Ashida-Michiue formula was chosen to calculate the bedload rate. Manning's roughness coefficient was set as 0.027 based on the Manning-Strickler equation. The morphological factor

was used to speed up the simulation: in one time-step, the morphological change was multiplied by the factor thus the total simulation time can be divided by the factor. In the simulation, the morphological factor was set to 2 thus the time of the original hydrograph was divided by the factor. The results were same with the morphological factor equal to 1, and larger value induced some differences. The equilibrium sediment transport rate was used at the inlet. The tangent value of the repose angle of bank collapse was increased from the default value 0.3 to 0.7 since significant bank collapse in the field was not observed in the field. The time step was set to 0.12 s to keep the simulation stable.

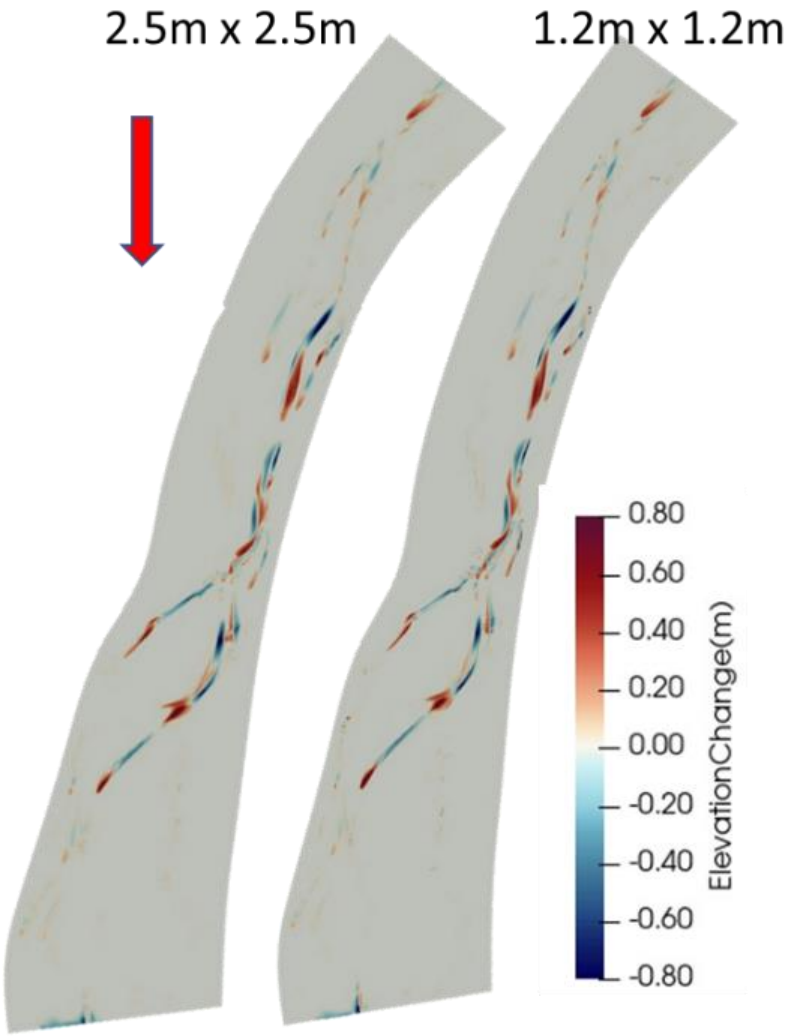

Figure 3.3 Comparison of elevation change between current grid and a finer grid.

3.3 Reproducibility of water surface elevation

The water surface is compared with field data to verify the simulation results. Since the data in the field is extremely limited, only water surface at the reopened channel at section S6 is compared. The water surface at peak discharge is shown in the **Figure 3.4**. The simulated result (blue line) has a relatively good agreement with the field data (green line) at the reopened side channel. In the main channel, the water surface elevation is inclined due to the centrifugal force.

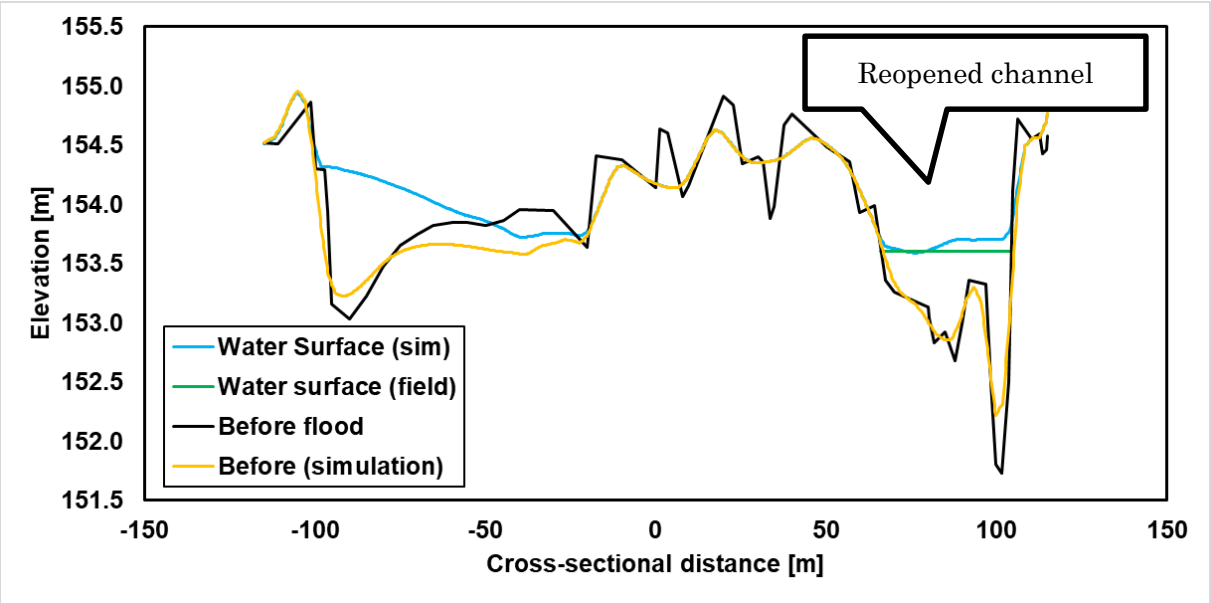

Figure 3.4 Water surface elevation and bed elevation at S6 section.

3.4 Predicting the morphological change around the bifurcation

Before and after the 2019 flushing flood, river cross-sectional profiles were measured by the river office. In addition, on June 22, 2020, the elevation of the centerline of the secondary channel was measured by RTK-GPS. Because no large flood happened after the flushing flood in 2019, the bed profiles measured on June 22, 2020 was considered to represent the topography after the flushing flood in 2019. The location of representative river sections surveyed is shown with the green lines in **Figure 3.1**.

Except measurement of the elevation, velocity in the reopened side channel was also measured by an image-based stream surface observation system. To obtain the discharge in the channel, the water depth was measure by a pressure sensor.

The results of simulated and surveyed cross-sectional change are compared in **Figure 3.5** and discussed below.

3.4.1 At the vicinity of the bifurcation

In section S2, deposition occurred in the channel (the purple ellipse in **Figure 3.5**a). In the simulation, the deposition can be observed although the amount of the deposited sediment is less, which can be attributed to the uniform grain size assumption used in the simulation. Since the sediment diameter is larger than the field (43.5 mm before the flood, and 63.5 mm after the flood), less amount of sediment could be transported (the purple ellipse in Fig. **Figure 3.5**b). In section S3, the deposition in the red box is presented by simulation but an erosion in the yellow rectangle is not represented.

3.4.2 In the main channel

The morphological change at the main channel is not simulated correctly. In the field measurement (**Figure 3.5**a), sediment deposited in the main channel at this cross-section S4 (the green filled-circle), and a middle bar (indicated with the green arrow in **Figure 3.5**) between the reopened side channel and the main channel was eroded. In the simulation, the river bed and the middle bar does not change during the flushing flood in the main channel at section S4 (the green filled-circle in **Figure 3.5**b). The difference in sediment diameter between the field and the simulation can be considered as the reason for the deposition in the main channel, and a lack of bank erosion model can be ascribed to the less erosion of the middle bar. In the field, sediment diameter was about 42.5 mm before the flushing flood, while in the simulation sediment diameter was 73.5 mm. Larger sediment in the simulation could hardly be transported in the main channel.

The location indicated with the black rectangle (**Figure 3.5**) is the left-hand side channel (which will be discussed later in Section 4), and the side channel was eroded in the field.

In section S5, bank erosion and deposition in the main channel (the red ellipses in **Figure 3.5**) can be observed in the field measurement, while in the simulation, bank erosion is at opposite side although deposition occurred at the same location. Overestimated erosion at the right bank of the main channel (indicated with the blue filled-circle) can be observed in the simulation, however, the armor effect may have happened in the field, and the large surface sediment prevented the bed from erosion.

In section S6, main channel erosion is observed in both field survey and simulation. The erosion is considered to be induced by the flow curvature (see the intersection of the black line showing the main channel and the S6 cross-section in **Figure 3.1**).

3.4.3 In the reopened side channel

In section S4, the erosion at the reopened side channel (indicated with the green triangle in **Figure 3.5**b) is overestimated in the simulation. At section S5 (**Figure 3.5**), a similar height of deposition can be observed in both simulation and field data (the blue triangles). In section S6, the erosion is not observed in the simulation, the possible reason is that in the field the morphological change is disturbed by a groin.

Longitudinal profiles of the side channel along the centerline are depicted in **Figure 3.6**. Ridge-trough sequences are observed in the field (the sky-blue and purple lines) and in the simulation (the green line). The depth of trough 1 in the simulation is similar to the trough 1 in the field survey. The D_{60} of trough 1 in the field is 90 mm which is larger compared with the D_{60} of the neighboring places including ridges 1 and 2, this implies the armoring effect prevented the erosion of the trough 1 in the field, while in the simulation the depth is limited. The stable topography around ridge 1 and the depth of trough 1 are well represented in the simulation, this

suggests the result can be applied to predict the discharge division since the discharge is mainly controlled by the morphology at the inlet.

The topography changes of simulated and measured profiles between 70 m to 120 m from the inlet do not correspond well (**Figure 3.6**). The trough 2 is observed in 130 m at the field data but the second trough is represented at 80 m in the simulation. Erosion occurs in the simulation while deposition in the field. The direct reason for the erosion can be ascribed to the overestimated sediment washout during the rising phase of the flushing flood, and the erosion is difficult to be backfilled during the falling phase.

The velocity and water depth estimated from the field survey are depicted in **Figure 3.7**. The discharge is about 17.2 m^3/s at the peak of the flushing flood. The discharge calculated from the numerical model in the reopened side channel is about 30 m^3/s at the peak. By comparing the discharge obtained by the field survey and numerical simulation, it can be concluded that the discharge is overestimated in the side channel. The exact reason for the overestimated discharge is not clear yet, but it is possibly attributed to the vegetation cover. The vegetation within the channel is not accounted for in the simulation; thus, the discharge distribution in the braiding network changes which may result in a larger portion of discharge that enters the side channel.

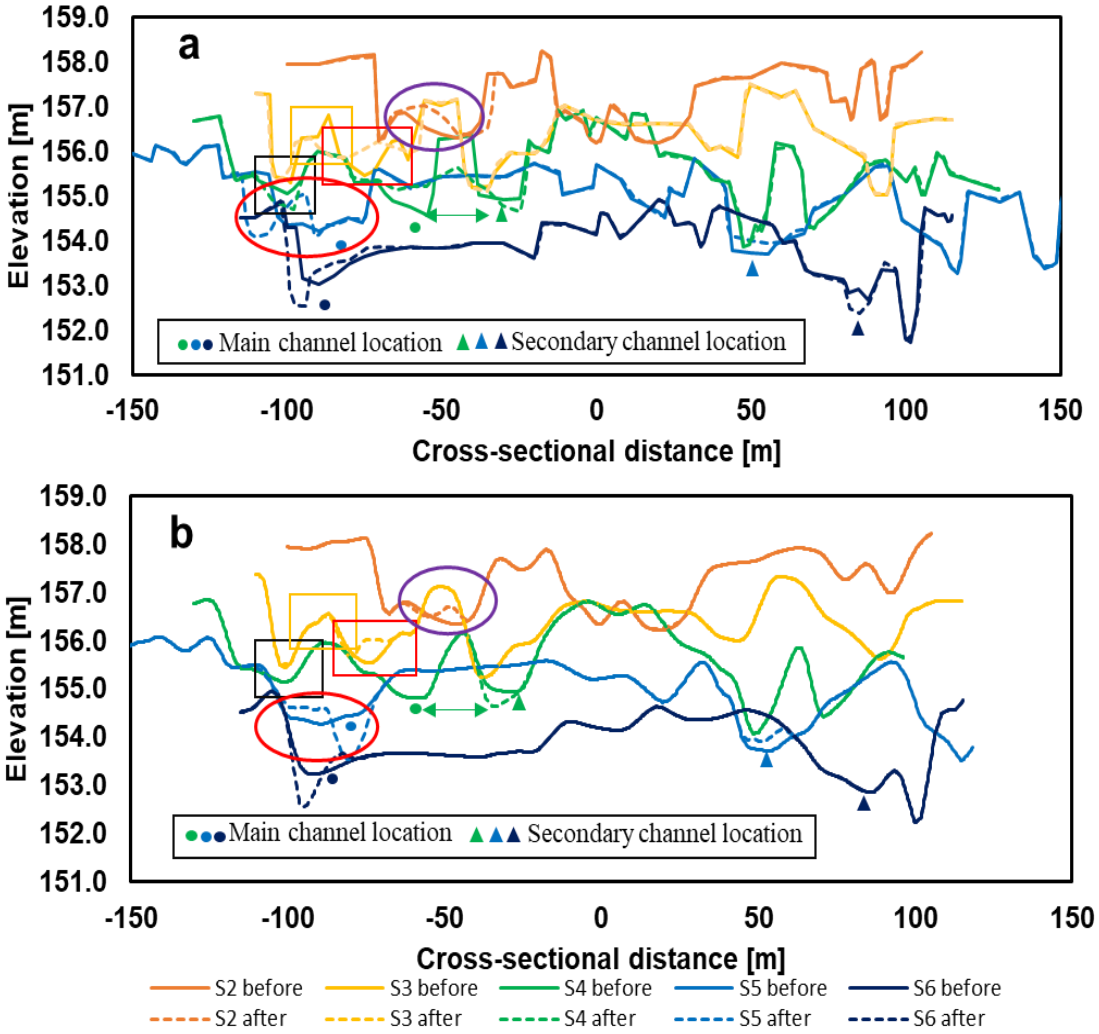

Figure 3.5 Cross-sectional profiles of sections S2 to S6 of (a) field measurement and (b) simulation.

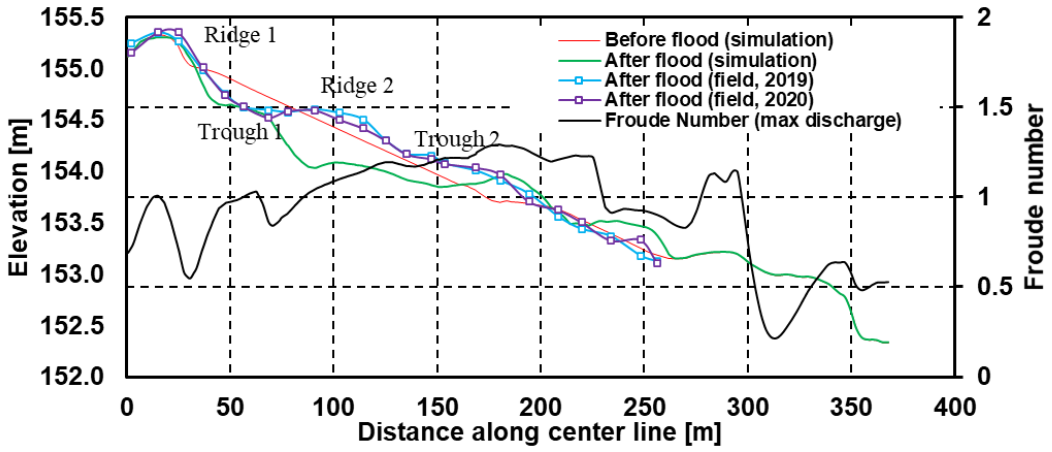

Figure 3.6 Bed elevation and Froude number along the reopened side channel. The start point of centerline was the cross point of the centerline of main channel and the reopened side channel.

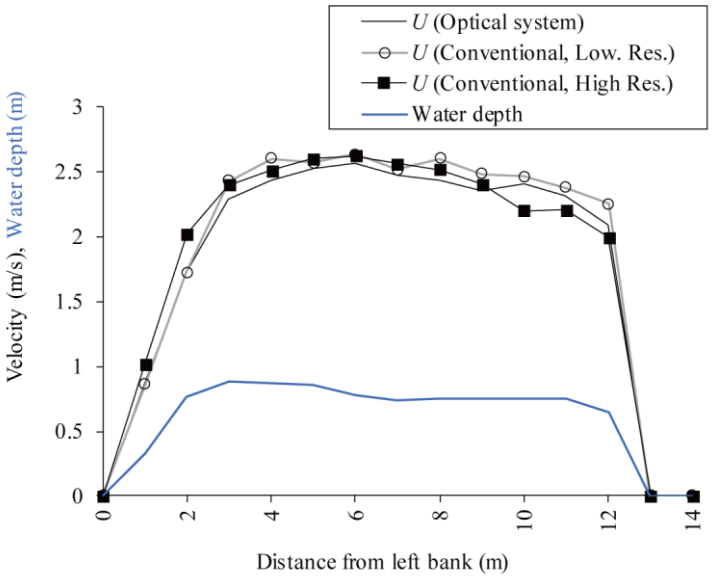

Figure 3.7 Mean water surface velocity and water depth measured by pressure sensor and an image-based stream surface observation system. Different makers of black lines show the velocity estimated by different method.

3.5 Morphological change and discharge division after narrowing the inlet of left-hand side channel

The targets of the reopened side channel include to mitigating the main channel meandering to the river embankments and to create the bare gravel bed (Sumitomo et al., 2018)s. To prevent the bank failure due to the main channel meandering, flow rate diversion to the reopened side channel is essential, and to increase the area of bare gravel bars requires active morphological change. After the flushing flood on June 24, 2020, the elevation of the centerline of the artificial channel is measured, and the change is quite limited (less than 0.1 m). The less flow capacity in the reopened side channel may bring limited morphological change during frequent small floods. To increase the efficiency of the reopened secondary channel to achieve its targets, it is important to increase the discharge flowing into the reopened side channel.

As illustrated in **Figure 3.8,** at the vicinity of the X node which is just located at the upstream of the bifurcation, a side channel (hereinafter referred to as left-hand side channel to distinguish from the reopened side channel) has reduced discharge entering the bifurcation. The water entered the left-hand side channel finally flows into the main channel (the yellow line) of the bifurcation. Thus, the discharge in the reopened side channel (the purple line) is reduced, and the discharge in the main channel increases relatively, which possibly leads to an increase in the risk of embankment erosion in the main channel due to the flow curvature.

Aiming to reduce the discharge entering the left-hand side channel, the following method is proposed: depositing sediment at the entrance of the left-hand side channel where is shown in the red rectangle of **Figure 3.8** to elevate its height to form an artificial mound and narrow its inlet. The elevation is elevated from 0.4 m to 1 m around the area to represent the mound. The discharges entering two channels diverted from the bifurcation are shown in **Figure 3.10** (the main channel is indicated by the yellow line in **Figure 3.8** and **Figure 3.9**, and the reopened side channel is indicated by the purple line in **Figure 3.8**). Without the artificial mound, the maximum total discharge entering the bifurcation during the flushing flood was 90 m^3/s, while with the artificial mound the maximum total discharge entering the bifurcation increased to 95 m^3/s. Because the maximum discharge is 110 m^3/s during the flushing flood, there is still space to increase the discharge entering the bifurcation. Compared to the discharge entering the reopened side channel, the change of discharge in the main channel changes relatively small. The discharge in the reopened side channel (dashed-lines in **Figure 3.10**) doubles at the end of the falling phase, and its value is larger than which in the main channel thus, an alternative mainstream change happens which is supposed to be effective in reactivating the morphological change (Hasegawa et al., 2003; Sumitomo et al., 2016). However, the alternative mainstream change is not observed without the artificial mound: the main channel always had a higher discharge.

The cross-sectional profiles at S4, S5 and S6 cross-sections with and without the artificial mound are as shown in **Figure 3.11**, respectively. In section S4, the reopened side secondary channel is eroded and deposition can be seen in the main channel. In section S5, the erosion of the main channel (indicated with the green filled-circle) is reduced. However, in the reopened side channel (the green triangle), the same deposition is still observed. This deposition occurrs due to the locally expanded width of the reopened side channel. In section S6, the erosion at the outer side of the bend of the main channel (the blue filled-circle) is slightly mitigated after the installation of the artificial mound. Because the eroded sediment from the main channel is transported downstream (depicted in **Figure 3.9**) where the reduced erosion is beneficial for the opening of downstream channels (the green line in **Figure 3.8** and **3.8**).

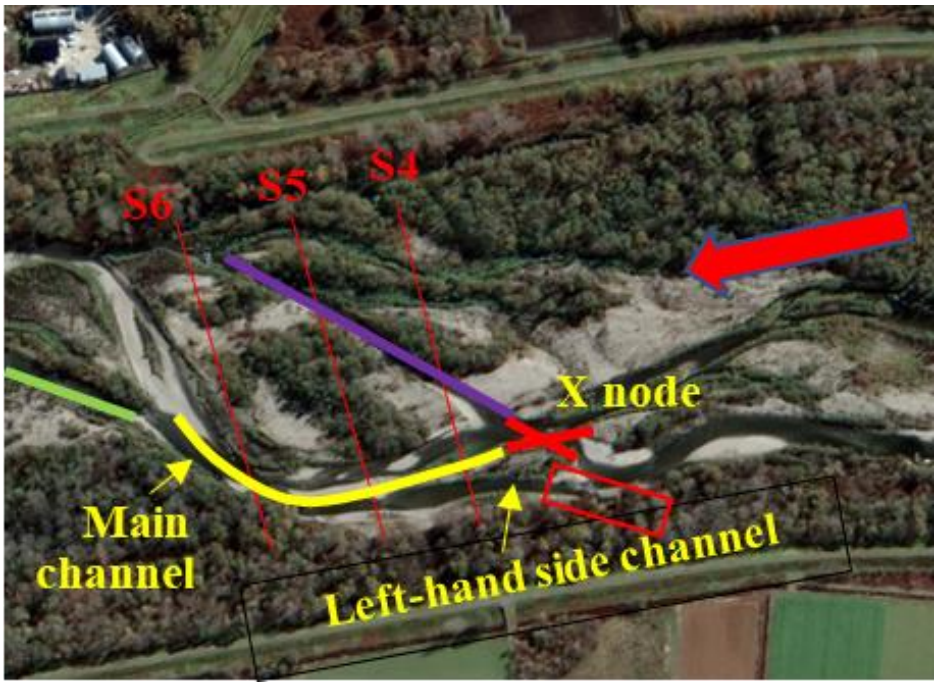

Figure 3.8 Aerial photo taken at Oct 28, 2019 around the bifurcation.

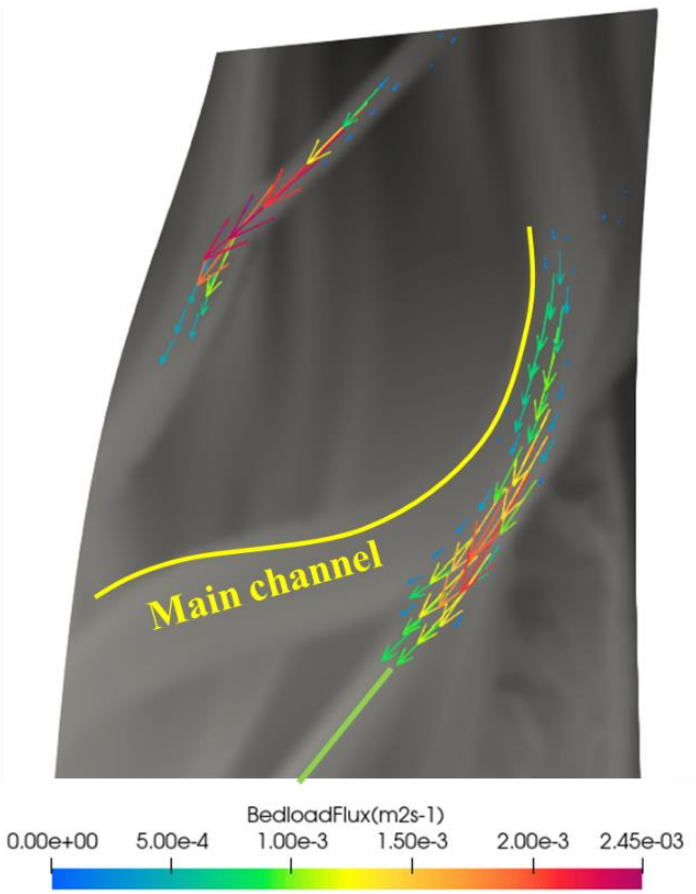

Figure 3.9 Bedload vector at the main channel and reopened side channel.

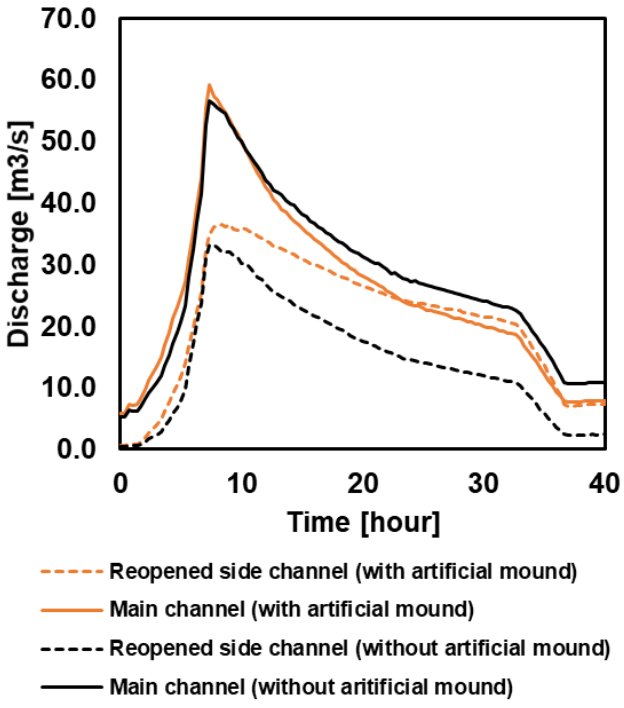

Figure 3.10 Discharge in the main channel and the reopened side channel.

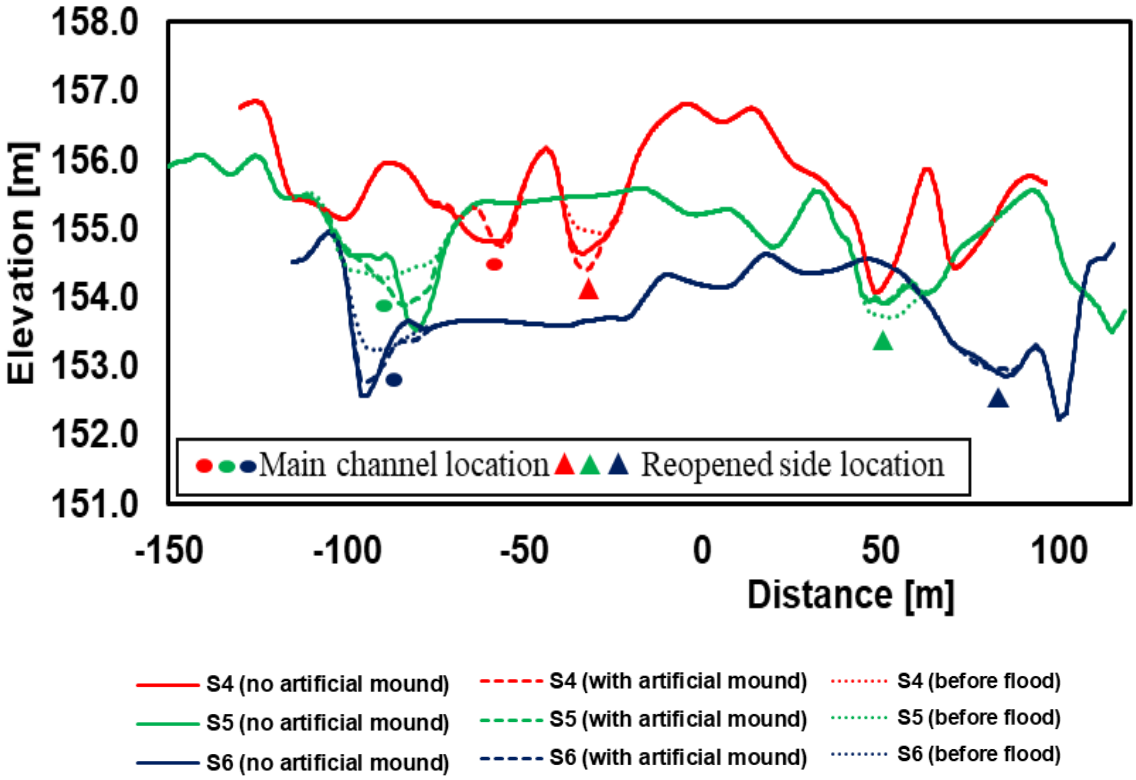

Figure 3.11 Profile at S4, S5 and S6 sections with and without artificial mound.

3.6 Conclusions

In this paper, numerical simulation is conducted for predicting the short-term morphological change around the bifurcation introduced by the reopening of the side channel to discuss how to activate the morphological change caused by the flushing flow. The simulated results have been compared with the field survey data and reasonable agreement has been confirmed in the morphological changes around the bifurcation. However, the morphological change at the reopened side channel is not reproduced well. The limited accuracy in the reopened side channel may be attributed to the overestimated discharge. The results imply the difficulties in reproducing the discharge distribution in a braiding river.

Based on field survey data, the reopened side channel is almost stable in the channel form after the flushing floods. By elevating the inlet of the left-hand side channel around the X node to form a mound and narrow the inlet, the discharge at the bifurcation can be increased and benefits the reopened side channel morphological change. Also, by reducing the discharge in the

main channel, the erosion and the risk of embankment failure are reduced. With the narrowed inlet of left-hand side channel, the alternative mainstream change is observed which is supposed to benefit the morphological change. The effects of the channel narrowing or closing suggest that not only the geometry of the reopened side channel should be carefully designed, but also the morphology around the bifurcation should be modified to increase the efficiency of the reopened side channel.

4 Effects of vegetation distribution along river transects on topographic characteristics in a braided river with gravel bed

4.1 Introduction

The interaction between hydrology, sediment transport, and vegetation creates diverse river morphology and landform (Millar, 2000; Tsujimoto, 1999). The role of vegetation is ineligible (Gurnell, 2014). Riparian vegetation decreases flow velocity within vegetation patch and can promote sediment deposition (Kim et al., 2015; Tsujimoto, 1999; Zong and Nepf, 2011). Vegetation patch in river also deflect water flow; thus, it also has far-field effect (Bywater-Reyes et al., 2018). Recent laboratory experiment has shown the effect of vegetation on single thread channel (Kyuka et al., 2021). By establishing stable floodplain, vegetation has the potential to transform a braided river into a single thread river(Gran and Paola, 2001; Tal and Paola, 2007).

Vegetation could colonize stabilized river bed if the water stage enables its growth (Mahoney and Rood, 1998). The spatial vegetation distribution depends on vegetation species, hydrological conditions and climate conditions (Camporeale and Ridolfi, 2006; Gurnell, 2014; Vargas-Luna et al., 2019). The discharge variability induced water flow disturbance and the water availability are important restriction factors that affect the transect distribution of vegetation (Camporeale and Ridolfi, 2006). Distribution along a river transect frequently has a peaked shape and the habitat extension depends on vegetation species (Johnson et al., 1995; Lytle and Merritt, 2004). The distribution of vegetation along the transect direction also results from the vegetation seed distribution method (Van Dijk et al., 2013). Artificial impact, e.g., dam construction, could also lead to the spatial change of vegetation (van Oorschot et al., 2018). Vegetation invasion could significantly change the vegetation spatial distribution depending on the propagule stress (van Oorschot et al., 2017). Climate change may induce the vegetation belt shifting and change the

species richness: vegetation belt may shrink or expand depending on the change of hydrological conditions and location of vegetation (Martínez-Fernández et al., 2018; Mosner et al., 2015; Ström et al., 2012).

Vegetation spatial distribution generates distinct river morphology. An early numerical study showed that non-uniform vegetation distribution on floodplains influenced the planform of meandering rivers (Camporeale et al., 2013; Perucca et al., 2007). The spatial distribution in the transverse direction has an impact on river with alternate bars (Bertoldi et al., 2014). Floodplain vegetation and vegetation on bar surfaces have different effect on river morphological change in a single thread river (Vargas-Luna et al., 2019). With vegetation establishment on floodplain, the river bank is more stable, while with vegetation on bar surface, river flow is deflected and induces local bank erosion. River with vegetation whose seeds are transported by water flow has a larger braiding intensity than river with vegetation whose seeds are transported by wind (Van Dijk et al., 2013).

Although studies have investigated the effect of vegetation distribution in wandering or single-thread rivers, the effect of vegetation distribution on braided river is rarely investigated. Along a braided river transection, vegetation may have different morphological effects depending on its location (Gurnell, 2014). Vegetation importance may reduce near mid-channel bars and on floodplains, since the disturbance from water flow is strong and submergence opportunity is low, respectively. Through numerical simulation and laboratory experiments, studies show that uniformly distributed vegetation transformed a braided river into a dynamic single-thread river (Murray and Paola, 2003; Tal and Paola, 2010, 2007). Vegetation could prevent a single-thread river from braiding and promote meandering during a large flood (Iwasaki et al., 2016a). Field observation has confirmed that the statistical properties of an island braiding river are related to the median elevation of vegetation patch (Bertoldi et al., 2011).

Studying the effects of different vegetation distribution along a transect on river morphology could be difficult in a laboratory experiment. With the development of depth-averaged two-

dimensional numerical models, it is possible to study such effects by simulation (Jourdain et al., 2020; van Oorschot et al., 2016; Weisscher et al., 2019). In this study, numerical simulations based on Delft3D were performed to study the effect of different vegetation distribution along transection on braided river morphology and its statistical properties.

Two different colonization patterns in a gravel-bed braided river are studied. The first pattern accounted for vegetation colonization near low water channel during normal flow condition where flow disturbance is relatively strong, and in the second pattern, the vegetation colonizes higher elevation where flow disturbance was relatively weak. By varying the colonization area, the morphology is quantitatively compared. The river is inspired by the Satsunai River and the Otofuke River in Hokkaido, Japan, which is heavily influenced by vegetation in the last decade (Iwasaki et al., 2016a; Weisscher et al., 2019), and the river configuration is also an typical gravel bed river that sensitive to vegetation expansion (Millar, 2005). The results have shown that two patterns have distinct influences on braiding river morphology.

4.1.1 Hydro-morphology model

Flow field and morphological development are obtained using the hydro-morphology model Delft3D. Details about the numerical method can be found in Lesser et al. (2004). The model solves the depth-averaged shallow water equation systems by the ADI method on boundary fitting grids and update the bed topography by solving the Exner equation. Bed load flux is estimated by the Meyer-Peter and Müller formula (Meyer-Peter and Muller, 1948).

Vegetation effects on the flow velocity is accounted for by adding a momentum source term representing the drag force exerting on the water flow (Jang and Shimizu, 2007):

$$F_x = \frac{1}{2} C_D \rho a_s h_v u \sqrt{u^2 + v^2} \quad (1)$$

$$F_y = \frac{1}{2} C_D \rho a_s h_v v \sqrt{u^2 + v^2} \quad (2)$$

where x is the longitudinal coordinate, y is the transverse coordinate, u is the velocity along the x direction, v is the velocity along the y direction, C_D is the drag coefficient, ρ is the water

density, a_s is the vegetation density that is the product of stem number per unit area and vegetation representative diameter, h_v is the smaller value in water depth and vegetation height.

The bedload flux direction is corrected by considering the secondary flow effect and bed slope effect. The secondary flow effect is induced by flow curvature and is critical for the formation of channel bars (Iwasaki et al., 2016b; Schuurman et al., 2013). The angle between the bedload transport and the downstream direction is calculated as:

$$\tan(\phi_\tau) = \frac{v}{u} - A\frac{h}{R} \quad (3)$$

$$A = \frac{2}{\kappa^2}\left(1 - \frac{\sqrt{g}}{\kappa C}\right) \quad (4)$$

where R is the radius of the streamline curvature, κ is constant value equal to 0.4, C is the Chezy roughness coefficient.

The effect of bed slope is accounted for by the following formulas:

$$\tan\phi_s = \frac{\sin\phi_\tau + f(\theta)\frac{\partial z_b}{\partial y}}{\cos\phi_\tau + f(\theta)\frac{\partial z_b}{\partial x}} \quad (5)$$

$$f(\theta) = \frac{1}{\alpha\theta^\beta} \quad (6)$$

where ϕ_s is corrected angle between bedload flux and downstream direction accounting for the bed slope effect, θ is the Shields number. Bed slope effect is critical for the simulation of braided river morphology. The selection of the parameter α significantly affects the braiding morphology, and a large value of α may lead to overestimated erosion (Baar et al., 2019; Schuurman et al., 2018, 2013).

4.1.2 Vegetation model

Vegetation dynamic includes the recruitment, growth, and mortality of vegetation (Camporeale et al., 2013; Solari et al., 2016; van Oorschot et al., 2016). In this study, vegetation disperses its seeds during a specified period. During the seed dispersal period, vegetation

establishes their community on the bare bed where water depth is smaller than a criteria value and the carrying capacity is larger than zero. When vegetation establishes in a grid, the grid is regarded as vegetated and cannot be colonized again until the vegetation is destructed by an external force.

Vegetation characteristics considered in this study include vegetation height, density, and root depth. Here, the density of vegetation represents the production of vegetation stem density and diameter.

Two mechanisms in the model can destroy the vegetation when certain conditions are satisfied. First, when cumulative scour depth in a grid becomes deeper than the root depth, the vegetation is destroyed (Edmaier et al., 2015). Second, when deposition in a grid is higher than the vegetation height in the grid, the vegetation is destroyed.

4.1.3 Simulation settings

Three groups of simulations are performed. The first group aims to investigate the influence of channel width, the second group aims to investigate the influence of sinuosity, and the third group aims to study the influence of meander bend length. Thus, the river is straight in the first group, and the width keeps constant in the second and the third group. The river does not represent a real river in nature, but the river with a width equal to 250 m has similar characteristics, including slope and peak discharge, with the Satsunai River, Japan, which is a braided river with a gravel bed. The river slope is 1/130, and the gravel size is 25 mm. Relating parameters of the numerical simulation are shown in **Table 2**. The initial bed developed from a compound channel and is fully braided. All simulation starts from this initial topography.

The whole simulation contains 200 cycles of floods, and between each cycle of flood vegetation can colonize on the river bed. Each cycle of flood contains a 12 hours rising phase and 24 hours of falling phase. The total time is enough for the morphology to reach an

equilibrium state. The magnitude of the flood is 300 m^3/s which is given by the average peak discharge in the Satsunai River (Nagata et al., 2016). The duration of the flood is typical in a mountainous region.

Two scenarios of vegetation distribution along the river transverse section, which is shown in **Figure 4.1**, are investigated: (1) In Scenario 1, vegetation establishes near the lower water channel and the upper limit of the colonization area varies from 0.2 m to 2.5 m (relative elevation, marked as RE_U) representing vegetation that sensitive to moisture availability (e.g., *Phragmites japonica*); (2) In Scenario 2, vegetation establishes on the bar top and the lower limit of the colonization area varies from 0.2 m to 1.5 m (relative elevation, marked as RE_L) representing vegetation that not sensitive to underground water table but flood disturbance.

The physical parameters of the vegetation being studied are shown in **Table 3**. Vegetation type C1 is similar to reedy grass in the riparian environment. However, reproducing a prototype in the field or studying the influence of specific vegetation are not the aims; hence, the root depth, density and time scale of vegetation being mature are modified to study the effects of different types of vegetation on the morphological characteristics. The parameters of vegetation are estimated in a physically real range (Crosato and Saleh, 2011; Tetsuya et al., 2003; van Oorschot et al., 2017; Andrés Vargas-Luna et al., 2016). The height of the vegetation is 2.5 m. For vegetation with a long growth time scale, the vegetation properties change linearly. Vegetation type D1 has the weakest resistance to flood impact in this study, while vegetation types A1 and A2 are the strongest. Simulation cases are provided in **Table 4**.

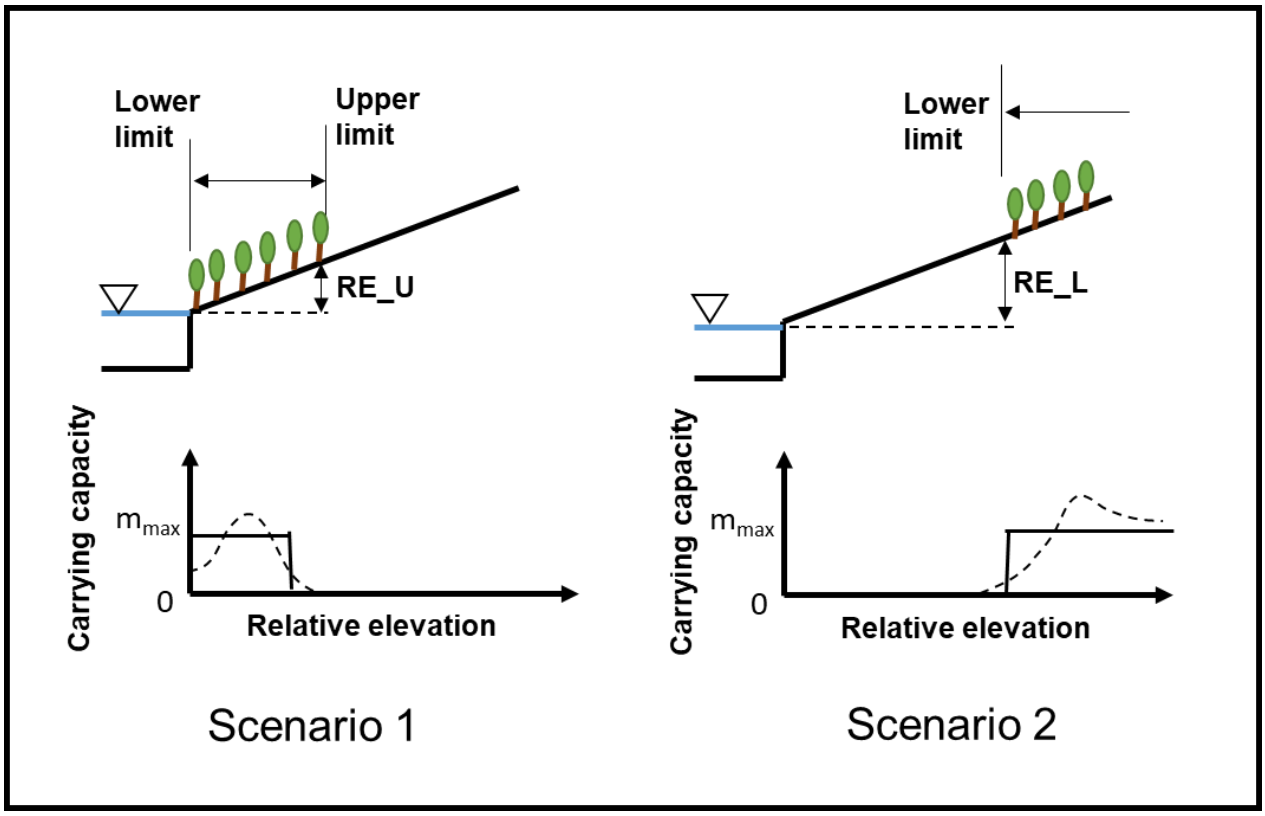

Figure 4.1 Schematic figure of two scenarios of vegetation distribution along river transverse sections. Dashed line shows the peaked pattern of distribution in the field (Camporeale and Ridolfi, 2006; Johnson et al., 1995), and solid line shows the simplified distribution in the numerical simulation.

Table 2. Settings of the numerical simulation

Item	Unit	Value	Reference
Channel width	m	250	Estimation based on field
Channel length	m	4,000	More than ten times of the channel width
Channel slope	-	1/130	Nagata et al. (2016)
Bed gravel size	mm	25	Iwasaki et al. (2016a)
Maximum discharge	m3/s	300	Nagata et al. (2016)
Mean annual normal flow (vegetation recruitment)	m3/s	30	Nagata et al. (2016)
Chezy roughness	m0.5/s	30	-
Sediment inlet	-	equilibrium condition	-
Sediment transport	-	Bedload	Determined by Shields stress and sediment diameter
Bed slope effect α	-	0.7	Physically real value based on Baar et al. (2019)
Grid size	m2	5x10	Balance between precision and computational resources
Time step	s	0.6	Keep simulation stable

Table 3. Parameters of different types of vegetation. Density and root depth are the values of a mature state. A linear growth is employed.

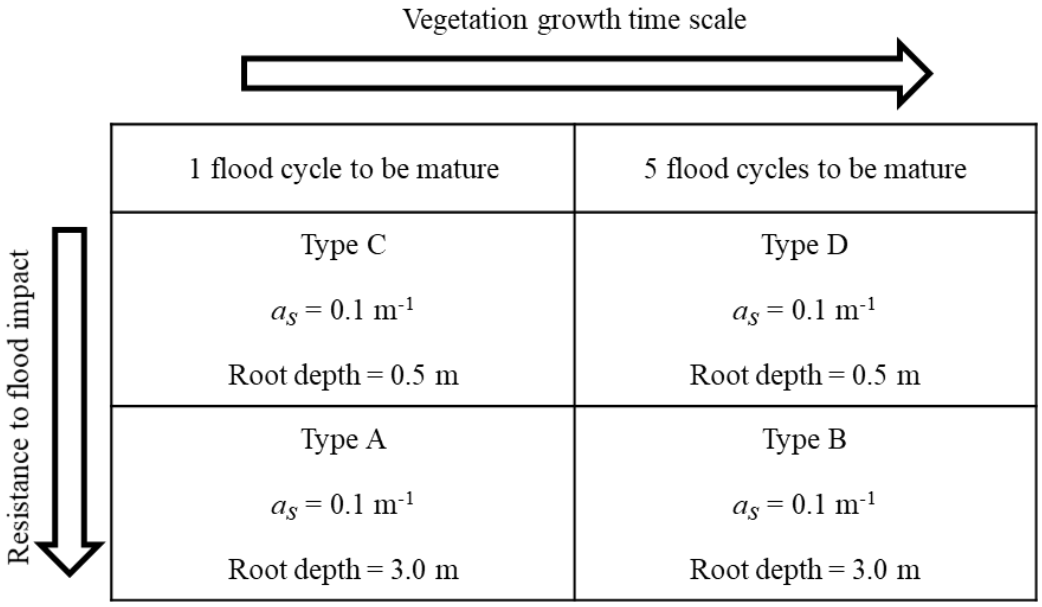

Table 4. Simulated cases

	Habitat Extension (Vertical distance from low water surface)	Vegetation type	Case name
Scenario 1	Lower limit (RE_L): 0 Upper limit (RE_U): 0.2, 0.5, 1.0, 1.5, 2.0, 2.5 m	A	S1-A
		B	S1-B
		C	S1-C
		D	S1-D
Scenario 2	Lower limit (RE_L): 0.2, 0.5, 1.0, 1.5 m Upper limit: No upper limit	A	S1-A
		B	S1-B
		C	S1-C
		D	S1-D
Full cover	Vegetation can cover all bare bed during the normal flow period	A	Ref-F-A
		B	Ref-F-B
		C	Ref-F-C
		D	Ref-F-D
Bare	Without vegetation cover	-	Ref-Bare

4.2 Results

4.2.1 General river morphology

The river morphology at the end of the simulation in the reference cases are shown in **Figure 4.2**. The green contour represents the age of vegetation patch rather than the age of vegetation. The river morphology is a single thread river when vegetation cover is Type A since it has the strongest resistance to flood. While in other cases, the river morphology shows a higher braiding intensity (e.g., Ref-F-C). The vegetation patch age is significantly older in Ref-F-A case than in the Ref-F-D case, showing a lower floodplain turnover rate with strong vegetation cover.

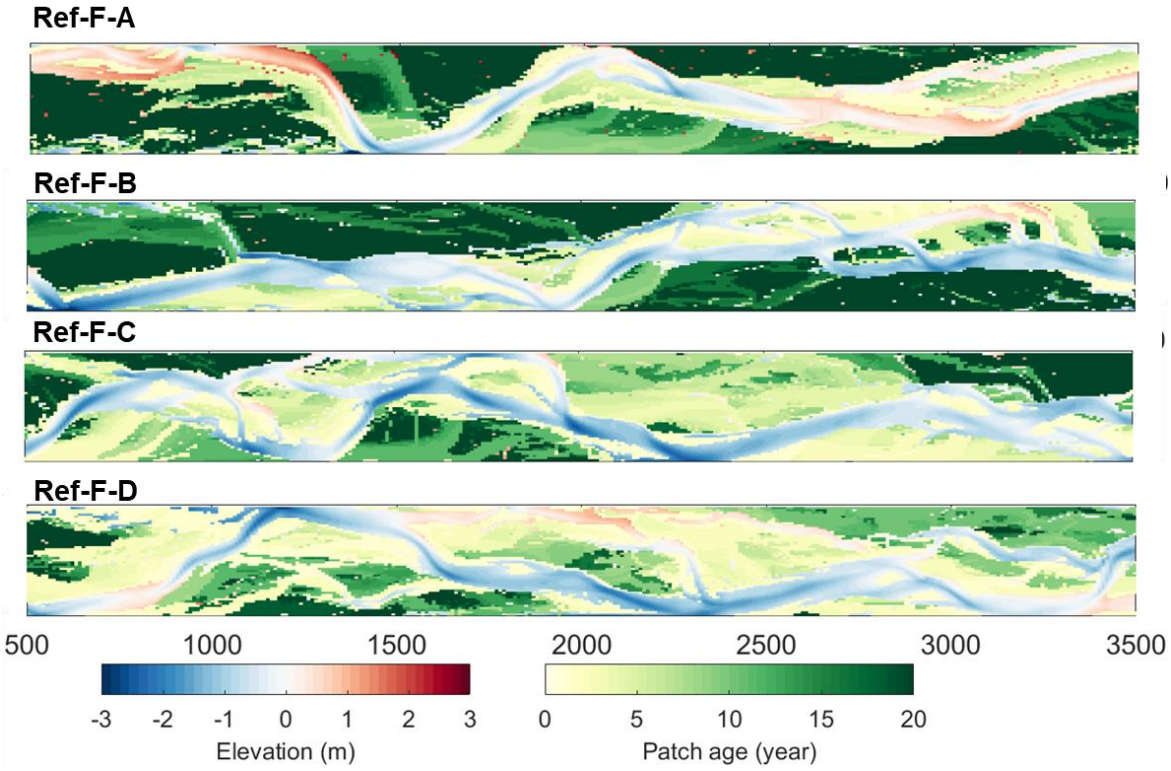

Figure 4.2 River morphology and vegetation cover in the reference cases. The green contour represents the age of vegetation patch. Flow direction is from the left.

The channel wet width and active width are depicted in **Figure 4.3**. The active width is the channel with bedload transport. In general, the width and active width are wider in Scenario 2 than which in Scenario 2. The width and active width decrease with the increase of habitat area since the bed roughness increases and flow are deflected to the main channel. Regarding the

active width, it decreases slowly when the vegetation area is small and faster when the habitat area ratio is larger than 0.6. It is attributed to that the higher place is inactive in the braided river; thus, vegetation on the bar top does not significantly influence the active width.

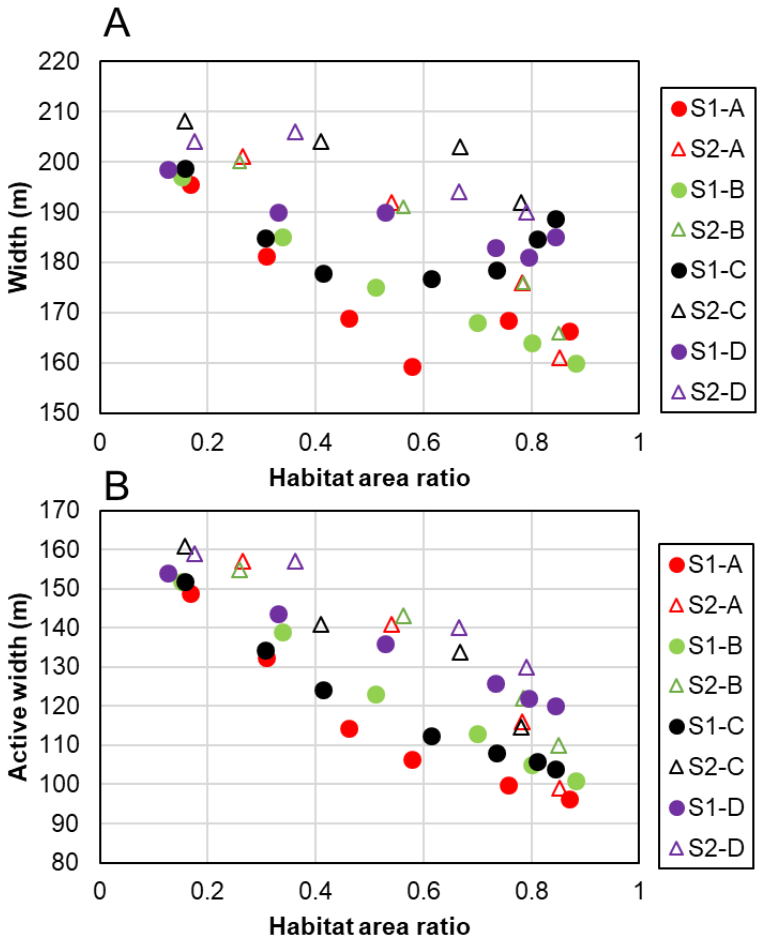

Figure 4.3 Wet width and active width (A and B, respectively) in each case during the peak discharge (300 m^3/s).

4.2.2 Statistical characteristics of bed elevation

The relationship between the statistical characteristics of bed elevation and vegetation cover is shown in **Figure 4.4**. Regarding the bed variance (**Figure 4.4**A), it increases with the increase of vegetation cover ratio in both scenarios. In Scenario 1, the variance increases rapidly and achieves a steady value when the cover ratio is about 0.4. In Scenario B, the variance value grows slowly before 0.6 and starts to grow rapidly with the vegetation cover ratio when the cover

ratio is larger than 0.6. The skewness of bed elevation increases monotonously with vegetation cover in Scenario 2, while in Scenario A, bed skewness first decreases and then increases (**Figure 4.4**B). The trend of bed kurtosis in Scenario 1 is also not monotonous: it increases first and then decreases (**Figure 4.4**C). In Scenario 2, the bed elevation has a negative skewness and positive kurtosis when the vegetation cover is low, and it has a larger skewness and a positive kurtosis when vegetation cover ratio becomes larger. In Scenario 1, bed elevation distribution always has a negative skewness and positive kurtosis. The results show that with different habitats, bed elevation subject to vegetation varies even with a same vegetation cover ratio.

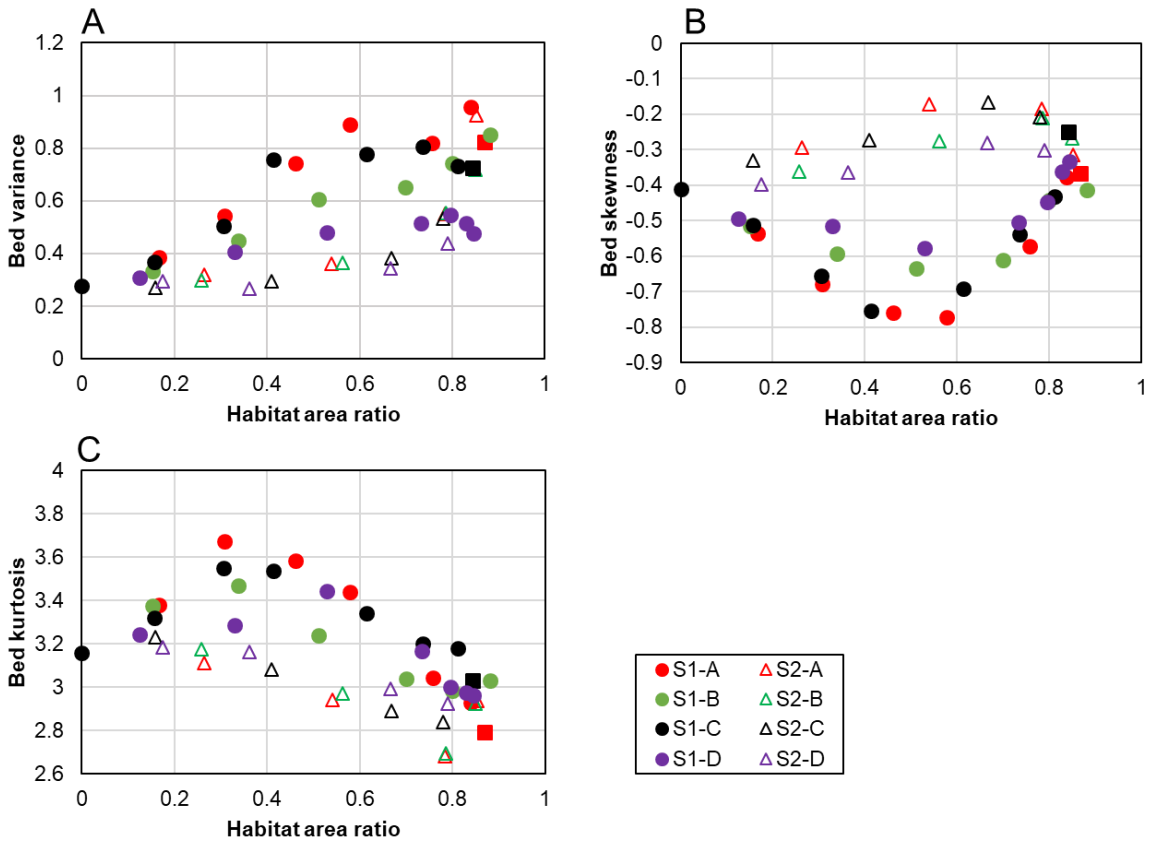

Figure 4.4 Relationship between bed statistical characteristics (A) bed variance, (B) bed skewness, and (C) bed kurtosis, and vegetation cover ratio.

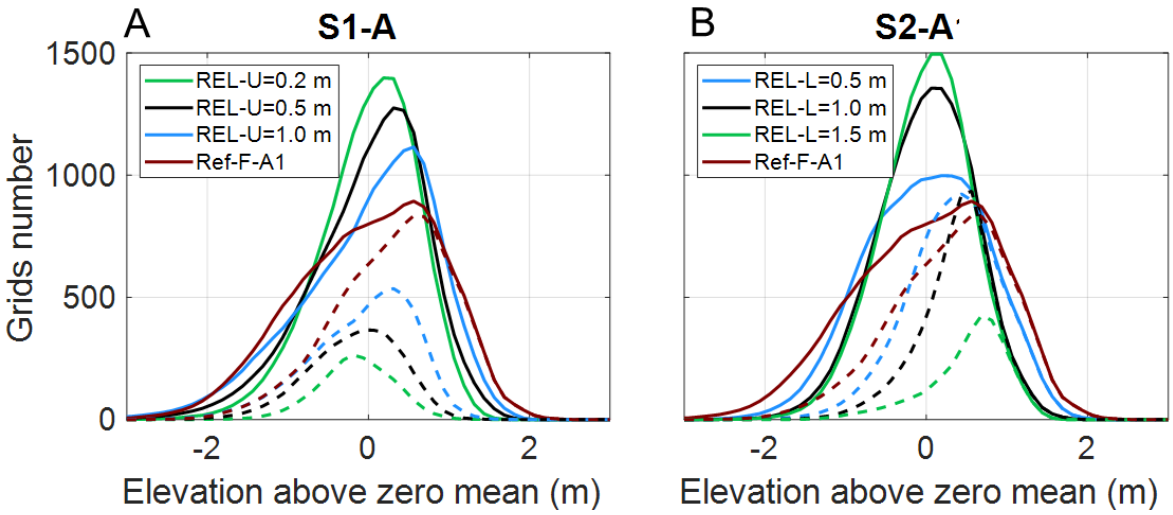

Figure 4.5 Distribution of elevation in case S1-A (A) and S2-A (B). The solid line shows the distribution of all grids, and the dashed line shows the distribution of vegetated grids.

The distribution of elevation is shown in **Figure 4.5**. Since the change of statistical properties has a similar trend in all cases, only vegetation type A is selected as an example. In Scenario 1 (**Figure 4.5**A), with the increase of the habitat upper limit, the peak value decreases, and the peak moves toward to the positive direction. The peak of the vegetated area moves from the negative to the positive. While in Scenario 2 (**Figure 4.5**B), the peak of vegetated area moves toward the negative direction. Compared to Scenario 2, the area with negative elevation and positive elevation both increase significantly with the increase of vegetated area in Scenario 1. In both cases, the peak value decreases with the increase of vegetated area.

4.2.3 Vegetation cover

Vegetation cover in case S1-C, S2-C and corresponding reference cases are shown in **Figure 4.6**A and B, respectively. Compared to the reference case without vegetation cover (Ref-Bare), the area of vegetated area in S1-C is smaller than the habitat area provided by the bare river, e.g., the area with a relative elevation smaller than 1 m is smaller in S1-C than in Ref-Bare **Figure 4.6**A). This result suggests the elevation with higher relative elevation has been created by the

vegetation. The vegetated area in S2-C is larger than the habitat area provided by the bare bed (**Figure 4.6**B). The larger river bed area with higher relative elevation shows vegetation induces accretion and creates habitat that has a higher relative elevation regardless of the location of vegetation. Compared to Scenario 1, in the fully covered case, vegetation cover ratio between same relative elevation is higher (**Figure 4.4**A). While comparing the case of S1-C, S2-C and Ref-F-C, vegetation habitat area with a higher relative elevation is less and habitat area with a lower relative elevation is larger (**Figure 4.6**A and B). The results show that the relationship between vegetation with lower relative elevation and vegetation with higher relative elevation is non-linear. The interaction between vegetation with a different relative elevation in the Ref-F-C case leads to a larger habitat area that has a smaller relative elevation.

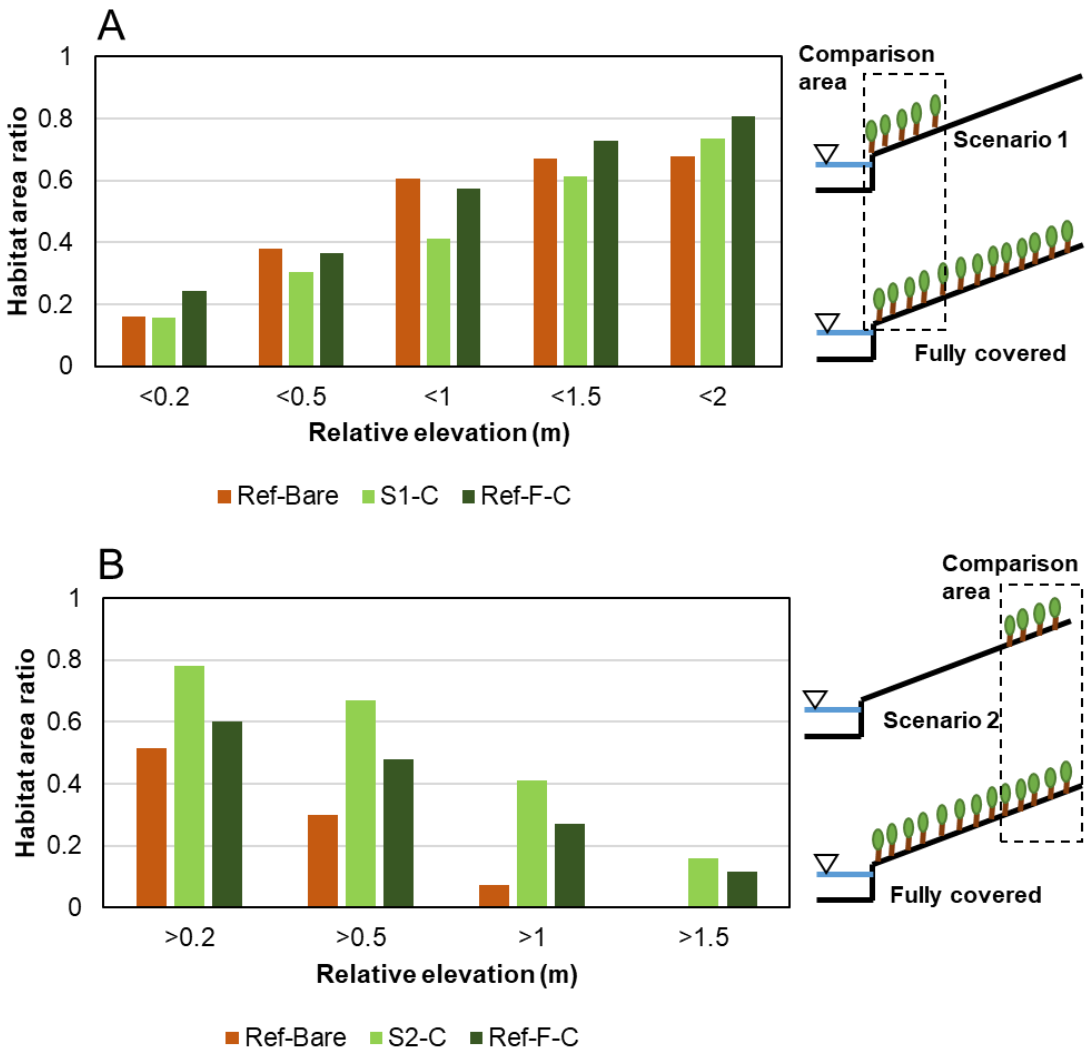

Figure 4.6 Vegetation cover ratio in S1-C, S2-C and corresponding reference cases.

4.2.4 Discussions

In this study, the effects of vegetation distribution along river transections on a braiding river morphology have been investigated. The reduction of braiding intensity with the influence of vegetation in the numerical model is well reproduced. The transformation is consistent with laboratory experiments and an early numerical simulation by cellular model (Bertoldi et al., 2015; Murray and Paola, 2003; Tal and Paola, 2010). The statistical characteristics of bed elevation and vegetation cover ratio are compared, and the results show that the change of statistical properties has two different relationships with the change of the vegetation cover ratio

depending on the vegetation transect distribution. The influence of vegetation transect distribution on bed statistical properties are summarized in

Table 5. Both distributions are positively related to habitat area ratio in term of bed variance and have opposite effects on bed skewness and bed kurtosis. The effects also explain the non-monotonous change in skewness and kurtosis with the increase of vegetation habitat area. For example, the decreasing trend of skewness in Scenario 2 when habitat area is larger than a critical value since the vegetation in lower place has an effect of reducing the bed skewness. In Scenario 1, the skewness decreases (i.e., more asymmetrical) with the increase of habitat upper limit until the upper limit reaches a critical value. In Scenario 1, since the vegetated area is around the local average elevation (0 m in **Figure 4.5**A) and vegetation induces both deposition and erosion, the distribution is more skewed. While in Scenario 2, vegetated area is mainly above the local average elevation (0 m in **Figure 4.5**B). Given the vegetation in higher place induces less erosion and still increase deposition (**Figure 4.6**B), the peak of the distribution will move toward the local mean elevation with the downward expansion of vegetation; therefore, the distribution becomes more symmetrical (i.e., an increasing skewness when starts from a negative skewness). In both scenarios, decreased peak hight can be observed, while the bed kurtosis increases in Scenario 1 and decreases in Scenario 2. The increase of kurtosis in Scenario 1 appears to be conflicting with the decreasing trend of the peak value, while it is attributed to that kurtosis is better to be described as a measure of tailedness rather than peakedness (Westfall, 2014). Suspended load is not considered in this study. Fine sediment can deposit on the top of the bar and it can fill the low place (Braudrick et al., 2009). Thus, with the consideration of fine sediment, the decrease of skewness in Scenario 1 may be mitigated.

Table 5. Relationship between bed statistical properties and the increase of habitat area ratio. The '+' represents the two values that are positively connected, and the '--' represents the two values that are negatively connected.

Distribution along transect	Bed variance	Bed skewness	Bed kurtosis
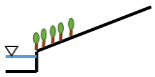	+ (strong)	--	+
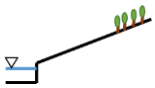	+ (weak)	+	--

In a field observation performed in the Tagliamento River in Italy, the skewness was found to be positively related to vegetation cover ratio, and the kurtosis was negatively related to vegetation cover ratio (Bertoldi et al., 2011), while in a flume experiment performed by Mao et al. (2020) the skewness decreased with the vegetation encroachment on bar surfaces. Mao et al. (2020) attributed the possible reason for the difference between the field observation in the Tagliamento River and their flume experiment to a lack of fine sediment in the laboratory experiment. However, the results imply that different pattern of vegetation distribution along river transect is another possible reason. In the flume experiment, vegetation expands its habitat from the bar top to a lower place, which can be confirmed in the Fig. 1 of Bertoldi et al. (2015). Such a situation is similar to Scenario 2 with a large habitat area in this study, and the study shows that the skewness decreases with the increase of vegetation cover when the habitat area ratio is larger than a critical value. In the Tagliamento River, the vegetation cover was mainly on locations with higher bed elevation, which was similar to Scenario 2 with a small habitat area ratio in this study. In addition, in the Tagliamento River, bed elevation with less vegetation cover was negatively skewed and had positive kurtosis, and the skewness became negligible and the kurtosis became negative with the increase of vegetation cover. The results of the relationship between skewness, kurtosis and vegetation cover ratio is consistent with the field observation.

In the field, the bed standard deviation is positively related with the vegetation cover, which also has an agreement with the results in this chapter. The negatively skewed distribution of cases without vegetation cover is observed in the laboratory experiment performed by Garcia Lugo et al. (2015). The change of the skewness and kurtosis with the vegetation cover ratio was more rapid in the field than in the simulation. A possible reason is that the root reinforcement effect of vegetation is not accounted for in the numerical simulation. The consistency between the numerical simulation and field observation shows that the numerical model has the potential to reflect the morphological change of braiding river with vegetation cover in the field quantitatively, although improvements are still needed.

Braided river is one of the most dynamic river patterns and provides support for fluvial ecosystem (Tockner et al., 2006). A global trend of reducing braided river was reported and one important factor is riparian vegetation expansion (Stecca et al., 2019). With the transformation from braided river to single thread river, the diversity of ecosystem may reduce. One recovery management strategy is removing the vegetation cover artificially (Leu et al., 2008). However, different removal methods exist depending on management objectives. Artificially released flushing flood is used to clear vegetation near the low water channel (Sumitomo et al., 2018, 2016). Cutting of vegetation on floodplain can improve the flow capacity during large flood (Toshimori and Miyamoto, 2014). This study shows that vegetation at different locations along river transections has distinct effects on river morphological development; thus, different removal methods of riparian vegetation may lead to different river morphological responses (**Figure 4.7**). In an originally braided but currently single-thread river, by removing vegetation near the low water channel, river morphology can recover rapidly and linearly to a status without or with less vegetation cover. By just removing vegetation from the floodplain, the effectiveness of the vegetation is lower and may generate a quite different river morphology considering the change of skewness and kurtosis. However, various vegetation removal methods can be applied to river management. The two methods discussed here are simplified. Vegetation removal should

also consider vegetation species and its ecological characteristics, such as growth and expansion. The methods discussed here can be applied to river where single vegetation species is in dominant.

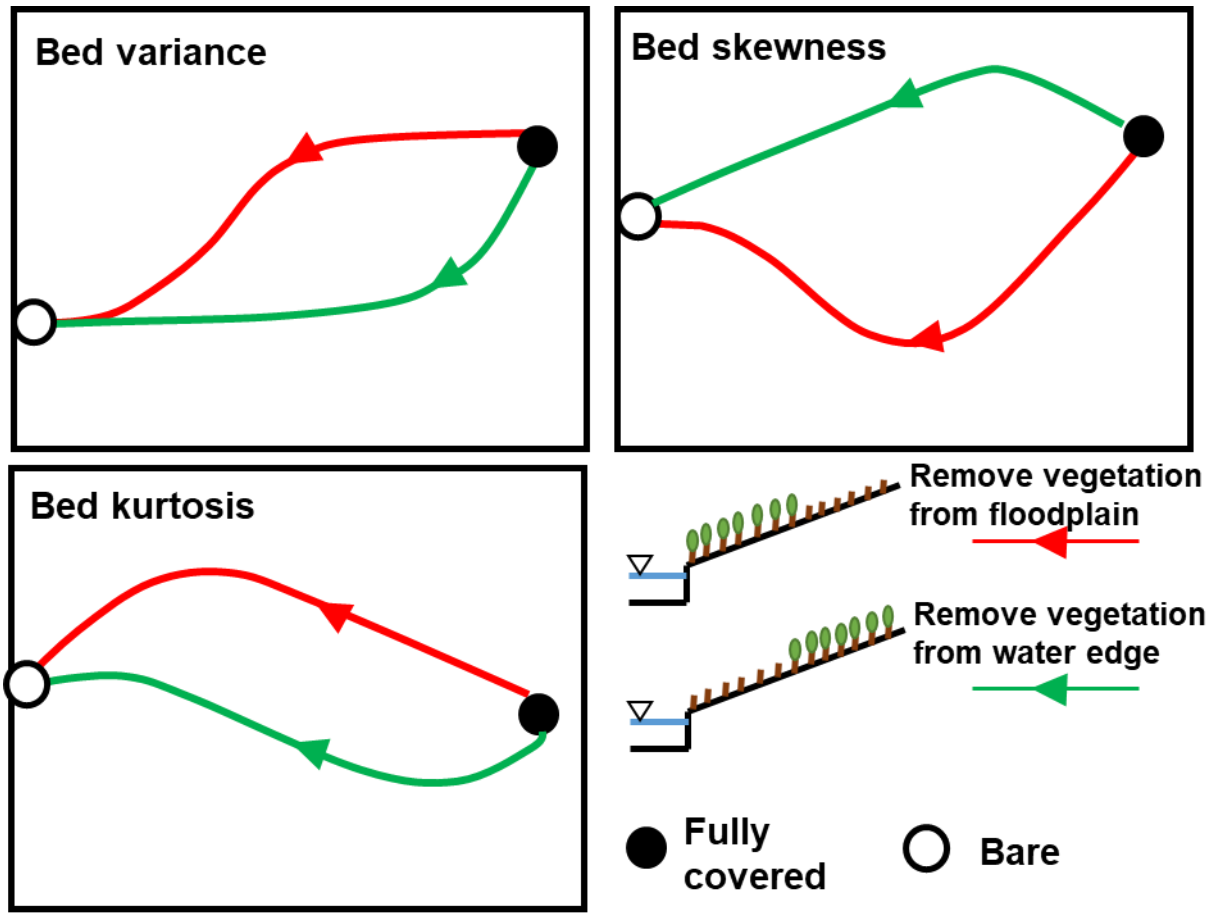

Figure 4.7 Schematic figure of two vegetation removing methods and response of river morphology in an originally braided but currently single-thread channel.

In the River Tech, vegetation location along transverse geomorphic gradient was found that have different effects on sediment accretion (Corenblit et al., 2009). Neither trees on the floodplain nor the herbs near the low water channel have the largest effect on sediment accretion, but the shrubs between the floodplain and low water channel affect the sediment deposition most. The vegetation near the low water channel captures sediment and maintains stable habitat for other species (Corenblit et al., 2020, 2009). The result in this thesis has confirmed the ability of vegetation to create habitat regardless of its distribution along the transect. However, by comparing the vegetation cover between partial coverage and full coverage (**Figure 4.6**), it is

found that the vegetated area with higher relative elevation is reduced in the full coverage situation, and the vegetated area with lower relative elevation has increased. The reduced area of vegetation with higher relative elevation is attributed to the sediment supply from the lower part of river. Sediment supply is a critical factor that influences the interaction between vegetation and braided river morphology, which has been confirmed both by numerical simulation and field observation (Gran et al., 2015; Murray and Paola, 2003). In an environment without enough sediment supply from the upstream, erosion rather than deposition may happen in the vegetation patch (Diehl et al., 2017; Kim et al., 2015). In the fully covered situation, the vegetation in the lower place may prevent the sediment from being transported to the higher place; thus, the vegetated area with higher relative elevation reduces.

In this study, the effects of different distribution of vegetation along river transverse gradient on braided river morphology are investigated. No specific vegetation type is discussed in this study. However, the major parameters of vegetation (density, root depth, and vegetation height) fall in a physically real range (Jourdain et al., 2020; van Oorschot et al., 2017, 2016; Andrés Vargas-Luna et al., 2016). Suspended load is not accounted for in the model. Thus, the results are more appropriate for gravel bed river. Vegetation preference on the habitat is explicitly controlled rather than modelling by physical process. The results show that a more sophisticated numerical model that accounts for the interaction between underground water and vegetation is necessary. It will also be interesting to study the effects of neglected factors, i.e., root reinforcement and fine sediment, in future research.

4.3 Conclusions

In this study, the influence of transverse vegetation distribution on braided river morphology development is investigated by numerical simulation. Two patterns of transverse distribution of vegetation have been investigated: (1) vegetation establishment on river bed near the lower channel; (2) vegetation establishment on the bar top. The numerical model has successfully

reproduced the reduction in the braiding index of the braided river undergoing the vegetation influence. Regardless of its distribution along river transect, vegetation can create a habitat with a higher relative elevation. However, such an effect is weakened if the vegetation can colonize the whole river bed. The results show that the transverse distribution of vegetation significantly influences the statistical characteristics of braided river. The bed elevation statistical characteristics show distinct relationship with the increase of vegetation habitat ratio. The variance positively relates to the increase of vegetation habitat area. The skewness and the kurtosis are negatively and positively related to the increase of vegetation habitat area, respectively, when the vegetation establishes habitat near the low channel. The skewness and the kurtosis have an opposite relationship with the increase of vegetation habitat area when the vegetation establishes habitat on the bar top. The influence of the vegetation transection distribution provides an explanation for the discrepancy in the bed skewness between field observation and laboratory experiments. The results also have implications for the recovery management of braided river with vegetation expansion problems.

5 Role of Riparian Vegetation Flexibility in a Bio-Hydro-Morphology Simulation

5.1 Introduction

Riparian vegetation's critical role in river morphology development has been widely recognized amongst river morphologists (Gurnell, 2014; Murray et al., 2008; Solari et al., 2016). Fluvial landscapes would be different from those we see today if vegetation had not participated (Gibling and Davies, 2012). Riparian and aquatic vegetation is an important part of fluvial systems (Tsujimoto, 1999; Vesipa et al., 2017). The expansion of vegetation within a river corridor may increase flooding risks and reduce bio-diversity (Erskine et al., 1999; Javernick et al., 2018). Thus, understanding vegetation's role within the fluvial system is of great significance in both a scientific and engineering context. Numerous studies have been performed for investigating the interaction between riparian vegetation and river morphology (Bertoldi et al., 2014; Crosato and Saleh, 2011; Tal and Paola, 2010, 2007; van Dijk et al., 2013). As such, noticeable progress has been made in quantitative research (Jourdain et al., 2020; Martínez-Fernández et al., 2018; van Oorschot et al., 2016).

Physical modelling and numerical simulations are two major ways of understanding the interaction between riparian vegetation and river morphology. Although a number of physical experiments have been performed, yielding fruitful results (e.g., Van Dijk et al. (2013) and Tal and Paola (2007)), several limitations are known (e.g., limited experimental duration and the scale effect on both sediment transport and vegetation dynamics (Lokhorst et al., 2019)). Given limitations for the experimental approach, numerical simulations could prove to be a promising way for clarifying processes related to vegetation-morphology interaction. Numerical simulations have several advantages, including: (1) controllable simulation conditions and (2) a

relatively short calculation time for long-term predictions as compared to physical modelling. Numerical models considering interactions between vegetation and river morphology can be referred to as bio-hydro-morphodynamic models. In previous studies, numerical investigations have been performed using bio-hydro-morphodynamic models and have revealed the effects of vegetation on meandering dynamics (Perucca et al., 2007; Schuurman et al., 2016) and the transformation of a river from a braided channel to a single-thread channel with floodplain vegetation (Crosato and Saleh, 2011; Weisscher et al., 2019). In past models, vegetation was considered static, not dynamic. Therefore, the characteristics of vegetation did not change with time evolution and important process such as vegetation growth were not accounted for in these models. Based on field observations and physical modelling, vegetation dynamics have been found to influence interactions amongst vegetation and morphological development. For example, seasonal changes in vegetation characteristics have been found to impact developed river morphology (Vargas-Luna et al., 2018). Laboratory experiments have revealed the influence of seed dispersal methods on river morphology (van Dijk et al., 2013). To investigate the effects of vegetation dynamics in numerical simulations, models incorporating vegetation dynamics, including growth, germination, and mortality, have emerged over the past decade (Bertoldi et al., 2014; Jourdain et al., 2020; Solari et al., 2016). A model accounting for competence and collaboration between species has also been developed (Sakai et al., 2013). Such numerical simulations have confirmed the influence of vegetation dynamics on river morphology and have presented its potential in quantitative research (Jourdain et al., 2019; van Oorschot et al., 2016).

Due to the complicated interaction between riparian vegetation and other elements in fluvial systems, several assumptions have been adopted in bio-hydro-morphodynamic models. In bio-hydro-morphodynamic models, the influence of vegetation is normally considered by adding a source term that represents the drag force exerted on water flow into the momentum equations or by changing bed roughness (Baptist et al., 2007; Bertoldi et al., 2014; Jang and Shimizu, 2007;

Vargas-Luna et al., 2015). When accounting for the drag force, vegetation stems are typically regarded as cylinders and uniformly distributed in simulation grids (Boothroyd et al., 2016; Ricardo et al., 2018; Andrés Vargas-Luna et al., 2016). This type of assumption neglects the complicated morphology of vegetation, such as leaves and canopies. Researchers have already shown that vegetation morphology changes surrounding flow structures and, thus, sediment transport rate (Boothroyd et al., 2017, 2016). Additionally, uniformly distributed vegetation within simulation grids may overestimate vegetation's influence when stem density is low (Crosato and Saleh, 2011; Andrés Vargas-Luna et al., 2016). Regarding biomechanical properties, for simplicity, the flexibility of vegetation is generally neglected.

Representing vegetation by assuming they are rigid is appropriate for tree-type vegetation, while for grass-type vegetation, the flexibility can hardly be neglected (Tsujimoto and Kitamura, 1998). As compared to rigid vegetation, flexible vegetation may lead to a smaller flow resistance due to a reduction of the area projected to flow since their posture is adjusted to water flow (Dijkstra and Uittenbogaard, 2010; Järvelä, 2005; Luhar and Nepf, 2011). By flume experiments and numerical investigations, the flexibility of vegetation was found to impact both flow structure and sediment transport (Dijkstra and Uittenbogaard, 2010; Marjoribanks et al., 2019; Nepf and Vivoni, 2000). However, the scale of the simulation and experiment was limited and mainly focused on the local flow field and sediment transport. Regarding the influence of flexible vegetation on bedform change, Chen et al. (2012) tested a flexible vegetation patch (represented by porous material) within a flume with a movable bed and found that channels with flexible vegetation have a smaller scouring depth between vegetation patches and the channel wall. Sediment deposition was found higher behind the flexible vegetation patch. Although flume experiments regarding reach scale river morphological evolution have been performed, and some experiments employed real vegetation (Braudrick et al., 2009; Kyuka et al., 2021; Tal and Paola, 2007), due to the scale effects, the vegetation should be regarded as trees rather than grass (Kyuka et al., 2021). Hitherto, a study investigating the effect of vegetation

flexibility on reach scale hydrodynamic and morphological change in a river is still lacking. Since grass-type vegetation could play an important role in fluvial vegetation communities, e.g., affecting river morphology or playing important role in vegetation succession (Corenblit et al., 2009; van Oorschot et al., 2017), investigating the possible effects of neglecting their flexibility in a morphological modelling (numerical or physical) is necessary.

However, to investigate the effects of vegetation flexibility in a flume experiment would be difficult since the Cauchy number must be the same between prototype and experiment, and very flexible material must be used in the experiment. Vargas-Luna et al. (2016) used woody sticks with a diameter equal to 2 mm in their laboratory experiment. The diameter of alfalfa was about 1 mm (Tal and Paola, 2010). To use flexible cylinders which has a diameter with similar order (e.g., 1 mm) to investigate the effects of flexibility in a 1:10 scale flume experiment, the Young's modulus of the material should be 0.1 GPa. A suitable material with similar Young's modulus is low-density polyethylene (LDPE). For a much smaller experiment, e.g., a 1:100 scale experiment, materials with much lower Young's modulus are needed, which is difficult to find. Thus, the numerical model could be a potential tool to simulate a more realistic environment.

Vegetation reduces velocity in the vegetation patch by increasing the drag force exerted on water flow. In addition to the increased flow resistance, vegetation patch also changes the flow structure and turbulent characteristics in the vegetation patch (Akahori et al., 2018; Nepf, 2011). The shear layer between the vegetation patch and water above the patch generates turbulence that can penetrate into vegetation patch. The turbulence generated by shear stress can possibly change the bed shear stress depending on the density of vegetation patch. However, since the velocity near bed is reduced by the vegetation resistance, the magnitude of turbulence near bed reduces. Thus, the effect of turbulence generated at the top of the vegetation patch onto the bed shear stress may be limited (Nepf, 1999; Zong and Nepf, 2011). However, the turbulence in both mixing-layer zone and wake zone (Akahori et al., 2018) may have major impact on suspended load. With flexible stem, vegetation stem may deflect during flood; thus, the frontal area reduces

(Aberle and Järvelä, 2015). The drag force exerted on water flow by the vegetation stem decreases due to the deflected vegetation. Reduced drag force leads to a reduced flow resistance. The turbulence generated by flexible vegetation patch and its effect on sediment transport is still under investigation. A three-dimensional simulation is difficult to apply to a reach-scale study since it requires extremely large computational resources (Tschisgale et al., 2021). Using resistance formula to investigate the effect of flexibility on reach-scale morphology is a reasonable solution. Vargas-Luna et al. (2015) compared the accuracy of different resistance formulas that accounted for vegetation effects in hydrodynamic and sediment simulation and found that certain formulas reasonably fit with flume experiment results. Experiment also shows certain resistance formulas can be applied to flexible vegetation and reproduce reasonable depth-averaged velocity (Verschoren et al., 2016). Hence, in this study, the effect of flexibility was accounted for by changing bed resistance.

In this study, a modification is made to the classical Baptist method to account for the vegetation flexibility and a bio-hydro-morphodynamic simulation is performed in a gravel bed river with alternate bars to discuss the effects of flexibility in such scenarios. Following two questions are going to be answered: (1) What is the effect of neglecting vegetation flexibility in a numerical bio-geomorphology simulation; (2) In which situations the flexibility of vegetation can be neglected.

5.2 Method

The bio-hydro-morphodynamic model consisted of two sub-models: vegetation sub-model and hydro-morphodynamic sub-model. Two models were performed alternately. The vegetation sub-model employed the results from the hydro-morphodynamic sub-model, e.g., water depth, to simulate vegetation recruitment, destruction, and posture update. The simulation was based on the model proposed by van Oorschot et al. (2016). Delft3D was employed in the hydro-morphodynamic sub-model.

5.2.1 Vegetation sub-model

The following three processes are adopted in the vegetation sub-model: 1) recruitment of vegetation; 2) destruction of vegetation due to uprooting and burial, and 3) update of vegetation posture based on local flow conditions.

In the vegetation sub-model, vegetation seeds are assumed to be sufficiently supplied, and vegetation is recruited on bare grids that had a relative elevation (defined as vertical distance from normal flow condition) falls in a specified range. The condition aims to reflect the influence of flood disturbance and water availability (Camporeale and Ridolfi, 2006).

In the simulation, when sediment deposition is higher than the initial vegetation height, vegetation is regarded as buried and is numerically treated as a lack of vegetation within the grid. Similar to burial, when the cumulative erosion depth is deeper than the vegetation root depth, vegetation is regarded as uprooted and not to exist within the grid (Calvani et al., 2019; Edmaier et al., 2015).

Vegetation height determines the drag force and the submergence ratio (i.e., the ratio of vegetation height to water depth), which is essential in the resistance calculation (Baptist et al., 2007; Vargas-Luna et al., 2015; Wilson, 2007). The method proposed by Luhar and Nepf (2011, 2013) is adopted to calculate the flexible vegetation height that is subjected to water flow in this article. In their method, the incoming flow is assumed to be uniform over water depth, and form drag is the dominant hydrodynamic force. A buoyancy force is also included if the density of vegetative tissue is small. The drag coefficient is constant, and the vegetation is entirely submerged.

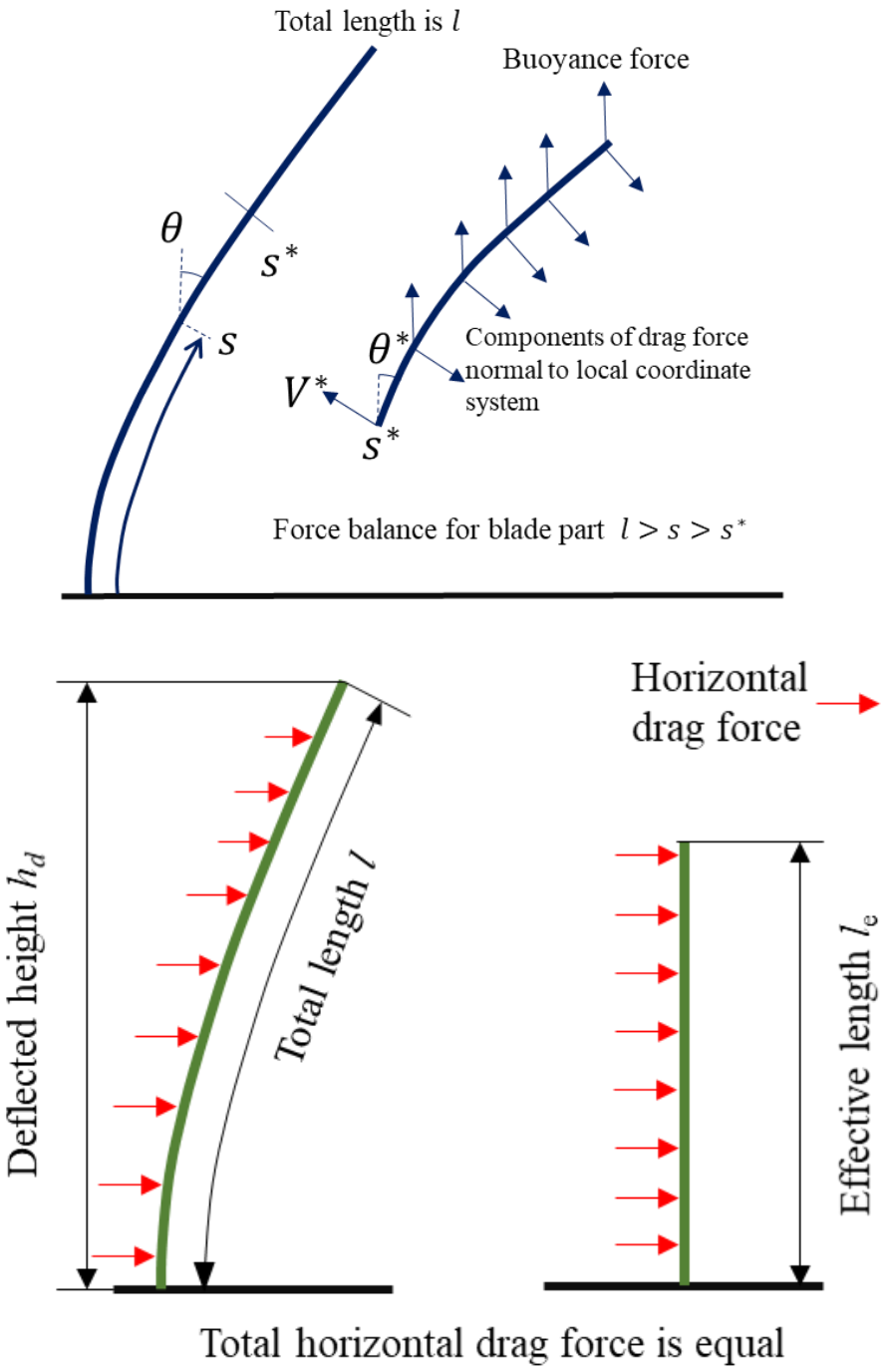

Figure 5.1 Upper: The curvilinear coordinate system and forces acting on a stem (Luhar & Nepf, 2011). Lower: A schematic of deflected height and effective length.

A curvilinear coordinate system is used to describe the posture of a vegetation stem. The coordinate system is shown in **Figure 5.1**. The coordinate of a point on the stem is denoted as *s*, and *s** represents an arbitrary point on a cylinder. The total length of the stem is *l*, and the stem

diameter is *d*. The local bending angle at *s* is denoted as θ. The normal component of the drag force exerted on a unit length of a vegetation blade is:

$$f_D = (1/2)\rho C_D dU^2 \cos^2\theta. \quad (7)$$

The restoring force caused by stiffness is:

$$V = -EI\frac{d^2\theta}{ds^2}, \quad (8)$$

where *E* is Young's modulus and *I* is the second moment of the area.

The buoyancy force exerted on a unit length of a blade can be described as:

$$f_B = 0.25\Delta\rho g\pi d^2 = 0.25(\rho - \rho_v)g\pi d^2 \quad (9)$$

where ρ is water density and ρ_v is the density of the vegetation stem.

The governing equation of the force for a stem beginning from a specific point s^* (**Figure 5.1**, the left) is:

$$V^*(s^*) + \int_{s^*}^{l} f_B \sin\theta^*(s^*)ds = \int_{s^*}^{l} \cos\{\theta(s) - \theta^*(s^*\} f_D\{\theta(s)\}ds, \quad (10)$$

where V^* is the stem-normal restoring force due to stiffness at $s = s^*$, and θ^* is the blending angle at s^*.

The non-dimensional form of the governing equation is:

$$-\frac{d^2\theta}{d\hat{s}^2}\bigg|_{\hat{s}^*} + B(1-\hat{s}^*)\sin\theta^* = \mathrm{Ca}\int_{\hat{s}^*}^{1} \cos(\theta - \theta^*)\cos^2\theta d\hat{s}. \quad (11)$$

here, $\hat{s}$ is the non-dimensional stem coordinate and is defined as $\hat{s} = s/l$. The non-dimensional parameters used in Equation (5) are defined as:

$$B = \frac{0.25\Delta\rho g\pi d^2 l^3}{EI}. \quad (12)$$

and:

$$\mathrm{Ca} = \frac{1}{2}\frac{\rho C_D dU^2 l^3}{EI}, \quad (13)$$

where *B* is defined as the ratio of the buoyancy force to the restoring force and Ca is the Cauchy number that represents the relationship between the drag force and restoring force.

To describe drag force reduction induced by vegetation reconfiguration in a manner compatible with the rigid vegetation model, Luhar and Nepf (2011) introduced a concept named effective length, l_e, that is the equivalent height of rigid vegetation suffering the same drag force acting on a flexible stem (**Figure 5.1**, right). The effective length is shorter than the stem length, l, and can be calculated as:

$$\frac{l_e}{l} = \frac{\int_0^l (1/2)\rho C_D dU^2 \cos^3\theta ds}{(1/2)\rho C_D dU^2} = \int_0^1 \cos^3\theta d\hat{s}. \quad (14)$$

Another variable needed for bed roughness and vegetation drag force calculations is the deflected height, h_d (**Figure 5.1**, right in the lower panel). The variable is defined as the vertical distance between the free end of a stem and the river bed. The deflected height of a flexible stem can be calculated as:

$$\frac{h_d}{l} = \int_0^1 \cos\theta d\hat{s}. \quad (15)$$

For the sake of reducing the simulation time for calculating Equations (5) to (8), an approximation formula from the article of Luhar and Nepf (2011) is adopted for evaluating the effective length, shown as follows:

$$\frac{l_e}{l} = 1 - \frac{(1 - 0.9\mathrm{Ca}^{-1/3})}{1 + \mathrm{Ca}^{-3/2}(8 + B^{3/2})}. \quad (16)$$

The deflected height can be calculated as (Luhar and Nepf, 2013):

$$\frac{h_d}{l} = 1 - \frac{1 - \mathrm{Ca}^{-1/4}}{1 + \mathrm{Ca}^{-3/5}(4 + B^{3/5}) + \mathrm{Ca}^{-2}(8 + B^2)}, \quad (17)$$

An iteration process is adopted for estimating velocity within a flexible vegetation patch and corresponding Cauchy number Ca (Luhar and Nepf, 2013). If the flow velocity is not large enough to bend the flexible vegetation so that it is fully submerged, reconfiguration of the stem is neglected.

5.2.2 Hydro-morphodynamic sub-model

The unsteady flow field is simulated in the hydro-morphodynamic sub-model by solving the depth-averaged shallow water equations. Sediment transport is calculated by bedload transport formula, and the river bed form is updated by solving the Exner equation. Since the bed slope effect model strongly affects the bed erosion and calibrating the model parameter depending on the situation is difficult, a physically reasonable value based on early research is used (Baar et al., 2019; Schuurman, 2015). Details can be found in the Delft3D manuscript and several relating papers (Crosato and Saleh, 2011; van Oorschot et al., 2016).

Within the simulation, the method proposed by Baptist et al. (2007) is used to account for the effects of vegetation on flow resistance. The approach consists of two parts: changing the bed roughness and adding a source term representing the vegetation-induced drag force to the momentum equations. River bed roughness accounting for vegetation drag, as well as actual bed roughness, is represented by the Chezy coefficient, C, as follows:

$$C = C_{\mathrm{b}} + \frac{\sqrt{g}}{\kappa} \ln\left(\frac{h}{h_v}\right) \sqrt{1 + \frac{C_{\mathrm{D}} m d h_v C_{\mathrm{b}}^2}{2g}}. \qquad (18)$$

In Equation (18), C_{b} is the bare bed roughness, and m is the vegetation stem density that represents the number of stems per unit area. In this research, parameter d represents the diameter of the vegetation stem. Variable h is the local water depth, and h_v is the height of rigid vegetation that is equivalent to the length, l, for rigid vegetation. Parameter κ is the von Kármán constant, and g is the gravitational acceleration.

The source term added to the momentum equations is $-\lambda u^2/2$, where the coefficient λ is calculated as:

$$\lambda = C_{\mathrm{D}} m d \frac{h_v}{h} \frac{C_{\mathrm{b}}^2}{C^2}. \qquad (19)$$

Although the original method proposed by Baptist (2007) assumed that vegetation is rigid, it works reasonably well as long as the deflected vegetation height is known when flexibility is accounted for in the model (Vargas-Luna et al., 2015; Verschoren et al., 2016). In this work, the

deflected height of flexible vegetation is calculated using Equation (16) and (17). Although vegetation height, h_v, in Equation (18), can be replaced by the deflected height, h_d, it is more reasonable to replace it by the effective length, l_e, since the square root portion in Equation (18) represents resistance induced by the river bed and the vegetation drag force (Verschoren et al., 2016). The deflected height is kept to simulate the relative submergence h/h_d since the inflection point of velocity profile is near the top of the deflected vegetation stem (Luhar and Nepf, 2011). In a similar manner, the h_v is replaced in Equation (19) by l_e. Therefore, by modifying Equations (18) and (19), following formulars are obtained:

$$\lambda = C_{\mathrm{D}} m d \frac{l_e}{h} \frac{C_{\mathrm{b}}^2}{C^2}, \text{ and} \quad (20)$$

$$C = C_{\mathrm{b}} + \frac{\sqrt{g}}{\kappa} \ln\left(\frac{h}{h_d}\right) \sqrt{1 + \frac{C_{\mathrm{D}} m d l_e C_{\mathrm{b}}^2}{2g}}. \quad (21)$$

Equation (21) is used for calculating the bed shear stress, and Equation (20) is accounted for in the momentum equations in order to calculate the drag force exerted by vegetation.

5.3 Simulation scenario

The simulated river reach is generalized from a downstream reach of the Kizu River in Japan. The rectangular simulation domain is 250 m in width with a length of 10,000 m. The river reach had a constant longitudinal slope of 1/1140. Sediment diameter within the river reach is set to 4 mm (Takebayashi & Egashira, 2001) and finer (down to 1 mm) and larger (up to 10 mm) simulations are also conducted to see the effect of the grain size. The domain is discretized by 10 x 25 m^2 structural grids. The upstream boundary condition is given by discharge, and an unsteady water level is used as the downstream boundary condition. The mean bed shear stress and sediment diameter determined that the bedload transport is dominant (Dade and Friend, 1998). Bedload entering the domain is calculated using the equilibrium condition, and bedload flux is calculated by the M.P.M formula.

The initial topography is a channel with developed alternate bars (**Figure 5.2**). The alternate bar has a similar wavelength to the alternate bars in the Kizu River. Two hydrographs, one with

a weak flood impact and the other with relatively strong flood impact, are used in the simulation. One year-cycle of the hydrograph is shown in **Figure 5.3**, and 80 year-cycles of the floods are performed to ensure the morphology reached a dynamic steady state. The maximum discharge is set to 2,000 m^3/s, and the lowest discharge is set to 100 m^3/s, depending on the flood in the Kizu River. Vegetation is recruited at the beginning of each year-cycle. It is noteworthy that reproducing the morphological development in the Kizu River is not the target of this research and this study aims to compare the difference introduced by neglecting vegetation flexibility. Due to the limited simulation resources, updating the vegetation posture in a short time interval is difficult. Considering the relatively steady discharge and slow morphological change during floods, the posture of vegetation is updated every 1 hour.

The target vegetation considered in this study is a type of reedy grass, namely *Phragmites japonica.* Cases containing a consideration of flexibility and those neglecting flexibility are tested in this research (referred to as the flexible and rigid cases, respectively). The geometry of the vegetation and stem rigidity are based on field surveys (Hattori, 2005; Nakagawa et al., 1995). The same geometric parameters were used for both flexible and rigid vegetation, with the exception of Young's modulus. The drag coefficient of the blade, C_D, is set to one (Jang and Shimizu, 2007). Root depth is set to 0.3 m. Vegetation is washed out when the scouring depth reaches the root depth (Calvani et al., 2019). The buoyancy force of the stems is neglected. The carrying capacity is set to 40 m^{-2} in the simulation, and vegetation stem density grows linearly after the recruitment on the bare bed to reflect the expansion and recruitment of reedy grass in the real environment (Aoki et al., 2007; Nakagawa et al., 1995). The growth rate of stem density is given by Δm. Since there is limited data regarding the growth rate of stem density, multiple Δm values ranging from 5 to 40 m^{-2} per year are tested. The value Δm could be understood as a measure of the changing rate of vegetation stem density from sparse to dense cover. Two recruitment conditions are considered. One is that the vegetation could be recruited on bare bed with a relative height between 0.3 and 2 m (Tetsuya et al., 2003), and the other is that vegetation

could be recruited above 0.3 m without the upper limit. Parameters regarding the vegetation used in this study are provided in **Table 6**. Cases name and simulation conditions are listed in **Table 7**.

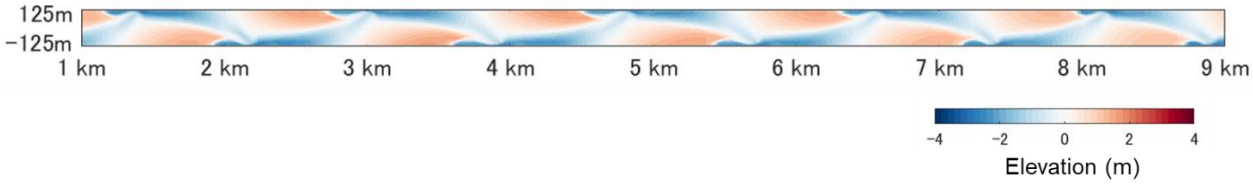

Figure 5.2 A plan view of the initial bed.

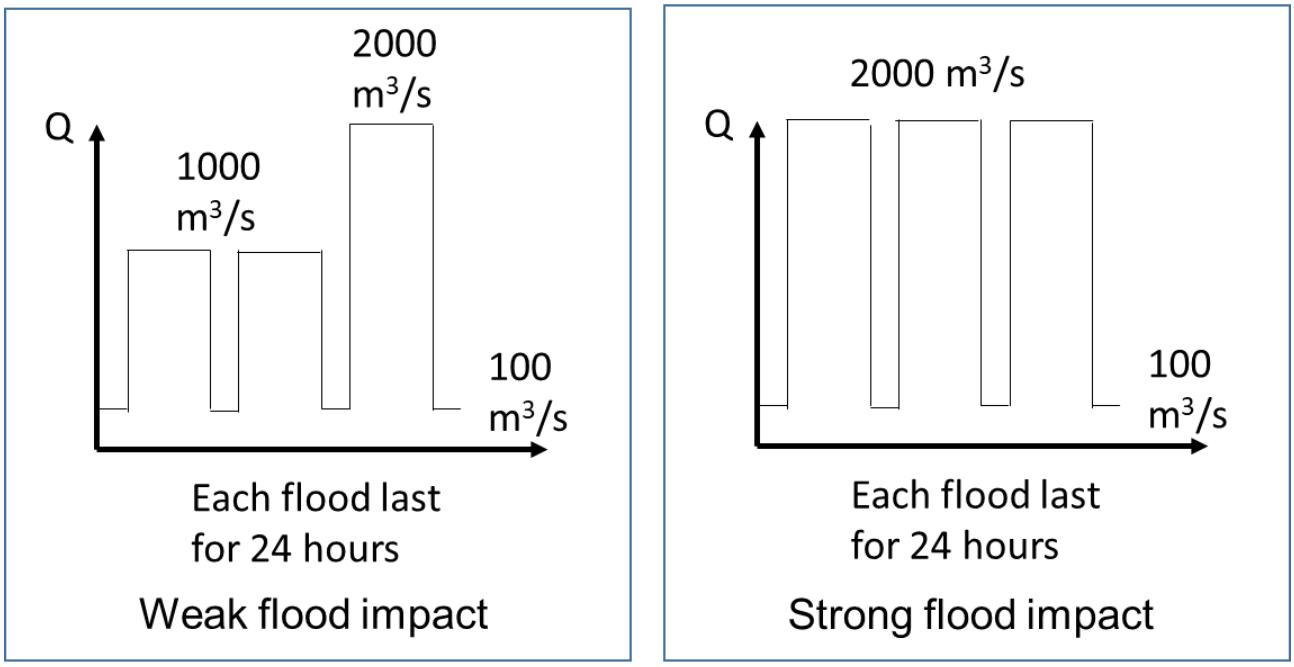

Figure 5.3 Hydrograph used in the simulation.

Table 6 Vegetation parameters

Items	Values	Reference
Vegetation height, l	1.5 m	Nakagawa et al. (1995)
Stem diameter	0.005 m	Vargas-Luna et al. (2016)
Root depth, r_d	0.3 m	Tetsuya et al. (2003)
Drag coefficient, C_D	1.0	Jang and Shimizu (2007)
Rigidity, EI	0.2 Nm^2	Hattori (2005)
Colonization water depth, h_c	0.1 m	Depending on the dry-wet criteria of the numerical model

Table 7 **Case name and related parameters. D stands for sediment diameter. G stands for the growth rate of stem density. F and R stands for flexible and rigid case, respectively.**

Scena-rio	Flow condition	Growth rate (G)	Bed sediment diameter (D)						Rigidity	Recruitment area
			1 mm	2 mm	4 mm	6 mm	8 mm	10 mm		
A	Weak flood impact (W)	5 $m^{-2}y^{-1}$			AW-G5-D4-F/R	AW-G5-D6-F/R			0.2 Nm^2	0.3 ~ 2 m
		10 $m^{-2}y^{-1}$	AW-G10-D1-F/R	AW-G10-D2-F/R	AW-G10-D4-F/R	AW-G10-D6-F/R	AW-G10-D8-F/R	AW-G10-D10-F/R		
		14 $m^{-2}y^{-1}$			AW-G14-D4-F/R					
		20 $m^{-2}y^{-1}$	AW-G20-D1-F/R	AW-G20-D2-F/R	AW-G20-D4-F/R	AW-G20-D6-F/R	AW-G20-D8-F/R	AW-G20-D10-F/R		
		40 $m^{-2}y^{-1}$			AW-G40-D4-F/R	AW-G40-D6-F/R				
B	Strong flood impact (S)	5 $m^{-2}y^{-1}$			BS-G5-D4-F/R	BS-G5-D6-F/R				
		10 $m^{-2}y^{-1}$	BS-G10-D1-F/R	BS-G10-D2-F/R	BS-G10-D4-F/R	BS-G10-D6-F/R	BS-G10-D8-F/R	BS-G10-D10-F/R		
		14 $m^{-2}y^{-1}$			BS-G14-D4-F/R					

Scena-rio	Flow condition	Growth rate (G)	Bed sediment diameter (D)						Rigidity	Recruitment area
			1 mm	2 mm	4 mm	6 mm	8 mm	10 mm		
		20 $m^{-2}y^{-1}$	BS-G20-D1-F/R	BS-G20-D2-F/R	BS-G20-D4-F/R	BS-G20-D6-F/R	BS-G20-D8-F/R	BS-G20-D10-F/R		
		40 $m^{-2}y^{-1}$			BS-G40-D4-F/R	BS-G40-D6-F/R				
C	Strong flood impact (S)	10 $m^{-2}y^{-1}$			CS-G10-D4-F/R				0.2 Nm^2	> 0.3 m
		14 $m^{-2}y^{-1}$			CS-G14-D4-F/R					
		20 $m^{-2}y^{-1}$			CS-G40-D4-F/R					
Rigidity sensitivity analysis (RS)	Weak flood impact (W)	10 $m^{-2}y^{-1}$			RSW-G10-F/R-1				0.1 Nm^2	0.3 ~ 2 m
		10 $m^{-2}y^{-1}$			RSW-G10-F/R-2				0.5 Nm^2	
		10 $m^{-2}y^{-1}$			RSW-G10-F/R-3				0.8 Nm^2	

5.4 Results

5.4.1 General geomorphology

River morphology at the end of the simulation of cases AW-G10-D4 and BS-G10-D4 are shown in **Figure 5.4**. In both cases, alternate bars had kept and are colonized by vegetation. In the AW-G10-D4 case, the pools induced by the alternate bars are shallower in the flexible case than which in the rigid case. With a weak flood impact (the lower panel of **Figure 5.4**), the vegetation covered bar top, while with strong flood impacts, the bar top is not covered by vegetation. In general, the flexibility does not significantly influence the bar geometry.

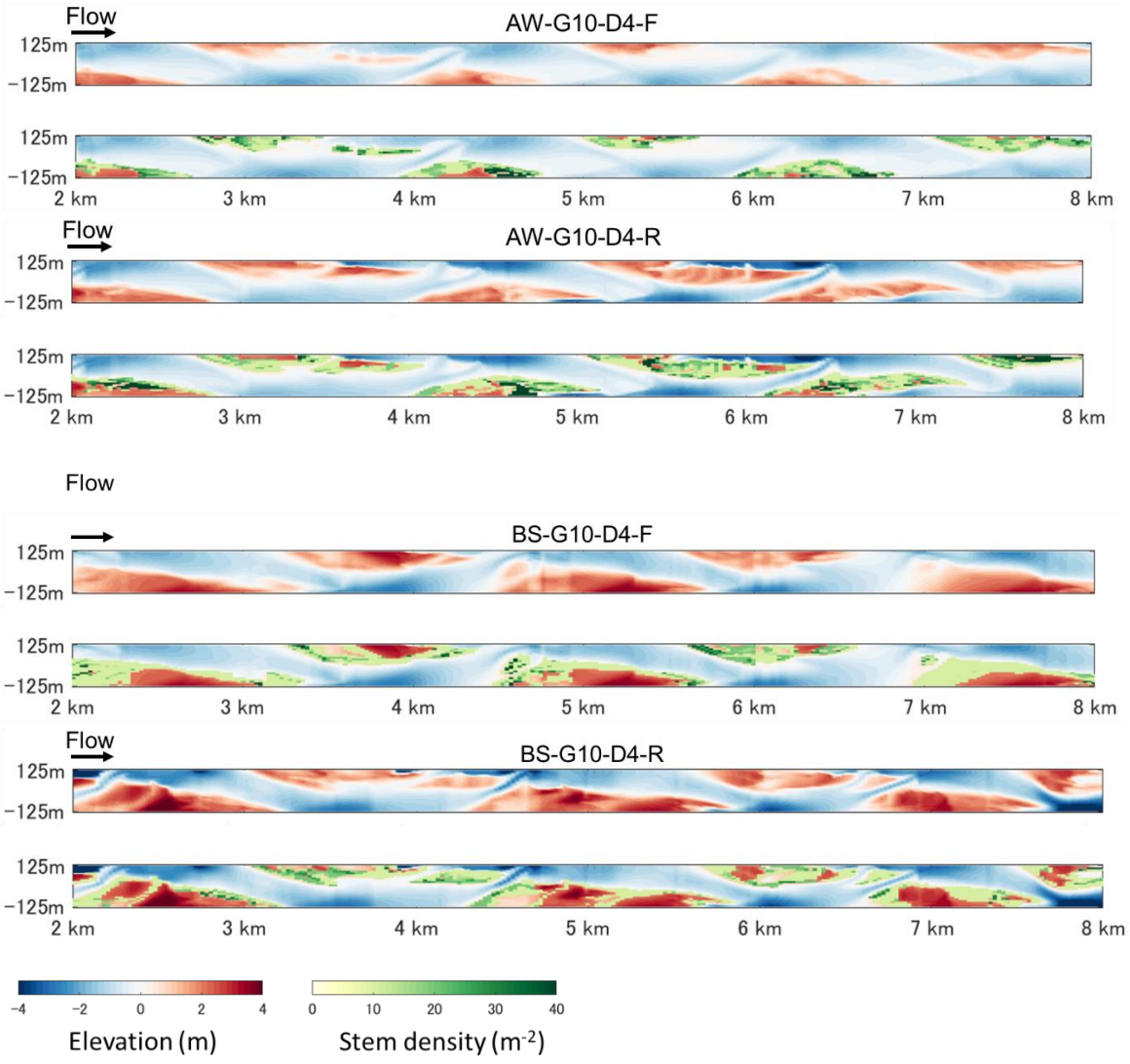

Figure 5.4 River morphology and vegetation cover at the end of the simulation in cases AW-G10-D4

and BS-G10-D4. The upper panel in each case shows the detrended bed elevation, and the lower panel shows the vegetation cover and stem density.

Figure 5.5 shows the time histories of relative height evolution of selected cases. The time histories have shown that the river morphology achieved a dynamic equilibrium state. The mean value of the relative height is similar between rigid and flexible cases, while the 95th percentile value is higher, and the 5th percentile value is smaller in the rigid case than the flexible case. The results show that the flexibility makes the distribution of relative height more concentrated. The results also show that the difference between flexible and rigid cases did not only occur after long-term evolution but appeared at almost the beginning of the simulation. The impact of floodplain has less influence on 5 percentile value when the stem growth rate is 20 $m^{-2}y^{-1}$. While the 5 percentile value is smaller in the case with strong flood impact when the stem growth rate equals to 10 $m^{-2}y^{-1}$.

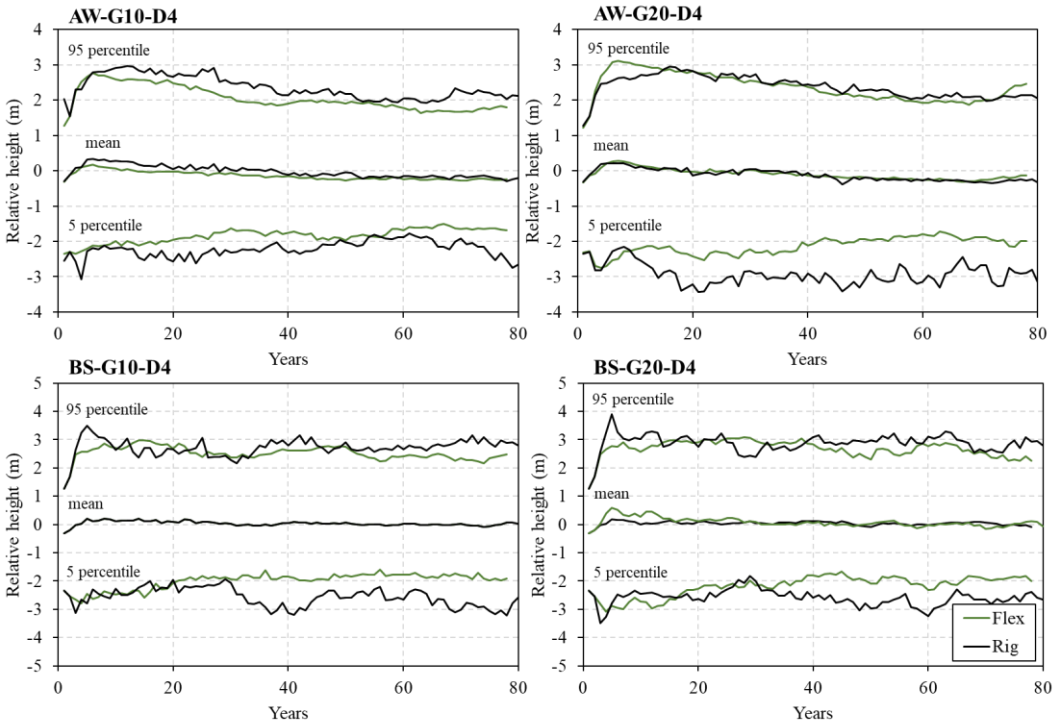

Figure 5.5 Time histories of 95th percentile, mean and 5th percentile value of the relative height. Case name is on the left-upper corner of each panel. The upper row shows the case with weak flood impact, and the lower row shows the case with strong flood impact. The left column shows the case has a slow growth rate, and the right column shows the case with a relatively faster growth rate.

The difference between flexible cases and rigid cases is shown by the distribution of relative height during the low discharge period in **Figure 5.6**. The mean value of the distribution is calculated from the last 30 years of each simulation. With the flexibility of vegetation considered, the erosion and deposition are reduced in the channel, and the area with a relative height between -2 and 0 m is larger than the rigid case. Regardless of the recruitment area (comparing the middle and the bottom row in **Figure 5.6**), the decreased deposition leads to a reduced habitat area in the flexible cases, showing a disadvantage brought by the flexibility. In the rigid case, the erosion increases more significantly with the increase of the growth rate than in the flexible case (e.g., the first row in **Figure 5.6**). Bi-modal distribution is observed in all rigid cases, while in the flexible case, the right peak of the bi-modal distribution is damped. With the increase of vegetation stem growth rate, the maximum peak value of the distribution reduces gradually. Compared to the reduced erosion, the reduced deposition appeared to be more significant in flexible cases when the stem density growth rate is higher (e.g., case AW-G20-D4).

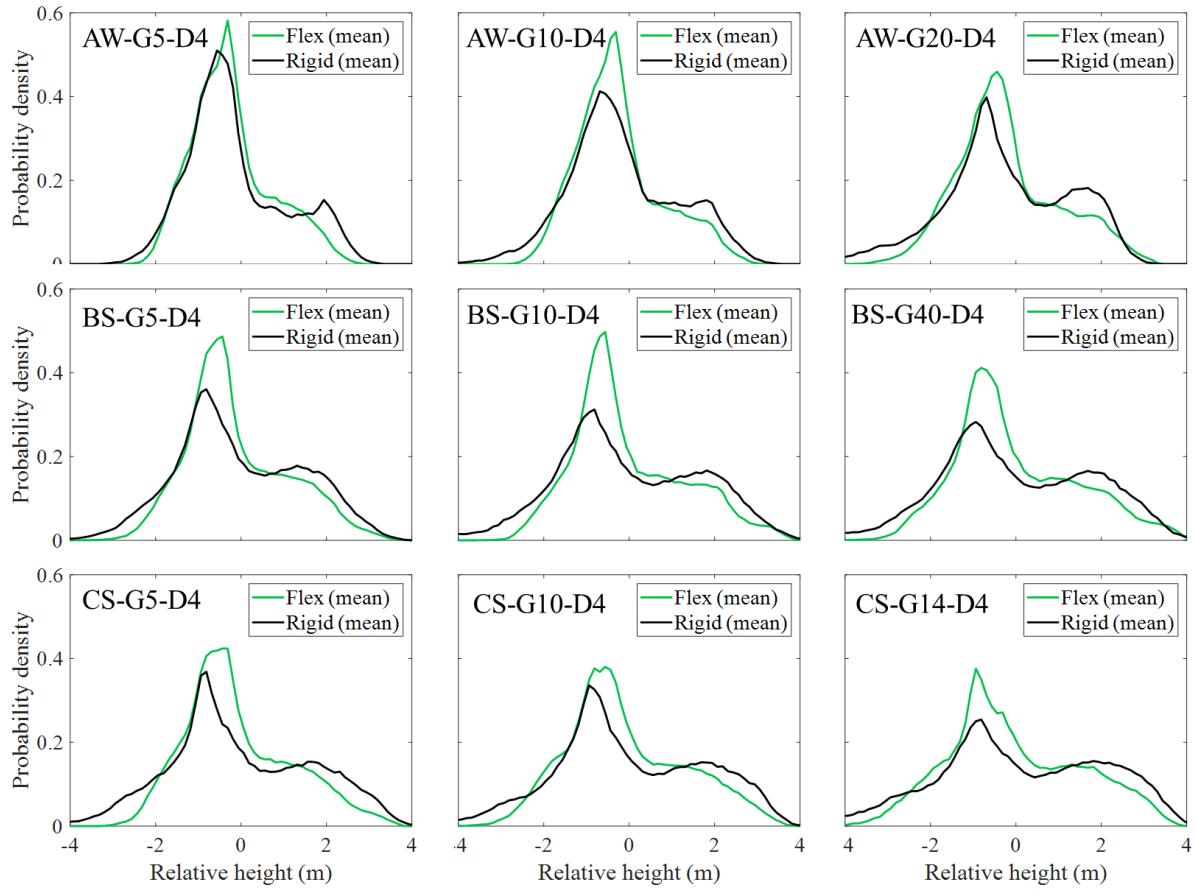

Figure 5.6 Distribution of relative height during the period of low discharge (Q=100 m^3/s). Each column has the same growth rate of the stem density. The first and the second row show cases undergoing different flood impact, and the third row shows cases without the upper limit of the recruitment zone.

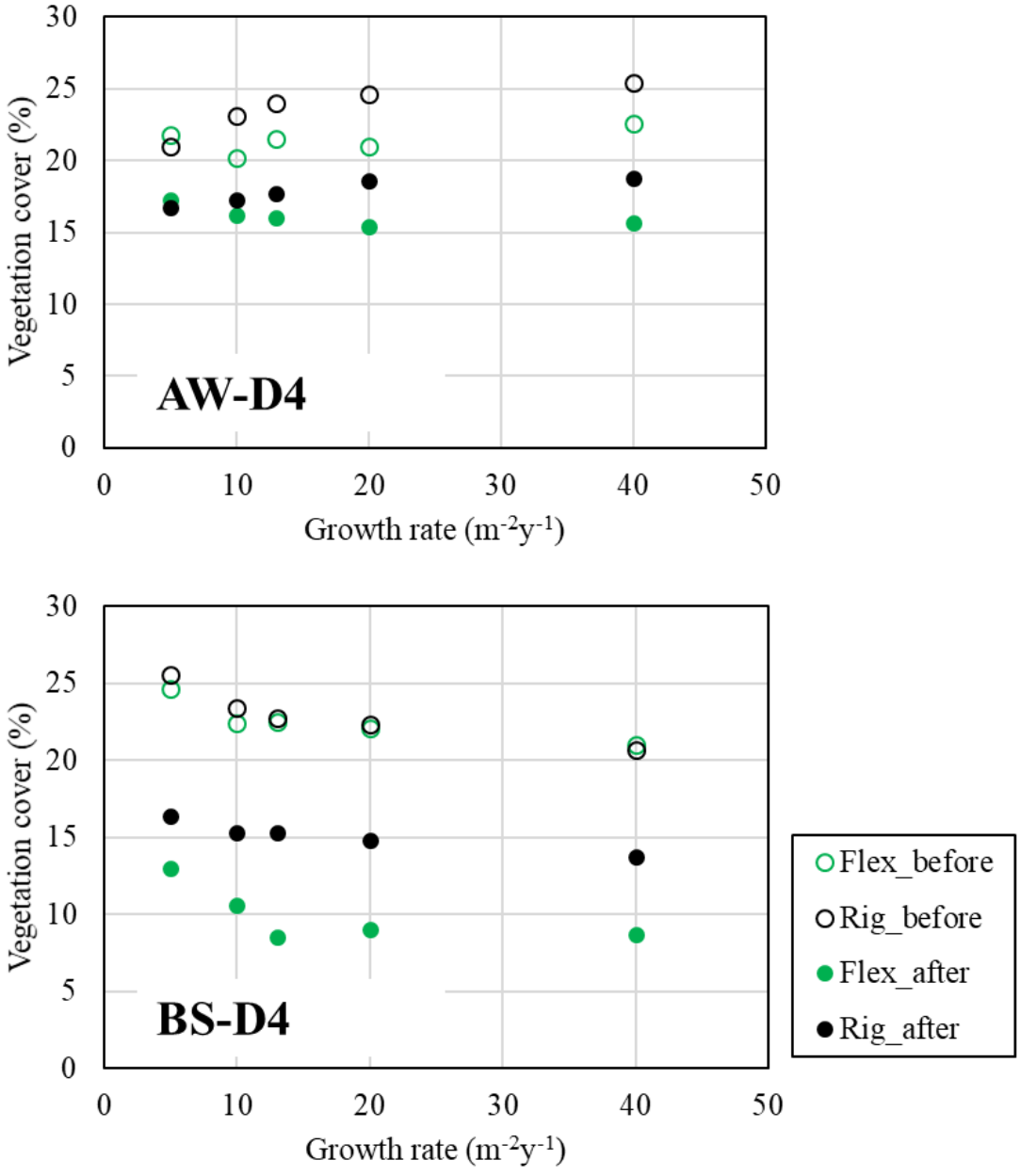

Figure 5.7 Mean value of vegetation cover before and after each year cycle of floods. Upper panel shows the cases with weak flood impact and the lower panel shows the cases with strong flood impact.

5.4.2 Vegetation cover

The vegetation cover before and after each year-cycle is shown in **Figure 5.7**. With a weak flood impact(the upper plot in **Figure 5.7**), the vegetation cover before each year-cycle is higher in the rigid case except when the growth rate equals to 5 $m^{-2}y^{-1}$. The vegetation area destroyed during the flood is similar between cases. Therefore, the vegetation area left after floods were smaller in the flexible cases than the rigid cases, which implies that the difference between flexible and rigid cases is mainly induced by reduced roughness. With a greater flood impact (the bottom plot in **Figure 5.7**), the vegetation cover before each year is similar between the flexible and rigid cases. However, the vegetation destroyed by the floods is more if the flexibility is accounted for. Thus, the vegetation cover after the flood is less in the flexible case. In cases with strong flood impacts, the difference brought by considering flexibility could come from the larger vegetation cover and reduced roughness. The results show that flexibility could be a disadvantage, i.e., smaller habitat area and higher vulnerability, for the vegetation. With the increase of stem density growth rate, the vegetation cover ratio before each year cycle decreases. The vegetation cover reduces because deposition in dense vegetation is less compared to sparse vegetation (Zong and Nepf, 2011).

5.4.3 Hydrodynamic during flood

Water depth during the floods is shown in **Figure 5.8**. With flexible vegetation, the water depth is shallower than the rigid cases. With the increase of growth rate, water depth increased in both flexible and rigid cases. Compared to total water depth, the reduced water depth is insignificant. **Figure 5.9** shows the relation between Shields stress in vegetation patches and stem density growth rate. Shields stress is higher in the flexible cases due to reduced roughness. The difference of the Shields stress between flexible and rigid cases decreased with the increase of the growth rate.

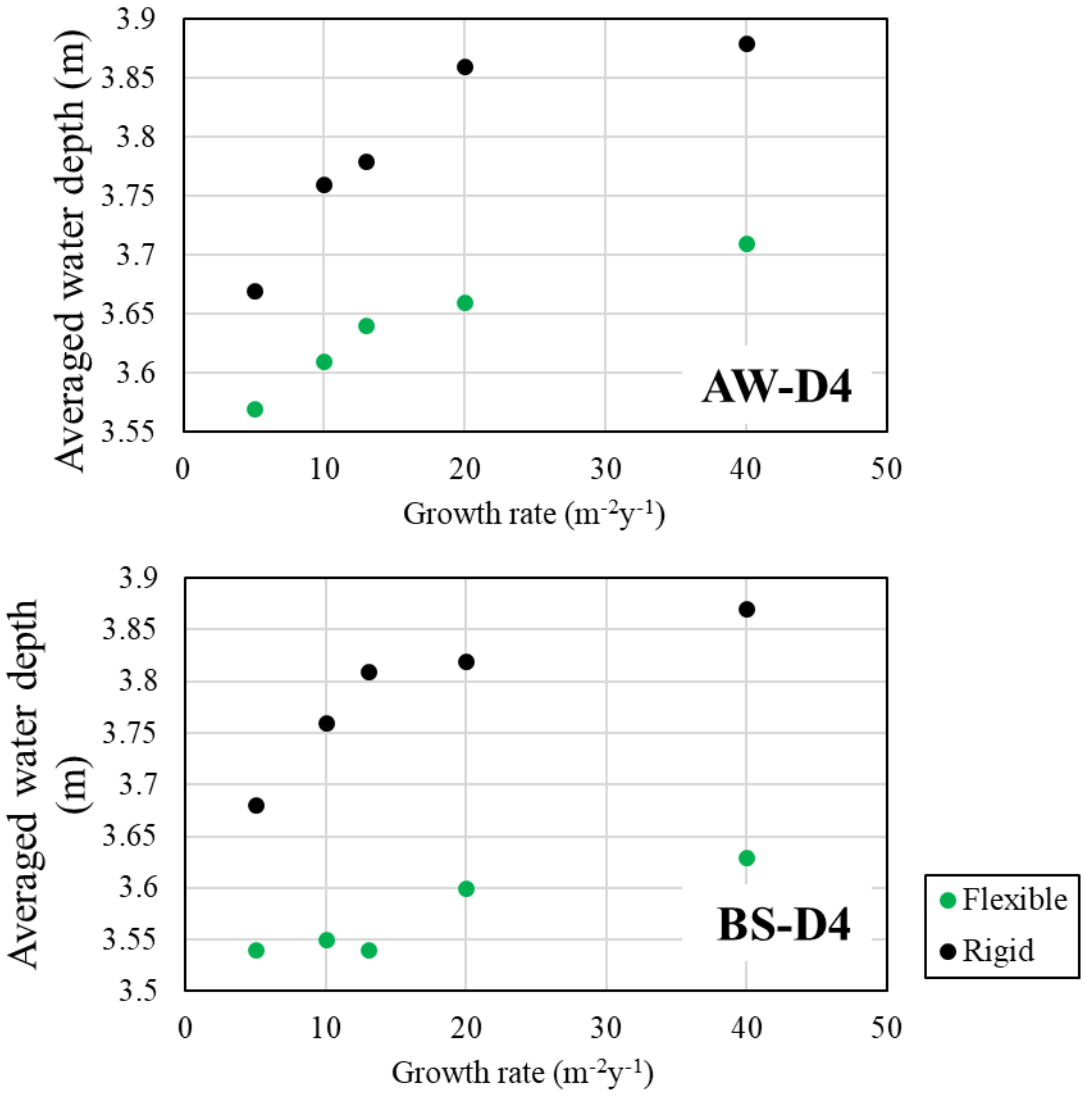

Figure 5.8 Averaged water depth in vegetation patch during floods (Q=2,000 m^3/s). Upper panel shows the cases with weak flood impact and the lower panel shows the cases with strong flood impact.

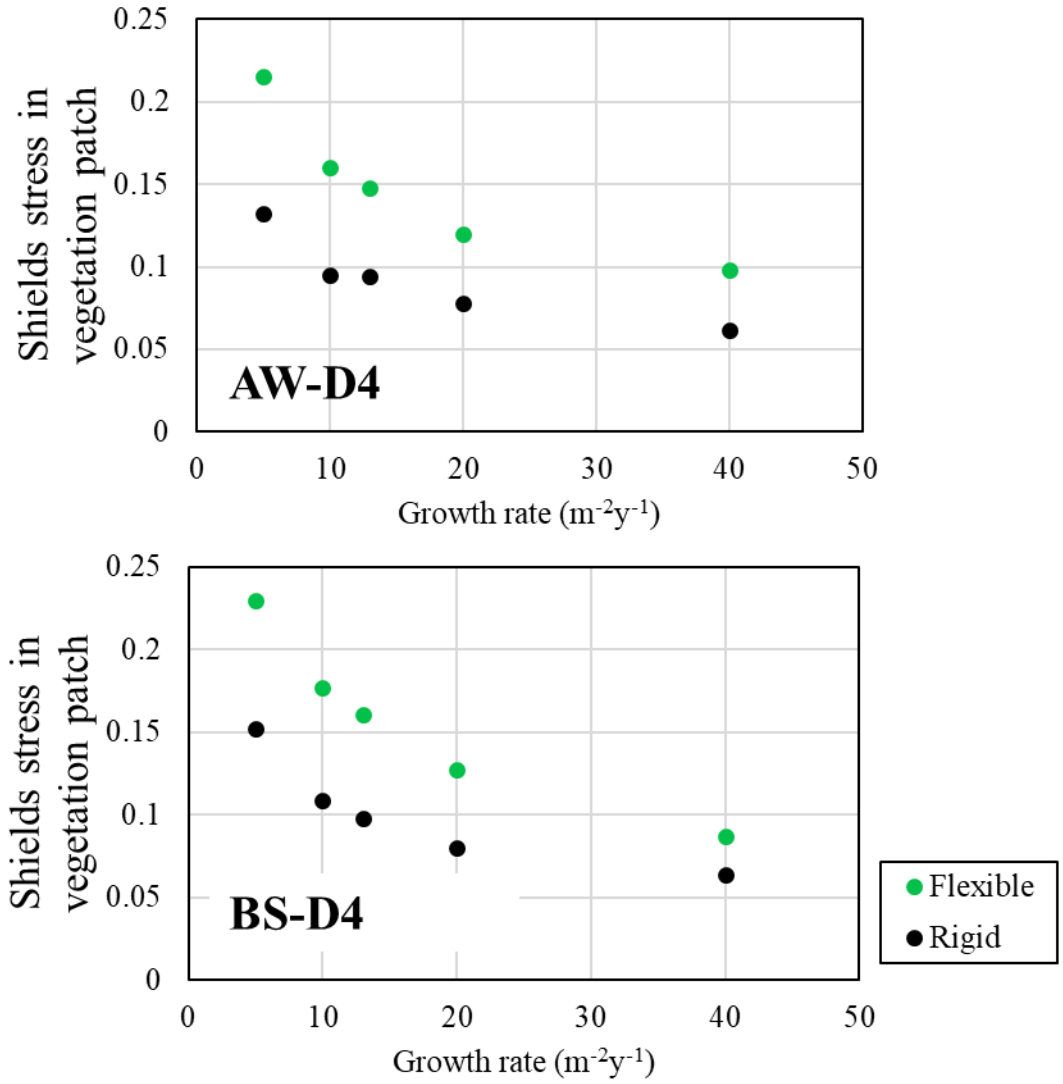

Figure 5.9 Shields stress in vegetation patch during floods (Q=2,000 m^3/s). Upper panel shows the cases with weak flood impact and the lower panel shows the cases with strong flood impact.

The change of active width, which is the channel width with bedload transport during floods (during the larger flood if the scenario is weak flood impact), with the varying growth rate of stem density is shown in **Figure 5.10**. When the growth rate was 5 $m^{-2}y^{-1}$, the active width in different cases is similar. With the increase of growth rate, the active width became narrower, and the difference between the rigid and flexible case become greater. The maximum difference is close to 20 m, which is about 10% of active width in the rigid case when the growth rate is 20 and 40 $m^{-2}y^{-1}$

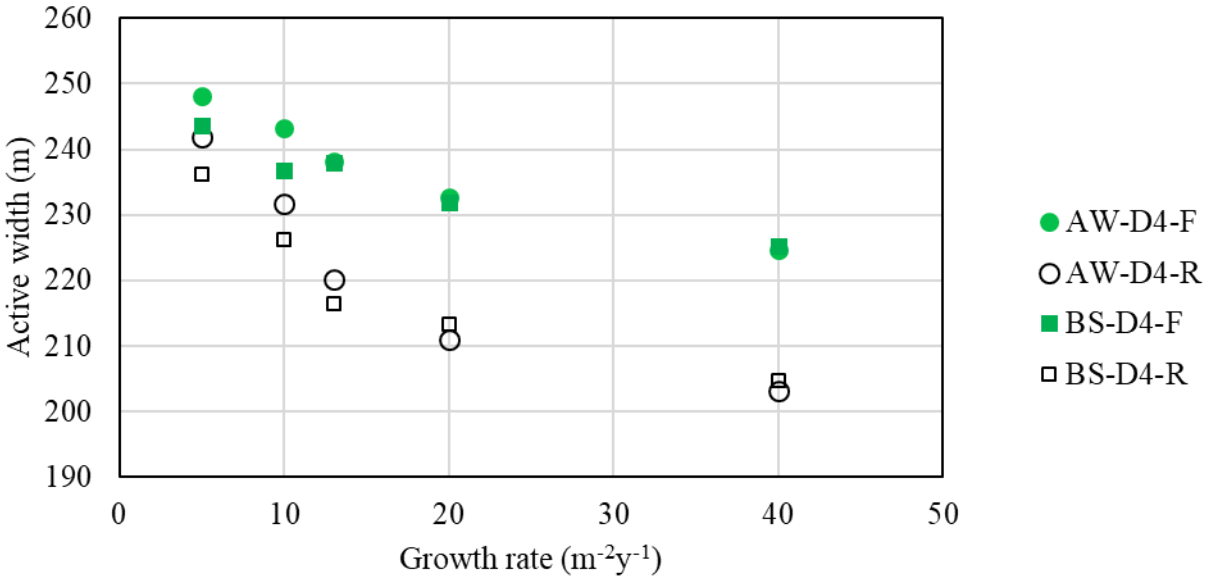

Figure 5.10 Active width with the varying growth rate of stem density.

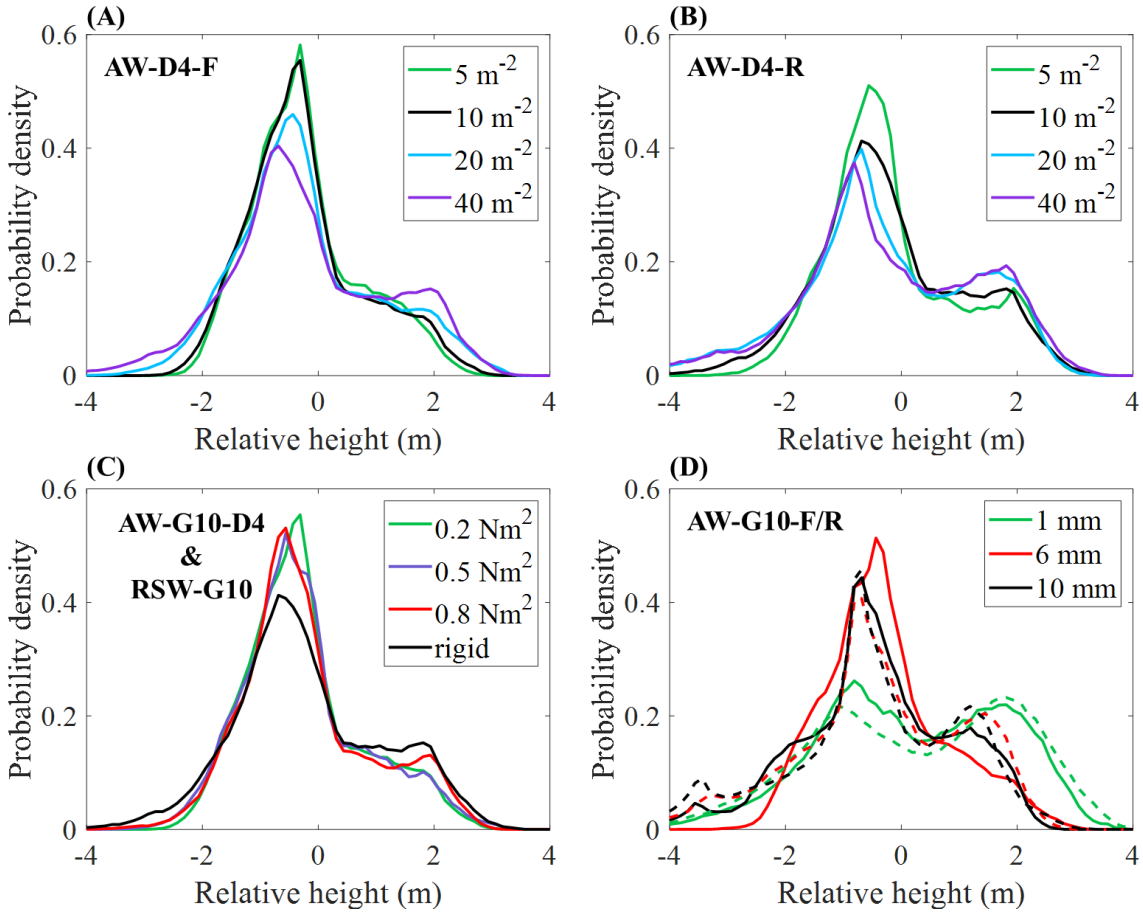

Figure 5.11 (A) Sensitivity to the growth rate of stem density with flexible vegetation. (B) Sensitivity to stem growth rate with rigid vegetation. (C) Sensitivity to rigidity. (D) Sensitivity to sediment diameter (solid lines represent flexible cases and dashed lines represent the rigid cases.).

5.4.4 Sensitivity analysis

The sensitivity of the relative height distribution to different parameters is shown in **Figure 5.11**. **Figure 5.11**(A) and (B) shows the sensitivity to various of growth rate of the flexible and rigid cases, respectively. With an increasing stem density growth rate, the erosion in the main channels and the deposition in the floodplains increase. In the rigid cases (**Figure 5.11** (B)), the change of distribution is relatively small between 20 $m^{-2}y^{-1}$ and 40 $m^{-2}\,y^{-1}$ cases. While in the flexible case (**Figure 5.11**(A)), erosion and deposition keep increasing when the growth rate increase from 20 $m^{-2}y^{-1}$ and 40 $m^{-2}\,y^{-1}$. The results suggest that the influence of vegetation has reached an upper limit in the rigid cases. In addition, the distribution has a similar shape between 40 $m^{-2}\,y^{-1}$ case in **Figure 5.11**(A) and 10 $m^{-2}\,y^{-1}$ case in **Figure 5.11**(B). **Figure 5.11**(C) shows the sensitivity of the distribution to varying rigidity. With increase in rigidity, the difference in the distribution between flexible and rigid cases become smaller: the effect of damping the right peak of the distribution reduces in the flexible case. **Figure 5.11**(D) shows the sensitivity of the distribution to sediment diameter. The results show that with finer (1 mm) and coarser (10 mm) sediment, the effect of neglecting flexibility could be small.

To quantitatively compare the differences in the relative height distributions between the rigid and flexible cases, the Euclidean distances between the relative height distribution of rigid and flexible cases is calculated and are shown in **Figure 5.12**. The Euclidean distance is frequently used as a metric to measure similarity in many fields, e.g., image recognition (Malkauthekar, 2013). If the Euclidean distance equals to 0, the two distributions are same. The difference between flexible and rigid cases reduces monotonously with the increase of the stem rigidity (**Figure 5.12**A), while a peak value exists with varying growth rate and sediment diameter (**Figure 5.12**B and C). Interestingly, the maximum difference only occurs when the bed material is fine or medium pebble (4 to 8 mm in the diamater, Blair and McPherson, 1999), which implies the flexibility can be neglected in a river with a coarse gravel bed (e.g., d > 8 mm in this study). Since the suspended load transport is dominant when the sediment diameter equal to 1 mm and

the sediment transport cannot be well predicted by the M.P.M. formula, the difference in the river with fine sediment still needs more investigation.

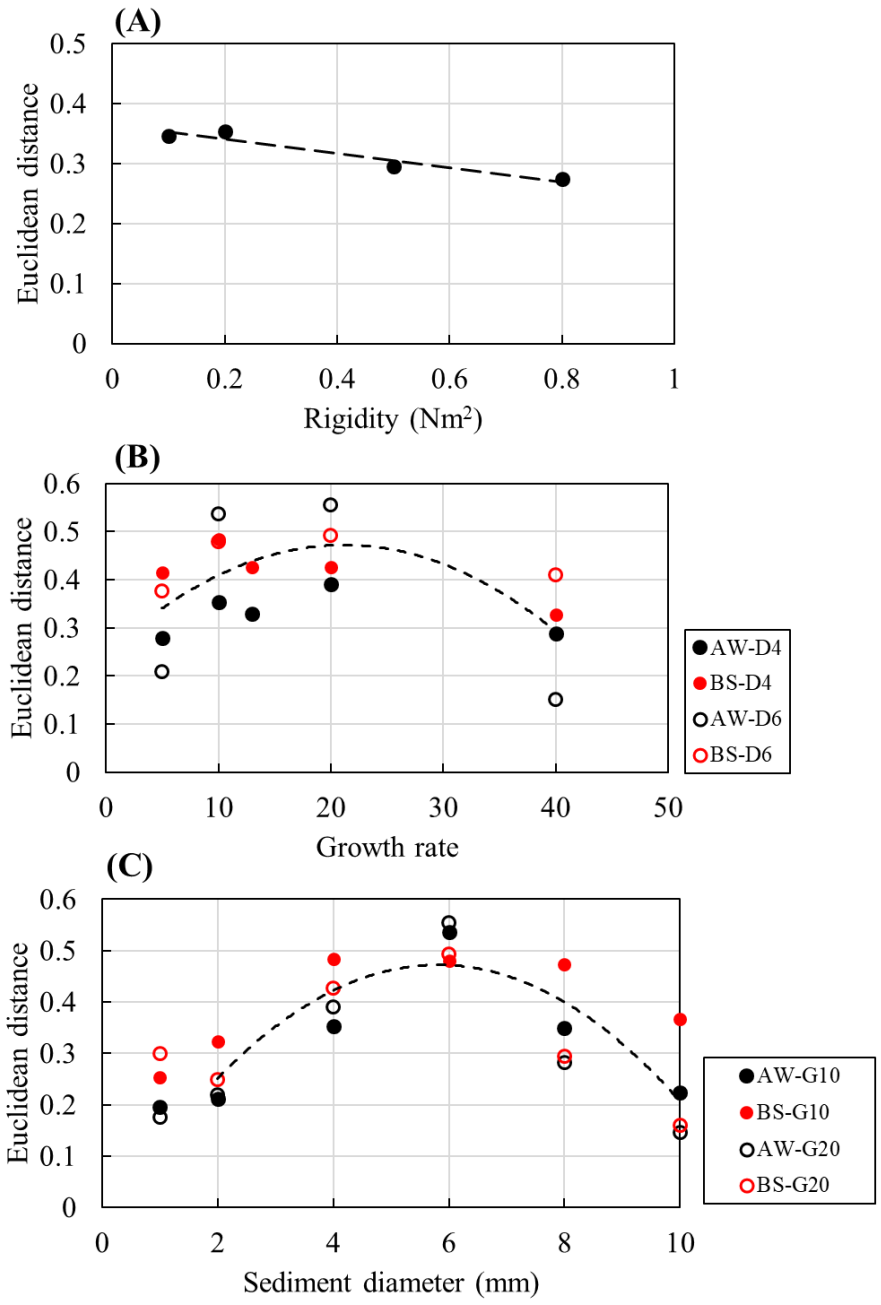

Figure 5.12 Euclidean distance of relative height distribution between rigid and flexible cases in scenarios A (weak flood) and B (strong flood) with varying (A) stem rigidity, (B) growth rate of stem density, and (C) the sediment diameter.

5.5 Discussions

A morphological simulation is employed combined with the vegetation model to investigate the effect of flexibility in the morphological simulation. The target river is a fine gravel-bed river with alternate bars. Although reproducing the real morphology is beyond the scope, the simulation shows some key features that are observed in earlier studies. For example, without the flexibility, the distribution of relative height is bi-modal (**Figure 5.11**B), which has been observed in an earlier numerical simulation aiming to study the effects of poplar on alternate bars (Jourdain et al., 2020) and also in the field study (Bertoldi et al., 2011). The erosion in the river is reduced due to the flexibility, which is consistent with flume experiment results (S. C. Chen et al., 2012). With increasing rigidity of the flexible stem, the influence of flexibility becomes smaller (**Figure 5.12**A), which agrees qualitatively with early numerical and flume experiments (Dijkstra and Uittenbogaard, 2010).

In the simulation, the major differences induced by flexibility are reducing erosion in the main channel and deposition on the floodplain. The reason is attributed to reduced bed roughness (**Figure 5.9**) and vegetation cover (**Figure 5.7**). The reduced deposition is partly attributed to the higher shields stress within the vegetation patch. Since higher Shields stress provides greater sediment carrying capacity, less deposition occurs in the vegetation patch. In addition, the vegetation cover in the flexible cases is less; hence the effect of vegetation in stabilizing the bars is mitigated. The effect of accounting the flexibility depends on the growth rate of stem density, stem rigidity, and bed material size. Based on the results, the flexibility should be considered if the bed material and vegetation growth rate fell in a specific range: the growth rate is between 10 to 20 $m^{-2}y^{-1}$ or the grain size is between 4 to 6 mm in this study. The flexibility effects can be neglected when the bed material is large gravel. With a vegetation that is more flexible than *P. Japonica*, the range of conditions (grain size and growth rate) within which the flexibility needs to be considered may change. The effect of flexibility needs further studies when the suspended load is dominant since currently the model is not designated to account for the suspended load.

A study regarding the suspended load effect performed by Box et al. (2019) that has shown net deposition in flexible foliage vegetation is higher than rigid leafless vegetation when considering suspended load deposition, but the increased deposition may also be induced by the vegetation foliage rather than flexibility.

In this study, the target vegetation is a kind of reedy grass, i.e., *P. Japonica*. The major effect of flexibility considered is its influence on bed resistance. The flexibility of *P. Japonica*. is not high compared to very flexible vegetation, e.g., eelgrass. With high flexibility, the vegetation stem may be prone to the flow and cover the river bed behind the vegetation stem, and deposition can be found (Sezaki et al., 2000). In such a situation, sedimentation may occur behind vegetation and erosion may be prevented. Such a phenomenon is not accounted for in the current model. The influence and significance of such phenomenon still need further investigation.

5.6 Conclusions

For this work, a simple bio-hydro-morphodynamic model accounting for the flexibility of vegetation is developed. The vegetation investigated in this study is a type of reedy vegetation that widely existed in the riparian environment, i.e., *Phragmites japonica*. The hydrodynamic and morphological evolution with and without considering the flexibility of the vegetation in a channel under the alternate bar regime is compared.

The consideration of flexibility in the simulation reduces the flow resistance induced by vegetation due to the posture reconfiguration. Thus, with flexibility, the water surface elevation is found to be lower, but the averaged Shields stress in the flexible vegetation patch is larger than rigid cases. River bed width with sediment transport has increased with flexible vegetation cover. Flexibility can be a disadvantage for vegetation habitat expansion. With flexibility considered, vegetation has less coverage than the corresponding rigid case. If the flexibility is neglected, the vegetation cover after floods will be overestimated.

The consideration of flexibility alters not only the river morphology in a long-term future but also the transitional process. The effect of accounting for vegetation flexibility depends on the growth rate of stem density, stem rigidity, and bed materials. With the consideration of flexibility, the distribution of elevation is concentrated due to reduced erosion and deposition. Without flexibility considered, the elevation shows a bi-modal distribution, while flexibility damps the right peak of the bi-modal distribution. The difference without considering flexibility maximizes when the growth rate and bed material diameter were in specific ranges (around 20 m^{-2} y^{-1} in the growth rate of and around 6 mm in diameter), and the difference monotonously decreases with the increase of the stem rigidity. The results suggest that the influence of flexibility could be neglected except in a narrow range that is mainly determined by vegetation stem density and bed material.

6 Conclusions and future research

6.1 Conclusions

In this thesis, the effects of vegetation, i.e., vegetation distribution and vegetation flexibility, on the transitional process and equilibrium state of gravel bed river morphology development are discussed. The motivation of this research is to compensate the bio-hydro-geomorphology interaction triangle and deepen the understanding of the vegetation's role in the interaction. Gravel bed rivers are considered due to the sensitivity of river morphology to vegetation expansion. Fine sediment effect is neglected since uniform sediment model is considered enough to predict the interaction between vegetation and river morphology (Millar, 2005). Three problems, (1) the effects of uniformly distributed vegetation on floodplain, (2) the effects of vegetation distribution on river morphology development, and (3) the effects of vegetation flexibility are studied. The problems are investigated by depth-averaged shallow water model and field survey. Vegetation effects in the numerical model is accounted for by changing bed roughness or adding a source term to the momentum equations. The results have shown that vegetated floodplain has significant influence on transitional process of river morphological change; thus, it is valuable to modify the low water channel shape to control its transitional morphological response. The effects of vegetation transect distribution and the effect of vegetation flexibility on reach-scale river morphology has been firstly demonstrated. The major conclusions are shortly summarized as follows:

(1) Influence of uniformly distributed floodplain vegetation on transitional river morphological development

In Chapter 2, the role of initial low water channel planform and floodplain vegetation is compared. It is demonstrated that floodplain vegetation could play a more important role than the initial low water channel planform. It is found that without floodplain vegetation, braiding

can easily develop from initial low water channel. With vegetation coverage on floodplain, the bank erosion is enhanced at the outer bank, and meandering with sinuosity close to gravel rivers in the field can develop from both initial channels in the migration regime and no-migration regime. Vegetation recruitment on bare bars is not a necessary condition for meandering initiation in vegetated gravel rivers, and vegetated floodplain combined with a suitable initial channel is one sufficient condition. Suitable initial channel is not restricted to the channel in the no-migration regime: channel that forms alternate bar is also possible for meandering initiation. The meandering can be initiated is because the bar growth is restricted to the lateral direction and its downstream migration is limited by vegetation.

Given the results in Chapter 2, it is known that the low water channel combined with a vegetated floodplain has important influence on the transitional response of river morphology to flood impact, artificial modification of the planform can be employed to achieve certain engineering targets, i.e., reduce embankment failure risks and remove vegetation cover by activate morphological change. In Chapter 3, effects of different planform modification measures have been studied. In a vegetated braided river, channel reopening and closing can be applied as modification measures. However, channel reopening is not always effective in activate morphological change. In this study, it is demonstrated that by combining channel reopening and channel closing in the braiding network, flow can be concentrated in the reopened channel and improve its efficiency.

(2) Influence of vegetation distribution along river transect on river morphology

Vegetation distribution along river transect is a result of stochastic hydrological conditions, morphological change and vegetation species. The distribution of vegetation along river transect can also be resulted from artificial impact, e.g., vegetation removal. The problem regarding the effect of vegetation distribution is generalized and studied by varying the habitat extension in Chapter 4. The reason that induces various vegetation distribution is not specifically discusses. Two patterns of distribution are investigated in this study. The results show that transverse

distribution of vegetation significantly influences statistical characteristics of braided river. The bed elevation statistical characteristics show distinct relationship with the increase of vegetation habitat ratio. The variance positively relates to the increase of vegetation habitat area. The skewness and the kurtosis are negatively and positively related to the increase of vegetation habitat area, respectively, when the vegetation establishes habitat near the low channel. The skewness and the kurtosis have opposite relationship with the increase of vegetation habitat area when the vegetation establishes habitat on the bar top. The difference can be explained by the difference in the location where major morphological change happens. The results suggest that river management measures that changes the vegetation distribution along river transect should take into account that different measures may lead to different river morphological change.

(3) Influence of vegetation flexibility on river morphology

In Chapter 5, the effect of vegetation flexibility on river morphology is investigated in a fine gravel bed river with alternate bars. The role of flexibility in reach-scale river morphology simulation has been neglected for a long time. The target vegetation is a type of reedy grass. The results show that with the consideration of flexibility, erosion and deposition both reduce in the river. In addition, the bi-modal distribution of the river relative elevation distribution is damped by accounting for the vegetation flexibility. The influence of flexibility is related to several parameters, that is vegetation stem growth rate, stem rigidity and the bed material size. The influence of flexibility decreases with the increase of stem rigidity. The influence achieves a maximum value when the grain size or the stem growth rate falls in a certain range. The influence of flexibility can be neglected if the bed grain size is large or the vegetation stem density is sparse. For river managers, considering the flexibility of grass type vegetation can give a better estimation about floodplain and vegetation habitat formation rate, and improve the efficiency in vegetation management.

(4) Influence of water edge vegetation and its implications for vegetation management

In Chapter 2, the floodplain vegetation is shown to have significant influence on the transitional river morphology due to it affects the sediment transport in the interface between floodplain and main channel. In Chapter 4, vegetation near the water edge is also proved to affect the equilibrium morphology in a braided river. Smaller cover of water edge vegetation may induce relatively significant morphological change compared to vegetation on bar tops. The results of Chapter 2 and Chapter 4 suggest that river management regarding riparian vegetation should better focus on the vegetation near water edge. Vegetation clearance on location with high relative elevation (e.g., floodplain or bar top), may be less efficient. Early research has implied the water edge vegetation plays an important role in vegetation recruitment by promoting fine sediment deposition. In Chapter 5, the results suggest the deposition induced by water edge vegetation is highly related to its stem density growth rate and flexibility. Sparse and flexibility vegetation may be less efficient in creating habitat by promoting deposition. The results also imply that it is necessary to study other factors, e.g., fine sediment and vegetation morphology, for understanding the vegetation recruitment and expansion near water edge.

6.2 Future work

In this study, several factors in the bio-hydro-geomorphology triangle are studied. The investigation is mainly based on numerical simulations. There are still more works that needs to be done.

In Chapter 2, short-term river morphology development is investigated with different floodplain vegetation cover. In the numerical model, the effect of root system on stabilizing river bank is not accounted for explicitly. The sediment in the model is uniform and classified as gravel, while in the field sediment on the floodplain is finer. A sophisticated numerical model is needed to investigate such factors.

In Chapter 3, channel reopening and closing is proved to be potential modification measure of the initial river planform to reduce bank failure and activate morphological change. The

results have shown modification of the braiding river network can be a possible way to influence the short-term morphological response of braiding river. Studies have shown that network concept can be applied in braiding rivers (Marra et al., 2014). However, such concept has not been used in river management yet. By studying the relationship between network characteristics and river morphological response, it is possible to use network concept as a convenient and cheap approach to perform river management in a large scale rather than employing time-consuming numerical simulations.

In Chapter 4, influence of vegetation distribution along river transect is studied. However, the study does not take into account the stochastic properties of hydrological condition explicitly. Although several numerical simulation has considered a real discharge time series, e.g., Oorschot et al. (2018), it is not enough to predict long term distribution of vegetation. Gurnell et al. (2012) has demonstrated by a one dimensional model that flood with same stochastic properties can generate different vegetation distribution. To predict long term morphological change undergoing vegetation effects, the consideration of variability of hydrological condition is necessary. However, such goal is difficult to achieve since expensive computational resources are necessary and current model must be coupled with underground water model. More novel works are still needed.

In Chapter 5, the effect of flexibility has been studied. Since flexible vegetation may play an important role in vegetation expansion process by promoting fine sediment accretion, it is necessary to study the effect of non-uniform sediment influence when considering flexible vegetation. When studying the effect of flexibility on fine sediment deposition, different posture of flexible vegetation should be considered, since the posture of flexible vegetation influences the turbulence, which is related to fine sediment transport in vegetation patch.

7 References

Amlin, N., Rood, S.B., 2002. Comparative tolerances of riparian willows and cottonwoods to water-table decline. Wetlands 22, 338–346.

Aoki, S., Tanaka, N., Yagisawa, J., 2007. Effects of flood disturbance on the morphology, productivity and runner-expansion of Phragmites japonica 51, 1255–1260.

Asahi, K., Shimizu, Y., Nelson, J., Parker, G., 2013. Numerical simulation of river meandering with self-evolving banks. Journal of Geophysical Research: Earth Surface 118, 2208–2229. https://doi.org/10.1002/jgrf.20150

Baar, A.W., Boechat Albernaz, M., van Dijk, W.M., Kleinhans, M.G., 2019. Critical dependence of morphodynamic models of fluvial and tidal systems on empirical downslope sediment transport. Nature Communications 10, 4903. https://doi.org/10.1038/s41467-019-12753-x

Baptist, M.J., Babovic, V., Uthurburu, J.R., Keijzer, M., Uittenbogaard, R.E., Mynett, A., Verwey, A., 2007. On inducing equations for vegetation resistance. Journal of Hydraulic Research 45, 435–450. https://doi.org/10.1080/00221686.2007.9521778

Barfield, B.J., Tollner, E.W., Hayes, J.C., 1979. Filtration of Sediment by Simulated Vegetation I. Steady-State Flow with Homogeneous Sediment. Transactions of the ASAE 22, 0540–0545. https://doi.org/10.13031/2013.35057

Bertoldi, W., Gurnell, A.M., Drake, N.A., 2011. The topographic signature of vegetation development along a braided river: Results of a combined analysis of airborne lidar, color air photographs, and ground measurements. Water Resources Research 47, 1–13. https://doi.org/10.1029/2010WR010319

Bertoldi, W., Siviglia, A., Tettamanti, S., Toffolon, M., Vetsch, D., Francalanci, S., 2014. Modeling vegetation controls on fluvial morphological trajectories. Geophysical Research Letters 41, 7167–7175. https://doi.org/10.1002/2014GL061666

Bertoldi, W., Welber, M., Gurnell, A.M., Mao, L., Comiti, F., Tal, M., 2015. Physical modelling of the combined effect of vegetation and wood on river morphology. Geomorphology 246, 178–187. https://doi.org/10.1016/j.geomorph.2015.05.038

Blair, T.C., McPherson, J.G., 1999. Grain-size and textural classification of coarse sedimentary particles. Journal of Sedimentary Research 69, 6–19. https://doi.org/10.2110/jsr.69.6

Bolla Pittaluga, M., Repetto, R., Tubino, M., 2003. Channel bifurcation in braided rivers: Equilibrium configurations and stability. Water Resources Research 39, 1–13.

https://doi.org/10.1029/2001WR001112

Boothroyd, R.J., Hardy, R.J., Warburton, J., Marjoribanks, T.I., 2017. Modeling complex flow structures and drag around a submerged plant of varied posture. Water Resources Research 53, 2877–2901. https://doi.org/10.1002/2016WR020186

Boothroyd, R.J., Hardy, R.J., Warburton, J., Marjoribanks, T.I., 2016. The importance of accurately representing submerged vegetation morphology in the numerical prediction of complex river flow. Earth Surface Processes and Landforms 41, 567–576. https://doi.org/10.1002/esp.3871

Box, W., Västilä, K., Järvelä, J., 2019. The Interplay between Flow Field, Suspended Sediment Concentration, and Net Deposition in a Channel with Flexible Bank Vegetation. Water 11, 2250. https://doi.org/10.3390/w11112250

Braudrick, C.A., Dietrich, W.E., Leverich, G.T., Sklar, L.S., 2009. Experimental evidence for the conditions necessary to sustain meandering in coarse-bedded rivers. Proceedings of the National Academy of Sciences of the United States of America 106, 16936–16941. https://doi.org/10.1073/pnas.0909417106

Bywater-Reyes, S., 2015. The influence of pioneer riparian vegetation on river processes from the plant to reach scale. University of Montana.

Bywater-Reyes, S., Diehl, R.M., Wilcox, A.C., 2018. The influence of a vegetated bar on channel-bend flow dynamics. Earth Surface Dynamics 6, 487–503. https://doi.org/10.5194/esurf-6-487-2018

Calvani, G., Francalanci, S., Solari, L., 2019. A Physical Model for the Uprooting of Flexible Vegetation on River Bars. Journal of Geophysical Research: Earth Surface 2018JF004747. https://doi.org/10.1029/2018JF004747

Camporeale, C., Perucca, E., Ridolfi, L., Gurnell, A.M., 2013. Modeling the interactions between river morphodynamics and riparian vegetation. Reviews of Geophysics 51, 379–414. https://doi.org/10.1002/rog.20014

Camporeale, C., Ridolfi, L., 2006. Riparian vegetation distribution induced by river flow variability: A stochastic approach. Water Resources Research 42, 1–13. https://doi.org/10.1029/2006WR004933

Carson, M.A., 1984. The meandering-braided river threshold: A reappraisal. Journal of Hydrology 73, 315–334. https://doi.org/10.1016/0022-1694(84)90006-4

Carter Johnson, W., 2000. Tree recruitment and survival in rivers: influence of hydrological processes. Hydrological Processes 14, 3051–3074. https://doi.org/10.1002/1099-1085(200011/12)14:16/17<3051::AID-HYP134>3.0.CO;2-1

Castro, J.M., Thorne, C.R., 2019. The stream evolution triangle: Integrating geology, hydrology, and

biology. River Research and Applications rra.3421. https://doi.org/10.1002/rra.3421

Chen, S.C., Kuo, Y.M., Yen, H.C., 2012. Effects of submerged flexible vegetation and solid structure bars on channel bed scour. International Journal of Sediment Research 27, 323–336. https://doi.org/10.1016/S1001-6279(12)60038-9

Chen, Z., Ortiz, A., Zong, L., Nepf, H., 2012. The wake structure behind a porous obstruction and its implications for deposition near a finite patch of emergent vegetation. Water Resources Research 48, 2012WR012224. https://doi.org/10.1029/2012WR012224

Cooper, D.J., Merritt, D.M., Andersen, D.C., Chimner, R.A., 1999. Factors controlling the establishment of Fremont cottonwood seedlings on the Upper Green River, USA. Regulated Rivers: Research & Management 15, 419–440. https://doi.org/10.1002/(SICI)1099-1646(199909/10)15:5<419::AID-RRR555>3.0.CO;2-Y

Corenblit, D., Steiger, J., Gurnell, A.M., Tabacchi, E., Roques, L., 2009. Control of sediment dynamics by vegetation as a key function driving biogeomorphic succession within fluvial corridors. Earth Surface Processes and Landforms 34, 1790–1810. https://doi.org/10.1002/esp.1876

Corenblit, D., Vautier, F., González, E., Steiger, J., 2020. Formation and dynamics of vegetated fluvial landforms follow the biogeomorphological succession model in a channelized river. Earth Surface Processes and Landforms 45, 2020–2035. https://doi.org/10.1002/esp.4863

Crosato, A., Mosselman, E., 2009. Simple physics-based predictor for the number of river bars and the transition between meandering and braiding. Water Resources Research 45, 1–14. https://doi.org/10.1029/2008WR007242

Crosato, A., Saleh, M.S., 2011. Numerical study on the effects of floodplain vegetation on river planform style. Earth Surface Processes and Landforms 36, 711–720. https://doi.org/10.1002/esp.2088

D'Alpaos, A., Toffolon, M., Camporeale, C., 2016. Ecogeomorphological feedbacks of water fluxes, sediment transport and vegetation dynamics in rivers and estuaries. Advances in Water Resources 93, 151–155. https://doi.org/10.1016/j.advwatres.2016.05.019

Dade, W.B., Friend, P.F., 1998. Grain-Size, Sediment-Transport Regime, and Channel Slope in Alluvial Rivers. The Journal of Geology 106, 661–676. https://doi.org/10.1086/516052

Diehl, R.M., Wilcox, A.C., Stella, J.C., Kui, L., Sklar, L.S., Lightbody, A., 2017. Fluvial sediment supply and pioneer woody seedlings as a control on bar-surface topography. Earth Surface Processes and Landforms 42, 724–734. https://doi.org/10.1002/esp.4017

Dijk, W.M. Van, Schuurman, F., Lageweg, W.I. Van De, Kleinhans, M.G., 2014. Bifurcation instability and chute cutoff development in meandering. Geomorphology 213, 277–291.

https://doi.org/10.1016/j.geomorph.2014.01.018

Dijkstra, J.T., Uittenbogaard, R.E., 2010. Modeling the interaction between flow and highly flexible aquatic vegetation. Water Resources Research 46, 1–14. https://doi.org/10.1029/2010WR009246

Edmaier, K., Burlando, P., Perona, P., 2011. Mechanisms of vegetation uprooting by flow in alluvial non-cohesive sediment. Hydrology and Earth System Sciences 15, 1615–1627. https://doi.org/10.5194/hess-15-1615-2011

Edmaier, K., Crouzy, B., Perona, P., 2015. Experimental characterization of vegetation uprooting by flow. Journal of Geophysical Research G: Biogeosciences 120, 1812–1824. https://doi.org/10.1002/2014JG002898

Edwards, P.J., Kollmann, J., Gurnell, A.M., Petts, G.E., Tockner, K., Ward, J. V., 1999. A conceptual model of vegetation dynamics of gravel bars of a large Alpine river. Wetlands Ecology and Management 7, 141–153. https://doi.org/10.1023/A:1008411311774

Erskine, W.D., Terrazzolo, N., Warner, R.F., 1999. River rehabilitation from the hydrogeomorphic impacts of a large hydro-electric power project: Snowy River, Australia. Regulated Rivers: Research & Management 15, 3–24. https://doi.org/10.1002/(SICI)1099-1646(199901/06)15:1/3<3::AID-RRR532>3.0.CO;2-R

Follett, E.M., Nepf, H.M., 2012. Sediment patterns near a model patch of reedy emergent vegetation. Geomorphology 179, 141–151. https://doi.org/10.1016/j.geomorph.2012.08.006

Fukuoka, S., Takahashi, H., Kamura, D., 1997. Compound meandering flow and simple meandering flow in a compound meandering rivers. Proceedings of Hydraulic Engineering 41, 971–976.

Garcia Lugo, G.A., Bertoldi, W., Henshaw, A.J., Gurnell, A.M., 2015. The effect of lateral confinement on gravel bed river morphology. Water Resources Research 51, 7145–7158. https://doi.org/10.1002/2015WR017081

Garcia, M., Niño, Y., 1993. Dynamics of sediment bars in straight and meandering channels: experiments on the resonance phenomenon. Journal of Hydraulic Research 31, 739–761. https://doi.org/10.1080/00221689309498815

Ghani, U., Anjum, N., Pasha, G.A., Ahmad, M., 2019. Investigating the turbulent flow characteristics in an open channel with staggered vegetation patches. River Research and Applications 35, 966–978. https://doi.org/10.1002/rra.3460

Gibling, M.R., Davies, N.S., 2012. Palaeozoic landscapes shaped by plant evolution. Nature Geoscience 5, 99–105. https://doi.org/10.1038/ngeo1376

González, E., Comín, F.A., Muller, E., 2010. Seed dispersal, germination and early seedling establishment of Populus alba L. under simulated water table declines in different substrates. Trees 24, 151–163. https://doi.org/10.1007/s00468-009-0388-y

Gran, K., Paola, C., 2001. Riparian vegetation controls on braided stream dynamics. Water Resources Research 37, 3275–3283. https://doi.org/10.1029/2000WR000203

Gran, K.B., Tal, M., Wartman, E.D., 2015. Co-evolution of riparian vegetation and channel dynamics in an aggrading braided river system, Mount Pinatubo, Philippines. Earth Surface Processes and Landforms 40, 1101–1115. https://doi.org/10.1002/esp.3699

Gurnell, A., 2014. Plants as river system engineers. Earth Surface Processes and Landforms 39, 4–25. https://doi.org/10.1002/esp.3397

Gurnell, A.M., Bertoldi, W., Corenblit, D., 2012. Changing river channels: The roles of hydrological processes, plants and pioneer fluvial landforms in humid temperate, mixed load, gravel bed rivers. Earth-Science Reviews 111, 129–141. https://doi.org/10.1016/j.earscirev.2011.11.005

Gurnell, A.M., Petts, G.E., Hannah, D.M., Smith, B.P.G., Edwards, P.J., Kollmann, J., Ward, J. V, Tockner, K., 2001. Riparian vegetation and island formation along the gravel-bed Fiume Tagliamento, Italy. Earth Surface Processes and Landforms 26, 31–62. https://doi.org/10.1002/1096-9837(200101)26:1<31::AID-ESP155>3.0.CO;2-Y

Hasegawa, K., Hirose, K., Meguro, E., 2003. Experiments and analysis on alternating mainstream change in the bifurcated channel in mountain rivers. Proceedings of Hydraulic Engineering 47, 679–684.

Hattori, A., 2005. Hydraulic resistance by flexible and tall plant communities. Doboku Gakkai Ronbunshu 2005, 65–80. https://doi.org/10.2208/jscej.2005.782_65

Hyslop, J., Trowsdale, S., 2012. A review of hydrochory (seed dispersal by water) with implications for riparian rehabilitation. Journal of Hydrology (New Zealand) 51, 137–152. https://doi.org/https://www.jstor.org/stable/43945038

Iwasaki, T., Shimizu, Y., Kimura, I., 2016a. Numerical simulation of bar and bank erosion in a vegetated floodplain: A case study in the Otofuke River. Advances in Water Resources 93, 118–134. https://doi.org/10.1016/j.advwatres.2015.02.001

Iwasaki, T., Shimizu, Y., Kimura, I., 2016b. Sensitivity of free bar morphology in rivers to secondary flow modeling: Linear stability analysis and numerical simulation. Advances in Water Resources 92, 57–72. https://doi.org/10.1016/j.advwatres.2016.03.011

Jang, C.L., Shimizu, Y., 2007. Vegetation effects on the morphological behavior of alluvial channels. Journal of Hydraulic Research 45, 763–772. https://doi.org/10.1080/00221686.2007.9521814

Järvelä, J., 2005. Effect of submerged flexible vegetation on flow structure and resistance. Journal of Hydrology 307, 233–241. https://doi.org/10.1016/j.jhydrol.2004.10.013

Javernick, L., Redolfi, M., Bertoldi, W., 2018. Evaluation of a numerical model's ability to predict bed load transport observed in braided river experiments. Advances in Water Resources 115, 207–

218. https://doi.org/10.1016/j.advwatres.2018.03.012

Johansson, M.E., Nilsson, C., 1993. Hydrochory, Population Dynamics and Distribution of the Clonal Aquatic Plant Ranunculus Lingua. The Journal of Ecology 81, 81. https://doi.org/10.2307/2261226

Johnson, W., Dixon, M.D., Simons, R., Jenson, S., Larson, K., 1995. Mapping the response of riparian vegetation to possible flow reductions in the Snake River, Idaho. Geomorphology 13, 159–173. https://doi.org/10.1016/0169-555X(95)00048-A

Jourdain, C., Claude, N., Tassi, P., Cordier, F., Antoine, G., 2020. Morphodynamics of alternate bars in the presence of riparian vegetation. Earth Surface Processes and Landforms 45, 1100–1122. https://doi.org/10.1002/esp.4776

Kawamura, T., Watanabe, Y., 2015. Analysis of long term change properties at a steep rive. Advances in River Engineering 24, 259–264.

Kim, H.S., Kimura, I., Park, M., 2018. Numerical Simulation of Flow and Suspended Sediment Deposition Within and Around a Circular Patch of Vegetation on a Rigid Bed. Water Resources Research 54, 7231–7251. https://doi.org/10.1029/2017WR021087

Kim, H.S., Kimura, I., Shimizu, Y., 2015. Bed morphological changes around a finite patch of vegetation. Earth Surface Processes and Landforms 40, 375–388. https://doi.org/10.1002/esp.3639

Kleinhans, M.G., Ferguson, R.I., Lane, S.N., Hardy, R.J., 2013. Splitting rivers at their seams: Bifurcations and avulsion. Earth Surface Processes and Landforms 38, 47–61. https://doi.org/10.1002/esp.3268

Kui, L., Stella, J.C., Lightbody, A., Wilcox, A.C., 2014. Ecogeomorphic feedbacks and flood loss of riparian tree seedlings in meandering channel experiments. Water Resources Research 50, 9366–9384. https://doi.org/10.1002/2014WR015719

Kuroki, M., Kishi, T., 1984. Regime criteria on bars and braids in alluvial straight channels. Proceedings of the Japan Society of Civil Engineers 1984, 87–96.

Kyuka, T., Yamaguchi, S., 2018. Effects of floodplain vegetation along embankments on lateral channel migration. Journal of Japan Society of Civil Engineers, Ser. B1 (Hydraulic Engineering) 74, 1135–1140.

Kyuka, T., Yamaguchi, S., Inoue, Y., Arnez Ferrel, K.R., Kon, H., Shimizu, Y., 2021. Morphodynamic effects of vegetation life stage on experimental meandering channels. Earth Surface Processes and Landforms 46, 1225–1237. https://doi.org/10.1002/esp.5051

Leopold, L.B., Wolman, M.G., 1957. River channel patterns: braided, meandering, and straight. https://doi.org/10.3133/pp282B

Lesser, G.R., Roelvink, J.A., van Kester, J.A.T.M., Stelling, G.S., 2004. Development and validation of a three-dimensional morphological model. Coastal Engineering 51, 883–915. https://doi.org/10.1016/j.coastaleng.2004.07.014

Leu, J.M., Chan, H.C., Jia, Y., He, Z., Wang, S.S.Y., 2008. Cutting management of riparian vegetation by using hydrodynamic model simulations. Advances in Water Resources 31, 1299–1308. https://doi.org/10.1016/j.advwatres.2008.06.001

Lokhorst, I.R., Lange, S.I., Buiten, G., Selaković, S., Kleinhans, M.G., 2019. Species selection and assessment of eco-engineering effects of seedlings for biogeomorphological landscape experiments. Earth Surface Processes and Landforms 44, 2922–2935. https://doi.org/10.1002/esp.4702

López, F., García, M., 1998. Open-channel flow through simulated vegetation: Suspended sediment transport modeling. Water Resources Research 34, 2341–2352. https://doi.org/10.1029/98WR01922

Luhar, M., Nepf, H.M., 2013. From the blade scale to the reach scale: A characterization of aquatic vegetative drag. Advances in Water Resources 51, 305–316. https://doi.org/10.1016/j.advwatres.2012.02.002

Luhar, M., Nepf, H.M., 2011. Flow-induced reconfiguration of buoyant and flexible aquatic vegetation. Limnology and Oceanography 56, 2003–2017. https://doi.org/10.4319/lo.2011.56.6.2003

Lytle, D.A., Merritt, D.M., 2004. Hydrologic regimesand riparian forests: a structured population model for cottonwood. Ecology 85, 2493–2503. https://doi.org/10.1890/04-0282

Mahoney, J.M., Rood, S.B., 1998. Streamflow requirements for cottonwood seedling recruitment—An integrative model. Wetlands 18, 634–645. https://doi.org/10.1007/BF03161678

Malkauthekar, M.D., 2013. Analysis of euclidean distance and Manhattan distance measure in face recognition. Third International Conference on Computational Intelligence and Information Technology (CIIT 2013) 503–507. https://doi.org/10.1049/cp.2013.2636

Mao, L., Ravazzolo, D., Bertoldi, W., 2020. The role of vegetation and large wood on the topographic characteristics of braided river systems. Geomorphology 367, 107299. https://doi.org/10.1016/j.geomorph.2020.107299

Marjoribanks, T.I., Lague, D., Hardy, R.J., Boothroyd, R.J., Leroux, J., Mony, C., Puijalon, S., 2019. Flexural Rigidity and Shoot Reconfiguration Determine Wake Length Behind Saltmarsh Vegetation Patches. Journal of Geophysical Research: Earth Surface 124, 2176–2196. https://doi.org/10.1029/2019JF005012

Marra, W.A., Kleinhans, M.G., Addink, E.A., 2014. Network concepts to describe channel importance

and change in multichannel systems: Test results for the Jamuna River, Bangladesh. Earth Surface Processes and Landforms 39, 766–778. https://doi.org/10.1002/esp.3482

Martínez-Fernández, V., Van Oorschot, M., De Smit, J., González del Tánago, M., Buijse, A.D., 2018. Modelling feedbacks between geomorphological and riparian vegetation responses under climate change in a Mediterranean context. Earth Surface Processes and Landforms 43, 1825–1835. https://doi.org/10.1002/esp.4356

Meire, D.W.S.A., Kondziolka, J.M., Nepf, H.M., 2014. Interaction between neighboring vegetation patches: Impact on flow and deposition. Water Resources Research 50, 3809–3825. https://doi.org/10.1002/2013WR015070

Merritt, D.M., Wohl, E.E., 2006. Plant dispersal along rivers fragmented by dams. River Research and Applications 22, 1–26. https://doi.org/10.1002/rra.890

Merritt, D.M., Wohl, E.E., 2002. Processes governing hydrochory along rivers: Hydraulics, hydrology, and dispersal phenology. Ecological Applications 12, 1071–1087. https://doi.org/10.1890/1051-0761(2002)012[1071:PGHARH]2.0.CO;2

Meyer-Peter, E., Muller, R., 1948. Formulas for Bed Load Transport, in: Proceedings of 2nd Meeting of the International Association for Hydraulic Structures Research. pp. 39–64.

Millar, R.G., 2005. Theoretical regime equations for mobile gravel-bed rivers with stable banks. Geomorphology 64, 207–220. https://doi.org/10.1016/j.geomorph.2004.07.001

Millar, R.G., 2000. Influence of bank vegetation on alluvial channel patterns. Water Resources Research 36, 1109–1118. https://doi.org/10.1029/1999WR900346

Mosner, E., Weber, A., Carambia, M., Nilson, E., Schmitz, U., Zelle, B., Donath, T., Horchler, P., 2015. Climate change and floodplain vegetation-future prospects for riparian habitat availability along the Rhine River. Ecological Engineering 82, 493–511. https://doi.org/10.1016/j.ecoleng.2015.05.013

Murray, A.B., Knaapen, M.A.F., Tal, M., Kirwan, M.L., 2008. Biomorphodynamics: Physical-biological feedbacks that shape landscapes. Water Resources Research 44. https://doi.org/10.1029/2007WR006410

Murray, B.A., Paola, C., 2003. Modelling the effect of vegetation on channel pattern in bedload rivers. Earth Surface Processes and Landforms 28, 131–143. https://doi.org/10.1002/esp.428

Nagata, T., Watanabe, Y., Shimizu, Y., INnoue, T., Funaki, J., 2016. Study on dynamics of river channel and vegetation in gravel bed river. Journal of Japan Society of Civil Engineers, Ser. B1 (Hydraulic Engineering) 72, I_1081-I_1086. https://doi.org/10.2208/jscejhe.72.I_1081

Nagata, T., Watanabe, Y., Yasuda, H., Ito, A., 2014. Development of a meandering channel caused by the planform shape of the river bank. Earth Surface Dynamics 2, 255–270.

https://doi.org/10.5194/esurf-2-255-2014

Nagata, T., Watanabe, Y., Yasuda, H., Ito, A., 2013. Development of a meandering channel caused by a shape of the alternate bars. Journal of Japan Society of Civil Engineers, Ser. B1 (Hydraulic Engineering) 69, 1099–1104.

Nakagawa, H., Tsujimoto, T., Kitamura, T., Fujii, Y., 1995. Flow resistance on flexible vegetation-covered bed in open channels. The Journal of Japan Society of Civil Engineers, Ser. B1 39, 465–470.

Nanson, G.C., Knighton, A.D., 1996. ANABRANCHING RIVERS: THEIR CAUSE, CHARACTER AND CLASSIFICATION. Earth Surface Processes and Landforms 21, 217–239. https://doi.org/10.1002/(SICI)1096-9837(199603)21:3<217::AID-ESP611>3.0.CO;2-U

Nepf, H.M., 2011. Flow and Transport in Regions with Aquatic Vegetation. Annual Review of Fluid Mechanics 44, 123–142. https://doi.org/10.1146/annurev-fluid-120710-101048

Nepf, H.M., Mugnier, C.G., Zavistoski, R.A., 1997. The effects of vegetation on longitudinal dispersion. Estuarine, Coastal and Shelf Science 44, 675–684. https://doi.org/10.1006/ecss.1996.0169

Nepf, H.M., Vivoni, E.R., 2000. Flow structure in depth-limited, vegetated flow. Journal of Geophysical Research: Oceans 105, 28547–28557. https://doi.org/10.1029/2000JC900145

Okabe, K., Kyuka, T., Shimizu, Y., Hasegawa, K., Shinjo, K., Yamaguchi, S., 2018. Discharge fluctuation dominating factors influencing the pass of river —a case study on Otofuke River in Japan. Journal of Japan Society of Civil Engineers, Ser. B1 (Hydraulic Engineering) 74, 1501–1506.

Parolin, P., 2006. Ombrohydrochory: Rain-operated seed dispersal in plants – With special regard to jet-action dispersal in Aizoaceae. Flora - Morphology, Distribution, Functional Ecology of Plants 201, 511–518. https://doi.org/10.1016/j.flora.2005.11.003

Pearlstine, L., McKellar, H., Kitchens, W., 1985. Modelling the impacts of a river diversion on bottomland forest communities in the Santee River floodplain, South Carolina. Ecological Modelling 29, 283–302. https://doi.org/10.1016/0304-3800(85)90057-2

Perucca, E., Camporeale, C., Ridolfi, L., 2007. Significance of the riparian vegetation dynamics on meandering river morphodynamics. Water Resources Research 43, 1–10. https://doi.org/10.1029/2006WR005234

Raupach, M.R., Antonia, R.A., Rajagopalan, S., 1991. Rough-Wall Turbulent Boundary Layers. Applied Mechanics Reviews 44, 1–25. https://doi.org/10.1115/1.3119492

Ricardo, A.M., Grigoriadis, D.G.E., Ferreira, R.M.L., 2018. LES modelling of a flow within an infinite array of randomly placed cylinders: Anisotropy characterization. E3S Web of

Conferences 40, 7–9. https://doi.org/10.1051/e3sconf/20184002035

Rominger, J.T., Lightbody, A.F., Nepf, H.M., 2010. Effects of Added Vegetation on Sand Bar Stability and Stream Hydrodynamics. Journal of Hydraulic Engineering 136, 994–1002. https://doi.org/10.1061/(asce)hy.1943-7900.0000215

Sakai, N., Toda, Y., Tsujimoto, T., 2013. Numerical simulation of bar morphology and vegetation dynamics with consideration of interspecific competition and expansion of riparian vegetation. Journal of Japan Society of Civil Engineers, Ser. B1 (Hydraulic Engineering) 69, I_1357-I_1362. https://doi.org/10.2208/jscejhe.69.I_1357

Schumm, S.A., 1985. PATTERNS OF ALLUVIAL RIVERS. Annual Review of Earth and Planetary Sciences 13, 5–27. https://doi.org/10.1146/annurev.ea.13.050185.000253

Schuurman, F., 2015. Bar and channel evolution in meandering and braiding rivers using physics-based modeling, Utrecht Studies in Earth Sciences. https://doi.org/10.13140/RG.2.1.3582.3529

Schuurman, F., Marra, W.A., Kleinhans, M.G., 2013. Physics-based modeling of large braided sand-bed rivers: Bar pattern formation, dynamics, and sensitivity. Journal of Geophysical Research: Earth Surface 118, 2509–2527. https://doi.org/10.1002/2013JF002896

Schuurman, F., Shimizu, Y., Iwasaki, T., Kleinhans, M.G., 2016. Dynamic meandering in response to upstream perturbations and floodplain formation. Geomorphology 253, 94–109. https://doi.org/10.1016/j.geomorph.2015.05.039

Schuurman, F., Ta, W., Post, S., Sokolewicz, M., Busnelli, M., Kleinhans, M., 2018. Response of braiding channel morphodynamics to peak discharge changes in the Upper Yellow River. Earth Surface Processes and Landforms 43, 1648–1662. https://doi.org/10.1002/esp.4344

Seminara, G., Tubino, M., 1989. Alternate bars and meandering: Free, forced and mixed interactions. pp. 267–320. https://doi.org/10.1029/WM012p0267

Sezaki, T., Hattori, A., Kondo, K., Tokuda, M., Fujita, K., Yoshida, M., 2000. Field study on the destruction processes of herbaceous vegetation on gravel bars due to flood flows. PROCEEDINGS OF HYDRAULIC ENGINEERING 44, 825–830. https://doi.org/10.2208/prohe.44.825

Shimizu, Y., Nelson, J., Arnez Ferrel, K., Asahi, K., Giri, S., Inoue, T., Iwasaki, T., Jang, C.L., Kang, T., Kimura, I., Kyuka, T., Mishra, J., Nabi, M., Patsinghasanee, S., Yamaguchi, S., 2020. Advances in computational morphodynamics using the International River Interface Cooperative (iRIC) software. Earth Surface Processes and Landforms 45, 11–37. https://doi.org/10.1002/esp.4653

Solari, L., Van Oorschot, M., Belletti, B., Hendriks, D., Rinaldi, M., Vargas-Luna, A., 2016. Advances on Modelling Riparian Vegetation-Hydromorphology Interactions. River Research and

Applications 32, 164–178. https://doi.org/10.1002/rra.2910

Stecca, G., Zolezzi, G., Hicks, D.M., Surian, N., 2019. Reduced braiding of rivers in human-modified landscapes: Converging trajectories and diversity of causes. Earth-Science Reviews 188, 291–311. https://doi.org/10.1016/j.earscirev.2018.10.016

Ström, L., Jansson, R., Nilsson, C., 2012. Projected changes in plant species richness and extent of riparian vegetation belts as a result of climate-driven hydrological change along the Vindel River in Sweden. Freshwater Biology 57, 49–60. https://doi.org/10.1111/j.1365-2427.2011.02694.x

Sumitomo, K., Watanabe, Y., Izumi, N., Yamaguchi, S., Tokohama, H., 2016. Study on the maintenance of former watercourses by the artificial flood for river channel disturbance. Journal of Japan Society of Civil Engineers, Ser. B1 (Hydraulic Engineering) 72, I_751-I_756. https://doi.org/10.2208/jscejhe.72.I_751

Sumitomo, K., Watanabe, Y., Izumi, N., Yamaguchi, S., Yonemoto, M., 2018. The effect of branched channel maintenance on river channel evolution during floods. Journal of Japan Society of Civil Engineers, Ser. B1 (Hydraulic Engineering) 74, I_1003-I_1008. https://doi.org/10.2208/jscejhe.74.5_I_1003

Takebayashi, H., Egashira, S., 2001. Formative process and domain of a self-formed stream channel. Doboku Gakkai Ronbunshu 75–86. https://doi.org/10.2208/jscej.2001.677_75

Tal, M., Paola, C., 2010. Effects of vegetation on channel morphodynamics: Results and insights from laboratory experiments. Earth Surface Processes and Landforms 35, 1014–1028. https://doi.org/10.1002/esp.1908

Tal, M., Paola, C., 2007. Dynamic single-thread channels maintained by the interaction of flow and vegetation. Geology 35, 347–350. https://doi.org/10.1130/G23260A.1

Tetsuya, S., Tsunekawa, A., Tsujimoto, T., 2003. A study on physical environment and water-solute transport in surface substrate under vegetation on a sandbar in Kizu River. Advances in river engineering 9, 389–394.

Tockner, K., Paetzold, A., Karaus, U., Claret, C., Zettel, J., 2006. Ecology of Braided Rivers, in: Braided Rivers. Blackwell Publishing Ltd., Oxford, UK, pp. 339–359. https://doi.org/10.1002/9781444304374.ch17

Toshimori, N., Miyamoto, H., 2014. Probabilistic Evaluation for Flood Water Level Reduction By Thinning and Cutting-Down of a Vegetated Channel Using a Vegetation Dynamics Model. Journal of Japan Society of Civil Engineers, Ser. B1 (Hydraulic Engineering) 70, I_1381-I_1386. https://doi.org/10.2208/jscejhe.70.i_1381

Tsujimoto, T., 1999. Fluvial processes in streams with vegetation. Journal of Hydraulic Research 37, 789–803. https://doi.org/10.1080/00221689909498512

Tsujimoto, T., Kitamura, T., 1998. Study on Flow over Flexible Vegetation-Covered Bed. Doboku Gakkai Ronbunshu 1998, 29–44. https://doi.org/10.2208/jscej.1998.607_29

van den Berg, J.H., 1995. Prediction of alluvial channel pattern of perennial rivers. Geomorphology 12, 259–279. https://doi.org/10.1016/0169-555X(95)00014-V

van Dijk, W.M., Teske, R., van De Lageweg, W.I., Kleinhans, M.G., 2013. Effects of vegetation distribution on experimental river channel dynamics. Water Resources Research 49, 7558–7574. https://doi.org/10.1002/2013WR013574

Van Dijk, W.M., Teske, R., Van De Lageweg, W.I., Kleinhans, M.G., 2013. Effects of vegetation distribution on experimental river channel dynamics. Water Resources Research 49, 7558–7574. https://doi.org/10.1002/2013WR013574

van Oorschot, M., Kleinhans, M., Buijse, T., Geerling, G., Middelkoop, H., 2018. Combined effects of climate change and dam construction on riverine ecosystems. Ecological Engineering 120, 329–344. https://doi.org/10.1016/j.ecoleng.2018.05.037

van Oorschot, M., Kleinhans, M., Geerling, G., Middelkoop, H., 2016. Distinct patterns of interaction between vegetation and morphodynamics. Earth Surface Processes and Landforms 41, 791–808. https://doi.org/10.1002/esp.3864

van Oorschot, M., Kleinhans, M.G., Geerling, G.W., Egger, G., Leuven, R.S.E.W., Middelkoop, H., 2017. Modeling invasive alien plant species in river systems: Interaction with native ecosystem engineers and effects on hydro-morphodynamic processes. Water Resources Research 53, 6945–6969. https://doi.org/10.1002/2017WR020854

Vargas-Luna, A., Crosato, A., Anders, N., Hoitink, A.J.F., Keesstra, S.D., Uijttewaal, W.S.J., 2018. Morphodynamic effects of riparian vegetation growth after stream restoration. Earth Surface Processes and Landforms 43, 1591–1607. https://doi.org/10.1002/esp.4338

Vargas-Luna, Andrés, Crosato, A., Calvani, G., Uijttewaal, W.S.J., 2016. Representing plants as rigid cylinders in experiments and models. Advances in Water Resources 93, 205–222. https://doi.org/10.1016/j.advwatres.2015.10.004

Vargas-Luna, A., Crosato, A., Hoitink, A.J.F., Groot, J., Uijttewaal, W.S.J., 2016. Effects of riparian vegetation development in a restored lowland stream. River Flow - Proceedings of the International Conference on Fluvial Hydraulics, RIVER FLOW 2016 2197–2200. https://doi.org/10.1201/9781315644479-341

Vargas-Luna, A., Crosato, A., Uijttewaal, W.S.J., 2015. Effects of vegetation on flow and sediment transport: Comparative analyses and validation of predicting models. Earth Surface Processes and Landforms 40, 157–176. https://doi.org/10.1002/esp.3633

Vargas-Luna, A., Duró, G., Crosato, A., Uijttewaal, W., 2019. Morphological Adaptation of River

Channels to Vegetation Establishment: A Laboratory Study. Journal of Geophysical Research: Earth Surface 124, 1981–1995. https://doi.org/10.1029/2018JF004878

Verschoren, V., Meire, D., Schoelynck, J., Buis, K., Bal, K.D., Troch, P., Meire, P., Temmerman, S., 2016. Resistance and reconfiguration of natural flexible submerged vegetation in hydrodynamic river modelling. Environmental Fluid Mechanics 16, 245–265. https://doi.org/10.1007/s10652-015-9432-1

Vesipa, R., Camporeale, C., Ridolfi, L., 2017. Effect of river flow fluctuations on riparian vegetation dynamics: Processes and models. Advances in Water Resources 110, 29–50. https://doi.org/10.1016/j.advwatres.2017.09.028

Wang, Z.B., De Vries, M., Fokkink, R.J., Langerak, A., 1995. Stabilité des bifurcations de rivières dans des modèles morphodynamiques filaires. Journal of Hydraulic Research 33, 739–750. https://doi.org/10.1080/00221689509498549

Weisscher, S.A.H., Shimizu, Y., Kleinhans, M.G., 2019. Upstream perturbation and floodplain formation effects on chute-cutoff-dominated meandering river pattern and dynamics. Earth Surface Processes and Landforms 44, 2156–2169. https://doi.org/10.1002/esp.4638

Westfall, P.H., 2014. Kurtosis as Peakedness, 1905–2014. R.I.P. The American Statistician 68, 191–195. https://doi.org/10.1080/00031305.2014.917055

Whiting, P.J., Dietrich, W.E., 1993. Experimental Studies of bed topography and flow patterns in large-amplitude meanders: 2. Mechanisms. Water Resources Research 29, 3615–3622. https://doi.org/10.1029/93WR01756

Wilson, C.A.M.E., 2007. Flow resistance models for flexible submerged vegetation. Journal of Hydrology 342, 213–222. https://doi.org/10.1016/j.jhydrol.2007.04.022

Yamaguchi, S., Ito, A., 2014. Characteristics of meandering streams caused by bar formation with bank erosion and its numerical experiments. Journal of Japan Society of Civil Engineers, Ser. B1 (Hydraulic Engineering) 70, I_985-I_990. https://doi.org/10.2208/jscejhe.70.I_985

Zen, S., Perona, P., 2020. Biomorphodynamics of river banks in vegetated channels with self-formed width. Advances in Water Resources 135. https://doi.org/10.1016/j.advwatres.2019.103488

Zong, L., Nepf, H., 2011. Spatial distribution of deposition within a patch of vegetation. Water Resources Research 47, 1–12. https://doi.org/10.1029/2010WR009516